



HAL
open science

The komatiite testimony to ancient mantle heterogeneity

Igor Puchtel, Janne Blichert-Toft, Mary Horan, Mathieu Touboul, Richard Walker

► To cite this version:

Igor Puchtel, Janne Blichert-Toft, Mary Horan, Mathieu Touboul, Richard Walker. The komatiite testimony to ancient mantle heterogeneity. *Chemical Geology*, 2022, 594, pp.120776. 10.1016/j.chemgeo.2022.120776 . hal-03589592

HAL Id: hal-03589592

<https://hal.science/hal-03589592>

Submitted on 25 Feb 2022

HAL is a multi-disciplinary open access archive for the deposit and dissemination of scientific research documents, whether they are published or not. The documents may come from teaching and research institutions in France or abroad, or from public or private research centers.

L'archive ouverte pluridisciplinaire **HAL**, est destinée au dépôt et à la diffusion de documents scientifiques de niveau recherche, publiés ou non, émanant des établissements d'enseignement et de recherche français ou étrangers, des laboratoires publics ou privés.

The Komatiite Testimony to Ancient Mantle Heterogeneity

Igor S. Puchtel^{1*}, Janne Blichert-Toft², Mary F. Horan³,
Mathieu Touboul², and Richard J. Walker¹

¹Department of Geology, University of Maryland, 8000 Regents Drive, College Park, MD 20742, USA

²Laboratoire de Géologie de Lyon, Ecole Normale Supérieure de Lyon, CNRS UMR 5276, Université de
Lyon, 46 Allée d'Italie, 69007 Lyon, France

³Earth and Planets Laboratory, Carnegie Institution for Science, 5241 Broad Branch Road NW, Washington,
DC 20015, USA

*Corresponding author: ipuchtel@umd.edu

Revised for:

Chemical Geology

Invited Review Manuscript

Version: February 06, 2022

Keywords: Komatiites; early Earth; mantle heterogeneity; Hf-W, Sm-Nd, Lu-Hf, Re-Os, Pt-Os isotope systems; highly siderophile elements; grainy late accretion; primordial magma ocean, core-mantle interaction; mixing times of the mantle; Nd-Hf-Os isotope paradox.

36 **Abstract**

37 Komatiites are crystallized samples of high-temperature, high-MgO lavas that were
38 common during the Archean, but became increasingly rarer in the Proterozoic and
39 Phanerozoic. Although the origin of komatiites remains a subject of debate, all komatiites
40 included in this review, ranging in age from 3.6 to 2.0 Ga, are interpreted to have most likely
41 been derived from anhydrous melting in mantle plumes. These plumes are estimated to have
42 been initiated at different depths in the mantle, thus, providing important information about
43 the chemical evolution of the early Earth.

44 The $^{142,143}\text{Nd}$, ^{176}Hf , ^{182}W , ^{187}Os , and ^{186}Os systematics and trace- and highly siderophile
45 element (HSE) abundances of these komatiites provide strong evidence for the presence of
46 isotopic and chemical heterogeneities in the mantle during the first half of Earth history.
47 These heterogeneities likely reflect the combined effects of: (1) the co-existence of diverse
48 post-magma ocean silicate domains that were characterized by variably-fractionated lithophile
49 and siderophile element abundances; (2) the presence of distinct reservoirs that included
50 mantles and cores of late accreted, differentiated planetesimals; and (3) isotopic exchange
51 across the core-mantle boundary. These data highlight the complexity of komatiite mantle
52 sources, none of which were similar in composition to estimates for the modern bulk silicate
53 Earth (BSE). Moreover, no single petrogenetic model can account for the remarkably diverse
54 chemical and isotopic compositions of komatiites.

55 The disappearance of resolvable positive and negative ^{142}Nd anomalies, as well as
56 decoupled ^{143}Nd - ^{176}Hf isotopic signatures, in the mafic-ultramafic rock record by ~ 2.5 Ga
57 indicate that, by the end of the Archean, the earliest silicate reservoirs, formed through
58 primordial magma ocean crystallization, had been largely destroyed as a result of vigorous
59 convective mantle mixing. This implies that, during the Hadean and Archean, it took the
60 mantle ~ 1.5 Ga to mix away the early formed ^{142}Nd heterogeneities *via* wholesale mantle
61 convection. Similar to ^{142}Nd systematics, there appears to have been a shift from mostly
62 positive ^{182}W anomalies in pre-2.5 Ga komatiite mantle sources to no ^{182}W offsets in post-2.5
63 Ga komatiite mantle sources. Coupled with the disappearance of projected HSE depletions in
64 komatiite mantle sources at ~ 2.5 Ga, relative to the modern BSE, this shift may indicate that
65 by the end of the Archean, late accreted planetesimals had become largely homogenized
66 within the mantle, and core-mantle interaction took over as the main driving force of creating
67 ^{182}W isotope anomalies, possibly coincident with the timing of the onset of modern-style plate
68 tectonics on Earth.

69

70 **1. Introduction**

71 Accurately determining how the distribution of chemical elements within the Earth has
72 changed over time has been, and remains, one of the most fundamental challenges in Earth
73 science; it has far-reaching implications not only for the long-standing debate of how
74 terrestrial planets formed and evolved, but also for understanding ongoing processes on Earth.
75 The information pertaining to the origin and early evolution of Earth comes largely from the
76 geological rock record between ~4.0 and 2.0 Ga, which harbors isotopic and elemental
77 signatures generated in the terrestrial reservoirs *via* early chemical fractionation processes and
78 the radioactive decay of short- and long-lived refractory nuclides, including $^{146,147}\text{Sm}$, ^{176}Lu ,
79 ^{182}Hf , ^{187}Re , and ^{190}Pt .

80 The mantle is the largest of all the terrestrial reservoirs. Its chemically and isotopically
81 heterogeneous nature has long been established by numerous pioneering studies of the Earth's
82 rock record (*e.g.*, Hart and Brooks, 1977; Hofmann and Hart, 1978; Zindler et al., 1982; Hart
83 and Zindler, 1986; Zindler and Hart, 1986; Jacobsen, 1988; Galer and Goldstein, 1991). Some
84 of the heterogeneities have been argued to be primordial in nature, reflecting initial planetary
85 accretion/differentiation and magma ocean crystallization processes (Goldstein and Galer,
86 1992; Albarède et al., 2000; Drake, 2000; Boyet and Carlson, 2005; Frost et al., 2008; Caro,
87 2011; Touboul et al., 2012; Carlson et al., 2015; Jacobsen and Yu, 2015; Puchtel et al., 2016a;
88 Rizo et al., 2016; Boyet et al., 2021). Others likely were formed as a result of a protracted
89 terrestrial accretion history (*e.g.*, Willbold et al., 2011; 2015; Dale et al., 2017; Puchtel et al.,
90 2018; Archer et al., 2019) or later processes associated with the dynamic regime of the planet,
91 especially crustal recycling (*e.g.*, DePaolo, 1980; Armstrong, 1981; Hofmann and White,
92 1982; Patchett et al., 1984; Shirey and Hanson, 1986; Chase and Patchett, 1988; Galer et al.,
93 1989; Bowring and Housh, 1995; Bennett et al., 1996; Salters and White, 1998; Blichert-Toft
94 et al., 2015).

95 Despite these decades-long research efforts, still limited insights into the terrestrial mantle
96 mixing history mean that the nature, origin, scale, and longevity of early mantle
97 heterogeneities, in terms of different elements and isotopic systems, remain contentious. This
98 review is intended to fill some of the existing gaps in our understanding of early Earth
99 chemical evolution by synthesizing the existing short- and long-lived refractory radiogenic
100 isotopic and elemental abundance data for a representative set of well-preserved and well-
101 characterized komatiite and basalt systems that are especially advantageous for studying
102 processes that occurred within the first 2.5 billion years of Earth history. In parallel, we

103 address the question of the complex origins of komatiites and their usefulness as proxies for
104 the chemical composition of the early Earth mantle.

105 Here, we consider komatiite-basalt systems from 13 different localities around the globe:
106 the 3.55 Ga Schapenburg, 3.48 Ga Komati, and 3.26 Ga Weltevreden komatiites in the
107 Kaapvaal Craton of South Africa; the 3.53 Ga Coonterunah, 3.34 Ga Kelly, and 3.18 Ga Ruth
108 Well and Regal komatiites and basalts in the Pilbara Craton of Western Australia; the 2.82 Ga
109 Kostomuksha, 2.41 Ga Vetreny, and 2.05 Ga Lapland komatiites in the Fennoscandian Shield
110 of northern Europe; the 2.72 Ga Pyke Hill-Alexo and Boston Creek komatiites in the Superior
111 Craton of Canada, and the 2.7 Ga Belingwe komatiites in the Rhodesian Craton of South
112 Africa. These komatiite-basalt systems were chosen because of good preservation of their
113 primary mineralogical and textural features and chemical and isotopic compositions, and
114 because complete sets of published high-precision chemical and isotope data, obtained on the
115 same sample sets, are available for these systems. A schematic world map showing the
116 location of these komatiite-basalt systems is provided in the **Electronic Supplement**.

117 **2. Komatiites as probes of the early Earth mantle**

118 Komatiites are ultramafic lavas containing more than 18% MgO in the parental liquid
119 (Arndt and Nisbet, 1982). To be classified as a komatiite, the crystallized lava must either
120 contain spinifex texture, or be genetically related to lavas containing spinifex texture. Spinifex
121 texture is a crucial feature that distinguishes komatiites from other ultramafic lavas, such as
122 picrites, boninites, and meimechites. It is characterized by the presence of large, skeletal
123 crystals of olivine that form during rapid, *in situ* crystallization of high-MgO, superheated
124 (*i.e.*, heated to above liquidus temperatures) silicate liquids. Due to the absence of nucleation
125 sites, superheated liquids display a reluctance to nucleate, and olivine crystals that eventually
126 form do so rapidly upon cooling below the liquidus and are typically large and skeletal,
127 leading to the formation of spinifex texture (*e.g.*, Arndt, 1994; Arndt et al., 2008).

128 Ever since komatiites were first discovered and described in South Africa (Viljoen and
129 Viljoen, 1969), these rocks have served as a source of valuable information bearing on the
130 chemical and thermal evolution of the mantle (*e.g.*, Arndt et al., 2008). Owing to formation
131 *via* the highest degrees of partial melting of all mantle-derived magmas, komatiites have
132 compositions approaching that of mantle peridotite and, thus, represent the closest available
133 approximation of the chemical characteristics of the mantle among volcanic rocks (*e.g.*,
134 Arndt, 1977; Nesbitt et al., 1979; Herzberg, 1992). As high-degree, superheated, and low-
135 viscosity melts, komatiites extracted large proportions of highly siderophile elements (HSE,

136 including Re, Os, Ir, Ru, Pt, and Pd) from the mantle, experienced little differentiation prior to
137 emplacement, and likely sampled mantle domains on the order of tens of millions of cubic
138 kilometers, as evidenced by the sheer volumes of komatiitic magmas erupted in a number of
139 Archean terrains. Some of these occurrences are argued to be similar in volume to recent and
140 modern oceanic plateaus, such as the Ontong Java plateau (*e.g.*, Condie, 1975; Schubert and
141 Sandwell, 1989; Storey et al., 1991; Kusky and Kidd, 1992; Desrochers et al., 1993; Kimura
142 et al., 1993; Abbott, 1996; Kent et al., 1996; Puchtel et al., 1998; Arndt et al., 2001). During
143 crystallization of komatiite lava flows, major and trace elements, including HSE, behaved in
144 predictable manners relative to indices of magmatic differentiation, making it possible to
145 obtain precise chronological information, estimate element mobility, and determine HSE
146 abundances in the mantle sources of most komatiites. The ability of komatiites to provide a
147 reliable record of the chemical and isotopic characteristics of mantle domains that existed
148 during the first half of Earth history is the key underlying factor for focusing on komatiites in
149 this review, which is intended to summarize what komatiites have taught us about the
150 evolution of early Earth. On the other hand, although basalts are less informative as probes of
151 the HSE characteristics of the mantle, because of their inherently higher Nd, Hf, and W
152 abundances, they are shown here to be reliable recorders of mantle Nd, Hf, and W isotopic
153 compositions and have also been studied in several komatiite-basalt systems.

154 **3. The analytical toolbox to study the chemical evolution of the mantle**

155 The chemical evolution of the mantle has long been studied using radiogenic isotope
156 systems and lithophile and siderophile element abundances in mantle-derived rocks. The
157 lithophile element-based isotopic systems, particularly $^{142,143}\text{Nd}$ and ^{176}Hf , are, by way of their
158 refractory nature and optimal half-lives, powerful tools for examining possible primordial
159 magma ocean processes, as well as subsequent mantle melting and differentiation processes
160 (*e.g.*, DePaolo and Wasserburg, 1976; Jacobsen and Wasserburg, 1979; Patchett and
161 Tatsumoto, 1980; Patchett et al., 1981; White and Patchett, 1984; Zindler and Hart, 1986;
162 Sivell and McCulloch, 1991). Silicate melts have lower Sm/Nd and Lu/Hf than co-existing
163 silicate solids, and after separation, evolve to distinctive ^{143}Nd and ^{176}Hf compositions. If
164 Sm/Nd fractionated prior to ~ 4.0 Ga, while ^{146}Sm was still extant, variations in ^{142}Nd can also
165 be generated. Hence, application of the combined $^{142,143}\text{Nd}$ systems provides the temporal
166 resolution necessary for deciphering the timing and mechanisms of the earliest mantle
167 differentiation events (Goldstein and Galer, 1992; Harper and Jacobsen, 1992; Boyet et al.,
168 2003; Caro et al., 2003, 2006, 2017; Boyet and Carlson, 2005, 2006; Bennett et al., 2007;

169 O'Neil et al., 2008, 2012, 2016; Rizo et al., 2012, 2013, 2016; Roth et al., 2013, 2014).
170 Further combining the $^{142,143}\text{Nd}$ with the ^{176}Hf systematics allows identification of specific
171 processes that may have controlled mantle differentiation, including fractionation of the high-
172 pressure bridgmanite (Mg-perovskite) and Ca-perovskite assemblage during crystallization of
173 a primordial magma ocean (Caro et al., 2005; Hoffmann et al., 2011; Rizo et al., 2011;
174 Puchtel et al., 2013; 2016a; Hoffmann and Wilson, 2017; Boyet et al., 2021).

175 The short-lived ^{182}Hf - ^{182}W system can be used to detect fractionation of the lithophile
176 trace element Hf from the siderophile trace element W occurring within the first ~60 Ma of
177 Solar System history. This isotope system constitutes a high-resolution tool for identifying
178 magma ocean crystallization, the effects of late accretion, and, by virtue of its dual lithophile
179 and siderophile nature, potentially core-mantle interaction processes (Kleine et al., 2002,
180 2004, 2009; Yin et al., 2002, Jacobsen and Yu, 2015; Reimink et al., 2020; Willbold et al.,
181 2011, 2015; Touboul et al., 2012; Puchtel et al., 2018, 2020, 2022; Rizo et al., 2019; Mundl-
182 Petermeier et al., 2019, 2020). Further, application of the combined ^{142}Nd and ^{182}W tools can
183 help discriminate between early magma ocean differentiation processes and the effects of late
184 accretion (Harper and Jacobsen, 1996; Rizo et al., 2016; 2019; Puchtel et al., 2018; Peters et
185 al., 2021).

186 Abundances of HSE, combined with ^{186}Os and ^{187}Os systematics, provide additional
187 information about the chemical evolution of the mantle and the processes that operated early
188 in Earth history (*e.g.*, Righter et al., 2000; Walker, 2009, 2016; Day, 2013; Puchtel et al.,
189 2014; Day et al., 2016). The behavior of Re, Pt, and Os is governed by their strong
190 partitioning into metal or sulfide liquids relative to silicate melt (Crocket et al., 1997; Righter
191 and Drake, 1997). During mantle melting, Os is moderately to highly compatible with the
192 melting residue, whereas Pt and Re are incompatible to various degrees (*e.g.*, Barnes et al.,
193 1985; Rehkämper et al., 1999; Mallmann and O'Neill, 2007). Thus, the two Os isotopic
194 systems together with HSE abundances provide insight into some primordial processes to
195 which the lithophile element-based isotopic systems are not sensitive, including late-stage
196 planetary accretion and metal-silicate differentiation. Estimates of HSE abundances in
197 komatiite mantle sources can also be used to track the mixing rates of the mantle and the
198 timing of homogenization of late accreted materials within the mantle (*e.g.*, Maier et al.,
199 2009; Puchtel et al., 2018, 2020, 2022). In combination with Os isotope systematics and HSE
200 abundances, the ^{182}Hf - ^{182}W isotopic system can be used to discriminate between the effects of
201 early planetary differentiation, late accretion, and core-mantle interaction (*e.g.*, Touboul et al.,

202 2012; Puchtel et al., 2016a, 2018, 2020, 2022; Archer et al., 2019; Rizo et al., 2019; Tusch et
203 al., 2021).

204 The water content of a komatiitic lava is also an important parameter for assessing where
205 in the mantle the parental melt originated. Water is highly incompatible during mantle melting
206 (*e.g.*, Moore, 1970; Michael, 1995; Saal et al., 2002; Hauri et al., 2006; Cooper et al., 2012).
207 The water content of a given komatiite mantle source can be derived from that of a komatiite
208 lava provided that effects of secondary alteration can be corrected for. For example,
209 correlations between the abundances of water and other lithophile trace elements, *e.g.*, Ce, in
210 submarine basalt glasses have been used in a number of studies to establish H₂O contents of
211 mantle-derived melts (*e.g.*, Michael, 1995; Saal et al., 2002; Hauri et al., 2006; Cooper et al.,
212 2012). Mid-ocean ridge basalt (MORB) and ocean island basalt (OIB) magmas have H₂O/Ce
213 ≤ 370 (Hauri et al., 2006), similar to the mantle value of 200 ± 50 (Hirschmann, 2018); the
214 rather large range is due to the fact that during anhydrous mantle melting, spinel lherzolite has
215 a bulk solid/melt $D_{\text{H}_2\text{O}} \approx D_{\text{Ce}}$, whereas garnet lherzolite has a bulk solid/melt $D_{\text{H}_2\text{O}} = 0.5 \times D_{\text{Ce}}$.
216 By contrast, arc magmas have H₂O/Ce of 2,000 to 3,000, due to variable contributions of H₂O
217 from the subducting slab (Cooper et al., 2012).

218 The oxidation state of a komatiite magma and its source reflects important information
219 about the location and processes involved in its generation. For example, knowledge of $f\text{O}_2$
220 can potentially be used to distinguish between a hydrous (*i.e.*, subduction) versus anhydrous
221 (*i.e.*, plume) origin of komatiites. Canil (1997, 1999, 2002) and Canil and Fedortchouk (2001)
222 used V partitioning between liquidus olivine and komatiite liquid as a redox indicator. These
223 authors showed that the major factor controlling the distribution of V between olivine and
224 komatiitic melt ($D_V^{\text{ol/liq}}$) was oxygen fugacity, $f\text{O}_2$. More oxidized, water-rich island arc
225 magmas (higher $f\text{O}_2$) are invariably characterized by $D_V^{\text{ol/liq}} < 0.01$, whereas less oxidized,
226 anhydrous mantle plume-derived magmas (*e.g.*, OIB and MORB) exhibit $D_V^{\text{ol/liq}} = 0.025 -$
227 0.10 .

228 Additional diagnostic features pointing to the origins of komatiites include estimates of
229 potential temperatures of inferred mantle sources and depths of melting initiation. To compare
230 mantle temperatures at various localities, McKenzie and Bickle (1988) proposed the concept
231 of a mantle potential temperature (T_p) as a point of reference. Mantle potential temperature is
232 the temperature that the solid adiabatically-convecting asthenospheric mantle would have had
233 at the surface if it ascended without undergoing melting. Mantle potential temperature
234 determines the depth of melting initiation (*e.g.*, Richter, 1988; Herzberg, 1992, 1995;

235 Herzberg et al., 2007), which, in turn, governs the style of mantle melting and melt
236 segregation (fractional versus batch). The depth of melting initiation and subsequent melt
237 segregation determines the chemical composition of the resultant komatiite melts, including
238 MgO contents. Pressures >8 GPa (240 km depth) stabilize majorite garnet relative to olivine
239 and pyroxene in the source (e.g., Ohtani, 1984; Herzberg and Ohtani, 1988). If the
240 temperature of a plume core is sufficiently high to initiate melting in the majorite garnet
241 stability field, the melting results in the formation of Al-depleted komatiitic melts with
242 subchondritic Al₂O₃/TiO₂ and Gd/Yb, provided the melt separated from the melting residue
243 while still in the majorite garnet stability field. By contrast, melting and melt segregation at
244 lower pressures, within the spinel lherzolite stability field, produces Al-undepleted komatiitic
245 magmas with chondritic Al₂O₃/TiO₂ and Gd/Yb (e.g., Green, 1975; Ohtani, 1984; Kato et al.,
246 1988; Herzberg, 1995).

247 **4. Which parts of the mantle do komatiites sample?**

248 In order to assess the extents of early mantle isotopic and chemical heterogeneities
249 sampled by komatiites, it is important to determine where in the mantle komatiites originate.
250 The location of komatiite magma generation is almost certainly not the same for all
251 komatiites, given the extent of chemical and isotopic heterogeneity inferred for their mantle
252 sources. This, in turn, requires assessment of diverse komatiite formation models.

253 Komatiites were most common during the Archean and may, during this eon, have been
254 the volumetrically second most significant constituent among volcanic rocks, comprising as
255 much as 25% of the entire volume of volcanic sequences, the rest being composed mostly of
256 basalts (e.g., Condie, 1975, 1981, 1994; deWit and Ashwal, 1997). Some of these basalts were
257 also derived from komatiites *via* fractional crystallization processes, while others were lower-
258 degree partial melts generated from the same sources as the spatially associated komatiites
259 (Arndt et al., 1977; Campbell et al., 1989; Condie, 2005). The abrupt decline in the abundance
260 of komatiites at the Archean-Proterozoic boundary, as well as the decrease in the MgO
261 contents of emplaced komatiite lavas, have been interpreted as evidence for a significant, up
262 to 300°C, secular cooling of the mantle over the course of Earth history (e.g., Bickle, 1982;
263 Nisbet et al., 1993; Herzberg et al., 2007; Herzberg and Gazel, 2009). Some authors have
264 linked this to a transition from drip to subduction tectonics (Campbell and Griffiths, 2014),
265 arguing that an increasing abundance of subducted slabs allowed for formation of the core-
266 enveloping D'' insulating layer, which they in turn associate with a step-like drop in maximum
267 komatiite magma MgO contents and mantle potential temperatures between 2.7 and 2.0 Ga.

268 The origin of komatiites has been a subject of studies for the past half century (*e.g.*,
269 Green, 1975, 1981; Allègre, 1982; Arndt et al., 1998, 2008; Parman et al., 2001, 2004; Berry
270 et al., 2008; Sobolev et al., 2016, 2019; Sossi et al., 2016; Asafov et al., 2018). A common
271 interpretation is that the parental magmas to komatiites were produced in unusually hot
272 upwellings of mantle material, termed mantle plumes (*e.g.*, Cawthorn, 1975; Campbell et al.,
273 1989; Griffith and Campbell, 1990; Richards et al., 1991; Loper, 1991; Herzberg, 1995;
274 Richard et al., 1996). The plumes most likely initiated at one of the two major thermal
275 boundary layers in the mantle, *i.e.*, either the core-mantle boundary (CMB) at 2900 km, or the
276 660 km discontinuity, with the ensuing rise driven by a buoyancy contrast between the less
277 dense, hot plume material and the cooler and denser surrounding mantle (Campbell and
278 Griffiths, 1990, 1992, 1993; Farnetani and Richards, 1995; Farnetani, 1997). The initially
279 solid mantle plume material was partially melted upon reaching shallower depths as a result
280 of decompression. Based on experimental data, Campbell et al. (1989) argued that komatiites
281 were produced in the hotter plume core containing mostly materials derived from near the
282 thermal boundary layer, whereas spatially associated basalts were generated in the cooler
283 plume head which, upon arrival at the surface, would have contained a substantial amount of
284 entrained upper mantle material. However, later studies (*e.g.*, Farnetani and Richards, 1995)
285 argued that such entrainment was unlikely to contribute significantly to the erupted melts.

286 Two major types of modern mantle plumes have been proposed based on the depth of
287 their initiation, determined using recent high-resolution seismic tomography imaging data
288 (*e.g.*, Courtillot et al., 2003; Montelli et al., 2004; He et al., 2015; Bao et al., 2022). The first
289 type is “primary”, or Morganian, plumes that are commonly thought to originate in the
290 deepest parts of the lower mantle, perhaps from seismically anomalous regions. Early
291 geophysical studies (*e.g.*, Dziewonski et al., 1977) identified seismically anomalous zones
292 along the core-mantle boundary, the so-called Large Low Shear-Wave Velocity Provinces
293 (LLSVP) and Ultra-Low Velocity Zones (ULVZ). The origin of these regions in the mantle is
294 debated. It has been proposed that LLSVPs may be stratified into primordial bottom domains
295 near the core-mantle boundary, often referred to as the D" layer, and mafic shallow domains
296 that extend from ~1100 to 2300 km depths (*e.g.*, Ballmer et al., 2016; Koppers et al., 2021).
297 These regions in the mantle may serve as nurseries for the majority of "primary" mantle
298 plumes (French and Romanovicz, 2015; Totsvik et al., 2016; Koppers et al., 2021). Ocean
299 island basalt systems that have been associated with this type of plume include Azores,
300 Canary, Coral Sea, Easter, Galapagos, Hawaii, Iceland, Samoa, and Tahiti (Courtillot et al.,
301 2003).

302 The “secondary” type, or Andersonian, plumes have been proposed to originate at the 660
303 km discontinuity and, hence, would be an upper mantle feature. Ocean island basalt systems
304 that have been associated with this type of plumes include Ascension, Caroline, McDonald,
305 and Pitcairn islands (Courtillot et al., 2003).

306 Considering the difficulties in determining even present-day mantle plume characteristics
307 (*e.g.*, Fletcher and Wyman, 2015, and references therein), it is not surprising that there are
308 few reliable estimates of Archean plume parameters (Arndt et al., 2008). This is due to the
309 fact that, unlike modern plumes, ancient plumes are extinct mantle features and, therefore,
310 cannot be examined by geophysical methods. Consequently, indirect approaches must be
311 taken, such as geological field observations. For example, the size of postulated plumes can
312 potentially be constrained by the lateral extent of contemporaneous magmatic activity within
313 a given region. Envisioned parental plume heads of up to 2500 km in diameter for large
314 systems, such as the Yilgarn Craton in Western Australia (Campbell and Hill, 1988; Mole et
315 al., 2014; Barnes and Van Kranendonk, 2014; Barnes et al., 2016), have been argued to be
316 indicative of plumes that originated at the CMB. Smaller plume heads, estimated to range
317 from 200 km to 300 km in diameter, and leading to less widespread volcanism, such as the
318 komatiite-basalt systems of the Pilbara Craton in Western Australia and the Superior Craton
319 in Canada (Arndt et al., 2001; Van Kranendonk, 2008; Hickman and Van Kranendonk, 2012;
320 Dostal and Mueller, 2013; Wyman, 2013, 2018, 2020), are likely to be more typical of upper
321 mantle plumes originated at the 660 km discontinuity.

322 Puchtel et al. (2009b, 2013, 2016a) calculated H₂O contents of <0.2 wt. % in the Pyke
323 Hill, Belingwe, Schapenburg, Komati, and Weltevreden komatiites, and concluded that their
324 parental magmas were formed under dry, high-temperature melting conditions. Similar
325 estimates of water content have been obtained for the Belingwe komatiites on the basis of the
326 oxidation state of iron in melt inclusions in olivine (*e.g.*, Berry et al., 2008). Thus, it is a
327 common assumption that most komatiites originated from dry, deep-seated mantle sources
328 (Arndt et al., 1998, 2008).

329 Consistent with the interpretation of an anhydrous, deep mantle origin for most
330 komatiites, Nicklas et al. (2018, 2019) concluded, on the basis of a global survey of
331 partitioning behavior of V between olivine and emplaced komatiitic and picritic melts, that
332 the redox states of a variety of komatiite and OIB sources, ranging in age from 3.48 Ga to
333 present day, were either similar to, or lower than, those of modern MORB.

334 Recent studies of komatiitic olivine melt inclusions (*e.g.*, Sobolev et al., 2016, 2019;
335 Asafov et al., 2018), while maintaining an anhydrous, deep mantle plume origin for

336 komatiites, have argued for relatively high water contents in some komatiite magmas, with
337 water being added to rising, dry plume material from a thin hydrous layer located at the top of
338 the mantle transition zone (MTZ), between the 410- and 660- km seismic discontinuities.
339 The origin of these seismic interfaces is attributed to solid- solid phase transitions from
340 olivine to wadsleyite and ringwoodite to perovskite+magnesiowüstite, respectively (*e.g.*, Bina
341 and Helffrich, 1994). The hydrous layer is predicted by Bercovici and Karato (2003) in their
342 MTZ water filter model to occur at the 410 km depth.

343 Alternatively, it has been argued that komatiites in general, and Komati lavas from the
344 Kaapvaal Craton in South Africa in particular, were produced in a special type of Archean
345 subduction environment *via* hydrous melting of the mantle at shallow depths and at
346 temperatures similar to, or only slightly higher than, those of the ambient upper mantle (*e.g.*,
347 Allègre, 1982; Grove et al., 1997; Parman et al., 1997, 2001, 2004). An important initial
348 condition of this hypothesis is the requirement that the Komati komatiites represent intrusive
349 bodies, since magmatic water escapes outgassing only under pressure (Grove et al., 1997).
350 According to the hydrous komatiite model of Parman et al. (1997, 2001), the presence of
351 water determined both the crystallization sequence and composition of the magmatic minerals
352 of the Komati komatiites. Parman et al. (1997) carried out a detailed experimental study
353 crystallizing material of komatiitic composition under both anhydrous and hydrous
354 conditions, paying particular attention to the composition of the crystallizing pyroxene. Using
355 the pyroxene compositions, these authors estimated that the original Komati komatiite magma
356 contained between 4 and 6 wt. % H₂O. Such a large amount of water would require the
357 temperature in the Komati source to be ~250°C lower than in anhydrous melting models. In
358 their follow-up review paper, Grove and Parman (2004) argued that the Archean mantle was
359 ≤100°C hotter than the modern mantle, hence, offering a view on the thermal evolution of the
360 Earth that contrasts with those that are based on the traditional assumption of a substantially
361 hotter Archean mantle (*e.g.*, Richter, 1985, 1988; Bickle, 1986; Nisbet et al., 1993; Herzberg
362 et al., 2007, 2010).

363 The summary of estimates of the mantle potential temperatures (T_p °C) for the sources of
364 the komatiite systems considered here, as well as the liquidus temperatures of the emplaced
365 komatiite magmas (T_{liq} °C) and depths of melting initiation in the respective mantle plumes
366 ($D_{melt\ init}$), are presented in **Table 1**. These estimates were generally derived from the studies
367 for the particular komatiite systems referenced in **Table 1** and updated here on the basis of the
368 more recent estimates of the emplaced komatiite lava compositions from Nicklas et al. (2018,
369 2019), where available, coupled with the previous and more recent mantle melting

370 parameterization models of McKenzie and Bickle (1988), Herzberg and O'Hara (2002),
371 Herzberg and Asimow (2008), and Herzberg and Gazel (2009).

372 **5. Chemical and isotopic data**

373 A summary of the available chemical and isotopic data for the komatiite systems
374 considered in this review are given in **Tables 1 and 2**.

375 **5.1. Emplaced lava compositions, mantle potential temperatures, and depths of melting**

376 Estimates of emplaced komatiite lava compositions (MgO_{liq}), their liquidus temperatures
377 ($T_{liq}^{\circ\text{C}}$), mantle potential temperatures ($T_p^{\circ\text{C}}$), and depths of mantle melting initiation (D_{melt}
378 $_{init}$) are listed in **Table 1**. The details of the methodology used for calculating these parameters
379 are provided in the **Electronic Supplement**.

380 The calculated depths of melting initiation range between 605 and 203 km, while liquidus
381 temperatures vary between 1606°C and 1498°C. There is an apparent tendency for a decrease
382 in depth of melting initiation between 3.6 and 2.0 Ga. This is also reflected in the ~100°C
383 decrease in mantle potential temperatures of komatiite sources from 1841 to 1748°C and a
384 corresponding decrease in MgO contents of emplaced komatiite lavas from ~31 to 25 wt.%
385 over the same period of time. Two exceptions are the Coonterunah and Kelly komatiite
386 systems that are less MgO-rich than the other early Archean systems. Therefore, the data
387 place the depths of onset of melting for all komatiite systems considered here within and
388 above the present-day MTZ and provide minimum estimates for the depths of mantle plume
389 initiation. In the following sections, more clues, as to which parts of the mantle the studied
390 komatiite systems sampled (*i.e.*, depths of mantle plume initiation, $D_{plume\ init}$), will be
391 considered using the available geochemical and isotopic data (**Table 2**).

392 **5.2. Chemical composition and isotopic systematics**

393 **5.2.1. Major and lithophile trace elements**

394 The petrologically most important chemical element in komatiites, along with Mg, is Al;
395 as a result, variations in Al_2O_3 , and its rare earth element (REE) behavioral equivalent Yb,
396 form an integral part of all komatiite classifications (*e.g.*, Nesbitt et al., 1979; Jahn et al.,
397 1982). The komatiite systems reviewed here can be subdivided into two major petrological
398 groups on the basis of their Al_2O_3 and Yb contents at a given MgO content, namely Al-
399 depleted/enriched and Al-undepleted. The majority of the early Archean komatiite systems,
400 including the Schapenburg, Komati, Weltevreden, Ruth Well, and Regal systems, belong to
401 the Al-depleted/enriched type of lavas characterized by either sub- or supra-chondritic Al/Ti

402 and Gd/Yb ratios (**Table 1**). Exceptions are the Coonterunah and Kelly systems that belong to
403 the Al-undepleted type of lavas with $\text{Al}_2\text{O}_3/\text{TiO}_2 = 22.8$ and 23.1 and $\text{Gd}/\text{Yb}_N = 0.96$ and 0.91 ,
404 respectively (where N denotes BSE-normalized values of Hofmann, 1988). By contrast, the
405 majority of the late Archean komatiite systems, including the Pyke Hill-Alexo, Belingwe,
406 Vetreny, and Lapland systems, belong to the Al-undepleted type of lavas characterized by
407 generally chondritic Al/Ti and Gd/Yb ratios. The Boston Creek (Puchtel et al., 2018) and
408 Kostomuksha komatiites (Puchtel et al., 1998), with $\text{Al}_2\text{O}_3/\text{TiO}_2 = 5.1$ and 17.2 and $\text{Gd}/\text{Yb}_N =$
409 2.0 and 1.2 , respectively, are notable exceptions. Although the Lapland komatiites have low
410 $\text{Al}_2\text{O}_3/\text{TiO}_2 = 13.2$ and high $\text{Gd}/\text{Yb}_N = 1.5$, these features have been shown to be the result of
411 enrichment in Ti and middle REE (MREE), rather than depletions in Al and heavy REE
412 (Puchtel et al., 2020).

413 Owing to their high liquidus temperatures and low viscosities during their passage through
414 and/or emplacement onto the continental crust, komatiitic liquids are highly susceptible to
415 contamination by upper crustal rocks (Huppert et al., 1984; Huppert and Sparks, 1985).
416 Archean upper crustal rocks are strongly enriched in Th, U, and light REE (LREE), and
417 relatively depleted in Nb (Rudnick and Gao, 2014) as a result of subduction zone processes
418 involving retention of Nb-rich rutile in the eclogitic residue (Foley et al., 2000; Rudnick et al.,
419 2000). Because of that, upper crustal rocks are characterized by negative Nb anomalies
420 relative to elements with similar incompatibility during mantle melting (Th and La), *i.e.*, their
421 $\text{Nb}/\text{Nb}^* \ll 1.0$ (where $\text{Nb}/\text{Nb}^* = \text{Nb}_N/\sqrt{(\text{Th}_N \times \text{La}_N)}$). By contrast, primary komatiitic magmas
422 are expected to have $\text{Nb}/\text{Nb}^* \geq 1.0$ (*e.g.*, Hofmann et al., 1986; Jochum et al., 1991). Due to
423 large differences in highly incompatible lithophile trace element concentrations between the
424 upper crust and komatiitic melts, crustal contamination usually leads to sharp increases in the
425 abundances of Th, U, W, and LREE, but much less so of Nb, in the hybrid melts, which
426 acquire negative Nb anomalies in the process. Hence, the Nb/Nb^* ratio represents a
427 diagnostic tool that has been utilized to evaluate and mathematically correct for the effects of
428 crustal contamination (*e.g.*, Puchtel et al., 2016b, 2020, 2022).

429 The majority of the komatiite systems considered here are variably depleted in highly
430 incompatible lithophile trace elements, with the La/Sm_N ratios ranging between 0.14 (the 2.05
431 Ga Lapland system) and 0.97 (the 3.48 Ga Komati system). The 2.72 Ga Boston Creek lavas
432 are the sole exception ($\text{La}/\text{Sm}_N = 1.9$). Furthermore, all komatiite systems examined here have
433 $\text{Nb}/\text{Nb}^* \geq 1.0$, reflecting either a lack of crustal contamination, or that the effects of crustal
434 contamination have been mathematically corrected for, as indicated in **Table 2**. The details of
435 the correction protocol are provided in the **Electronic Supplement**.

436 5.2.2. Isotopic systems of the lithophile elements

437 **Table 2** presents the initial $\epsilon^{143}\text{Nd}$ and $\epsilon^{176}\text{Hf}$ values (defined as the deviation in parts per
438 10,000 of initial $^{143}\text{Nd}/^{144}\text{Nd}$ and $^{176}\text{Hf}/^{177}\text{Hf}$ in a given sample from those in the chondritic
439 reference at the time of lava emplacement) for each komatiite system, which represent
440 compositions of the respective komatiite-basalt mantle sources. These values were derived
441 from the respective Sm-Nd and Lu-Hf isochrons obtained for each komatiite-basalt system
442 and, where appropriate, corrected for crustal contamination, as indicated in **Table 2**, using the
443 lithophile trace element systematics discussed in the previous section. The resultant initial
444 $\epsilon^{143}\text{Nd}$ and $\epsilon^{176}\text{Hf}$ values are all positive, ranging between +0.46 and +4.9 and +1.7 and +10.2,
445 respectively, indicating that all the komatiite-basalt systems considered were derived from
446 mantle sources with time-integrated supra-chondritic Sm/Nd and Lu/Hf.

447 By contrast, Blichert-Toft et al. (2015) reported ^{143}Nd and ^{176}Hf data for a suite of heavily
448 altered Komati drill core samples from several flows. That study produced a much greater
449 scatter, and both positive and negative initial $\epsilon^{143}\text{Nd}$ and $\epsilon^{176}\text{Hf}$ values for whole-rock
450 samples, than for the initial values obtained from the individual Sm-Nd and Lu-Hf isochrons
451 for the remarkably well preserved Komati komatiite samples from the Puchtel et al. (2013)
452 study reported in **Table 2**. Blichert-Toft et al. (2015) also reported data for variably leached
453 clinopyroxene separates, which yielded initial $\epsilon^{143}\text{Nd}$ and $\epsilon^{176}\text{Hf}$ values of -2 and $+5$,
454 respectively. This may indicate more complex magmatic and/or alteration history of the
455 samples studied by Blichert-Toft et al. (2015) than for the Komati samples studied by Puchtel
456 et al. (2013).

457 The time-integrated Sm/Nd and Lu/Hf ratios in the mantle sources of komatiite systems
458 derived from the respective Sm-Nd and Lu-Hf isochron sets are plotted in **Fig. 1**. These ratios
459 were calculated by assuming the minimum-degree fractionation from either the chondritic
460 values or the values defined by the combined $^{142,143}\text{Nd}$ systematics (where available) to those
461 required to bring the $\epsilon^{143}\text{Nd}$ and $\epsilon^{176}\text{Hf}$ to the measured initial $\epsilon^{143}\text{Nd}$ and $\epsilon^{176}\text{Hf}$ of the
462 respective mantle sources by the time of komatiite-basalt system formation. All of these
463 komatiite systems were derived from mantle sources having time-integrated $^{147}\text{Sm}/^{144}\text{Nd}$ and
464 $^{176}\text{Lu}/^{177}\text{Hf}$ ratios between those of CHUR and DMM. An important feature of the data is that,
465 while all komatiite-basalt systems younger than ~ 3.0 Ga follow the terrestrial Nd-Hf mantle
466 evolution array, indicating long-term “coupled”, or congruent, behavior of the Nd and Hf
467 isotope systematics in the post-3.0 Ga komatiite mantle sources, the komatiite systems older
468 than ~ 3.0 Ga (with the exception of the Pilbara Craton komatiite-basalt systems) plot above

469 the terrestrial evolution curve, indicating long-term “decoupled”, or incongruent, behavior of
470 the Nd and Hf isotope systematics in their mantle sources. All these early Archean systems
471 are from the Kaapvaal Craton in South Africa. The processes that might have been
472 responsible for producing such Nd-Hf isotope decoupling are discussed in **Section 6.1**.

473 Relatively limited ^{142}Nd data are available for the komatiite systems reviewed in this
474 study (**Table 2**). The komatiite systems, for which these data are available, mostly exhibit
475 $\mu^{142}\text{Nd}$ values indistinguishable from the standard reference value, where $\mu^{142}\text{Nd}$ is defined as
476 the deviation in parts per million of $^{142}\text{Nd}/^{144}\text{Nd}$ in a given komatiite sample from the
477 laboratory reference materials (AMES or JNdi), which are considered to represent the
478 composition of the modern BSE. The Schapenburg and Komati komatiite systems have small
479 $\mu^{142}\text{Nd}$ deficits, averaging -5.0 ± 2.8 (2SD; Puchtel et al., 2016a) and -4.0 ± 4.1 (2SD; Boyet et
480 al., 2021), respectively.

481 5.2.3. Tungsten abundance and isotope systematics

482 The ^{182}W data are reported as $\mu^{182}\text{W}$, which is the deviation in parts per million of
483 $^{182}\text{W}/^{184}\text{W}$ in a given sample from that of the in-house *Alfa Aesar* laboratory W reference
484 material. The $\mu^{182}\text{W}$ value of 0 for the reference material is considered to represent the
485 composition of the BSE. This is based on the observation that a limited number of data for
486 modern MORB (Willbold et al., 2011; Rizo et al., 2016; Mundl et al., 2017), numerous data
487 for OIB with low $^3\text{He}/^4\text{He}$ (Mundl-Petermeier et al., 2020), and data for Proterozoic and
488 Phanerozoic glacial diamictites and granites (Mundl et al., 2018; Nakanishi et al., 2021) are
489 all characterized by $\mu^{182}\text{W}$ values of ~ 0 .

490 In contrast to ^{142}Nd , the majority of komatiite systems examined here exhibit either
491 positive (all the Pilbara, the Kostomuksha, and the Boston Creek komatiite systems), or
492 negative (the Schapenburg and Lapland komatiite systems) ^{182}W anomalies, with only the
493 Komati and Vetreny komatiite systems lacking an ^{182}W anomaly.

494 The behavior of W during magmatic processes is governed mainly by the redox state of
495 the magmatic system in question (Newsom et al., 1996; Arevalo and McDonough, 2008;
496 König et al., 2011). Under reducing conditions, such as those that likely existed during
497 metallic core formation, W behaves as a moderately siderophile element (MSE),
498 concentrating largely in the metal relative to the silicate melt. During mantle melting under
499 relatively oxidizing conditions in the absence of a metal phase, such as typical of the modern
500 upper mantle, W behaves as a highly incompatible element, concentrating in the silicate melt
501 relative to the melting residue, with a degree of incompatibility similar to that of Th and U.

502 The Archean mantle was recently shown to be only slightly (by ~ 1.3 Δ FMQ log units) less
503 oxidized than, whereas the Proterozoic mantle was found to be similarly oxidized to, the
504 modern mantle (Nicklas et al., 2018, 2019). Therefore, it is expected that during the mantle
505 melting that produced the komatiite-basalt systems considered in this review, W behaved
506 similarly to Th and U and, hence, that in undisturbed komatiite-basalt systems, $W/Th \approx$
507 W/Th_{BSE} , where $W/Th_{BSE} = 0.19$ (McDonough and Sun, 1995). Indeed, in modern OIB and
508 MORB, for which W is characterized by a primary, magmatic distribution, the W/Th ratios
509 are similar to the BSE value of 0.19 (*e.g.*, König et al., 2008, 2011; Jenner and O'Neill, 2012).
510 Modern island arc lavas, on the other hand, show uniformly elevated W/Th ratios relative to
511 the BSE value attributed to various contributions of fluid-borne W to the arc mantle from the
512 subducted slab (König et al., 2008, 2011). Although some komatiite systems (*e.g.*, the
513 Komati, Vetreny, and Lapland systems) have average W/Th ratios within the uncertainty
514 limits of the BSE value, and in that respect are similar to modern OIB and MORB, others are
515 variably either enriched (most common) or depleted in W over Th (**Table 1**). In addition, the
516 lack of correlation between W concentrations and indices of magmatic differentiation, such as
517 MgO content, indicates either W mobility after lava emplacement in most komatiite-basalt
518 systems (*e.g.*, Touboul et al., 2012; Puchtel et al., 2016a, 2018, 2020, 2022; Tusch et al.,
519 2021) or involvement of a yet-unaccounted-for magmatic process.

520 The issue of the origin of W in Archean and Proterozoic komatiite-basalt systems is,
521 therefore, controversial. Recent studies have shown that W abundance and isotopic
522 systematics can be affected by crustal contamination, hydrothermal alteration, and
523 metamorphism (*e.g.*, Touboul et al., 2014; Liu et al., 2016; Puchtel et al., 2016a,b, 2018,
524 2020, 2022; Tusch et al., 2019, 2021), resulting mostly in W enrichments relative to immobile
525 trace elements with similar degree of incompatibility, *e.g.*, Th. Two mechanisms, based on the
526 origin of W, have been proposed to account for the elevated W/Th ratios in komatiites and
527 basalts. The first mechanism advocates derivation of W from an endogenous source, whereby
528 W originated within the komatiite-basalt system. The second mechanism assumes an
529 exogeneous origin, whereby W is introduced into the komatiite-basalt systems from
530 genetically unrelated sources. We address these two mechanisms in more detail below.

531 **Endogenous** origin of W in komatiite-basalt systems have been advocated for the
532 Kostomuksha (Touboul et al., 2012), Schapenburg (Puchtel et al., 2016a), Boston Creek
533 (Puchtel et al., 2018), and the Coonterunah and Kelly systems (Puchtel et al., 2022). In case of
534 the two Pilbara komatiite-basalt systems, the komatiites are characterized by high W/Th
535 ratios, whereas the basalts, that are spatially associated and genetically related to komatiites,

536 are depleted to only slightly enriched in W relative to Th. In these komatiite-basalt systems,
537 and also in many other Archean komatiite-basalt systems around the globe, komatiites
538 constitute 5-10% of the sequence by volume, the rest consisting of basalts (Condie, 1981; de
539 Wit and Ashwal, 1997; Smithies et al., 2007). Originally, basalts contain significantly higher
540 abundances of all highly incompatible trace elements, including W, compared to komatiites.
541 During secondary alteration, komatiites are turned into serpentinites, whereas basalts are
542 transformed into amphibolites. Serpentine is a major host for W and can accommodate several
543 orders of magnitude more W than the precursor mineral olivine, whereas W shows a lower
544 affinity for amphibole (Liu et al., 2016). Therefore, if W is mobilized and redistributed within
545 a komatiite-basalt volcanic sequence, it is expected to be preferentially captured by komatiites
546 during serpentinization of the primary mineral assemblage. The effect of this relative W
547 enrichment is amplified by the low trace element concentrations in komatiites, resulting in
548 high W/Th ratios (Puchtel et al., 2022).

549 In the case of the Boston Creek system, samples collected across a differentiated lava flow
550 have remarkably uniform ^{182}W compositions, but show a wide range of W/Th ratios, from
551 enriched in the lower olivine cumulate part to BSE-like in the low-Mg basaltic layer, with
552 strong inverse correlation between MgO content (*i.e.*, amount of modal serpentine) and W/Th
553 (Puchtel et al., 2018). The above features were argued by these authors to reflect an
554 endogenous nature of W in the Boston Creek system, with isotopically uniform W having
555 been redistributed within the lava flow and hence reflecting the primary magmatic signature.

556 The above scenarios have been argued to be applicable to several other komatiite-basalt
557 systems, including the Kostomuksha (Touboul et al., 2012), and the Schapenburg (Puchtel et
558 al., 2016a) systems.

559 **Exogenous** W in the komatiite-basalt systems considered in this review has been shown
560 to be derived from upper crustal rocks either during passage of mafic-ultramafic magmas
561 through the continental crust *en route* to the surface (the Vetreny and Lapland systems:
562 Puchtel et al., 2016b, 2020), or as a result of interaction with upper crustal rocks during both
563 the magmatic stage *via* crustal contamination, and the post-magmatic stage *via* fluid-rock
564 interaction (the Ruth Well and Regal systems: Puchtel et al., 2022).

565 Due to the generally high W abundances in upper crustal rocks (*e.g.*, Rudnick and Gao,
566 2014), crustal contamination has the potential to modify both W concentrations and ^{182}W
567 compositions of komatiite-basalt magmas during ascent, as has been argued to be the case for
568 the Vetreny, Lapland, Ruth Well, and Regal systems on the basis of studies of lithophile trace
569 element systematics (Puchtel et al., 2016b, 2020, 2022). In order to mathematically correct for

570 the effects of magmatic crustal contamination, these authors performed un-mixing
571 calculations using the degrees of crustal contamination estimated on the basis of trace element
572 systematics and assumptions about the W isotopic composition and abundances in the most
573 likely potential crustal contaminant.

574 Being a highly fluid-mobile element (*e.g.*, König et al., 2008), W can be transferred from
575 spatially associated granitic rocks to komatiite-basalt sequences *via* W-rich fluids. Such a
576 mechanism has been proposed to affect the W isotopic composition of the Ruth Well and
577 Regal komatiite systems on the basis of the high W/Th ratios in both komatiites and basalts
578 and the similarity in ^{182}W compositions between the most W-enriched komatiites and the
579 spatially associated 3.5 Ga tonalites of the Pilbara Craton (Puchtel et al., 2022). These authors
580 were able to evaluate the W isotopic composition of the primary lavas by assuming that their
581 ^{182}W composition was similar to that of the least affected basalts from Tusch et al. (2021) and
582 Puchtel et al. (2022), with W/Th ratios closest to that in the BSE estimate.

583 After corrections have been applied where needed, the $\mu^{182}\text{W}$ values reported in **Table 2**
584 are considered to reflect those in the sources of the respective komatiite-basalt systems.

585 **5.3. Os isotope systematics and HSE abundances**

586 The $^{186,187}\text{Os}$ data are listed in **Table 2** and plotted in **Fig. 2**. The majority of the komatiite
587 systems have $\gamma^{187}\text{Os}$ values (defined as percent deviation of the $^{187}\text{Os}/^{188}\text{Os}$ ratio in a given
588 komatiite sample from a chondritic reference value at the time of komatiite lava
589 emplacement) plotting within the chondritic range, indicating evolution of their mantle
590 sources with time-integrated near-chondritic Re/Os ratios. The only exceptions are the
591 Schapenburg and Kostomuksha komatiite systems that have more radiogenic $\gamma^{187}\text{Os}$ values of
592 +3.7 and +2.5, respectively, implying that their mantle sources evolved with long-term
593 slightly suprachondritic Re/Os.

594 The limited ^{186}Os data available indicate that, out of the seven systems studied, only three
595 (the Pyke Hill, Belingwe, and Vetreny systems) have initial $\mu^{186}\text{Os}$ values (defined as the
596 deviation in ppm of the $^{186}\text{Os}/^{188}\text{Os}$ ratio in a given komatiite sample from a chondritic
597 reference value at the time of the komatiite lava emplacement) that plot within the chondritic
598 range, indicating that their mantle sources evolved with time-integrated near-chondritic Pt/Os
599 ratios. The other four komatiite systems have non-chondritic initial $\mu^{186}\text{Os}$ values and, thus,
600 evolved with either suprachondritic (the Weltevreden, Kostomuksha, and Lapland systems) or
601 subchondritic (the Komati system) time-integrated Pt/Os ratios. Importantly, among the
602 mantle sources with non-chondritic Re-Os and/or Pt-Os systematics, only in the Kostomuksha

603 komatiite source are these isotope systematics coupled, whereas in the others, they are
604 decoupled.

605 The total HSE abundances in the komatiite mantle sources have been calculated using the
606 bootstrap method of Puchtel et al. (2004b) that was refined in subsequent studies (*e.g.*,
607 Puchtel et al., 2020, 2022). This method combines the $^{186,187}\text{Os}$ isotopic and HSE abundance
608 data for a suite of komatiitic lavas derived from a common primary magma and related by
609 fractional crystallization of olivine after lava emplacement. The details of the analytical
610 protocol used in the bootstrap method of Puchtel et al. (2004b) are provided in the **Electronic**
611 **Supplement**.

612 The total HSE abundances in the sources of the komatiite systems considered in this
613 review, calculated as percent of those in the estimates of the modern BSE of Becker et al.
614 (2006), are presented in **Table 2** and plotted as a function of their age in **Fig. 3**. The
615 calculated total HSE abundances range from ~30% in the 3.55 Ga Schapenburg and 3.53 Ga
616 Coonterunah systems to ~120% in the 2.05 Ga Lapland system. Overall, the entire dataset,
617 except for the obvious outliers (*e.g.*, the 2.72 Ga Boston Creek, 2.69 Ga Belingwe, and 2.41
618 Ga Vetreny systems), exhibits a broad trend of increasing HSE abundances in the komatiite
619 mantle sources with time. This trend is generally consistent with that defined by the much
620 more scattered data of Maier et al. (2009).

621 In the following sections, the data reviewed in **Section 5** will be discussed in light of the
622 possible mechanisms responsible for creating these early chemical and isotopic
623 heterogeneities in the mantle.

624 **6. Mechanisms for creating early mantle heterogeneities**

625 **6.1. Primordial differentiation of the mantle**

626 Crystallization of a primordial magma ocean(s) is one possible mechanism for generating
627 early chemical and isotopic heterogeneities in the mantle (*e.g.*, Boyet et al., 2003, 2021; Boyet
628 and Carlson, 2005, 2006; Caro et al., 2005, 2017; Brown et al., 2014; Puchtel et al., 2016a;
629 Byerly et al., 2017; Morino et al., 2017). Periodic magma oceans are likely a direct
630 consequence of planetary growth due to gravitational energy release from core formation and
631 high-energy collisions during final stages of accretion (*e.g.*, Tonks and Melosh, 1993; Bottke
632 et al., 2010; Rubie et al., 2011). Crystallization of a magma ocean results in stratification
633 controlled by fractionation of mineral assemblages, the composition of which depends on the
634 depth of the magma ocean and the composition of the melted domain. Some studies have
635 argued for occasional, near-complete melting of the silicate Earth, such as may have occurred

636 during the putative giant impact that led to formation of the Moon (Rubie et al., 2011; Canup,
637 2012; Elkins-Tanton, 2012; Young et al., 2016). The pressures and temperatures near the
638 bottom of such a magma ocean would have stabilized bridgmanite (Mg-perovskite) and Ca-
639 perovskite (Kato et al., 1988; Abe, 1997; Walter et al., 2004). Because most trace elements
640 are variably compatible in Ca-perovskite, with the degree of compatibility decreasing in the
641 order Lu>Hf>Sm>Nd (Corgne et al., 2005), the presence of Ca-perovskite in the fractionating
642 assemblage would result in stronger fractionation of Lu/Hf relative to Sm/Nd than that
643 observed under upper mantle conditions. Over time, this would result in Nd-Hf isotopic
644 decoupling in the mantle domains derived from magma ocean differentiation products,
645 relative to the coupling of these two isotope systems observed in the sources of modern
646 MORB and most OIB, which together define the modern Nd-Hf mantle array, or terrestrial
647 evolution curve (e.g., Salters and White, 1998).

648 The Nd-Hf mantle array owes its origin to the coupled, or congruent, Nd-Hf isotope
649 systematics of most terrestrial rocks that arise from similar partitioning behavior of the parent
650 (^{147}Sm , ^{176}Lu) and daughter (^{143}Nd , ^{176}Hf) isotopes of the Sm-Nd and Lu-Hf systems during
651 upper mantle differentiation and crust-forming processes (e.g., Patchett et al., 1981; Salters
652 and White, 1998; Vervoort and Blichert-Toft, 1999; Vervoort et al., 1999, 2000). During
653 mantle melting, both parent isotopes are less incompatible with the melt fraction than the
654 daughter isotopes, which results in higher Sm/Nd and Lu/Hf ratios in the melting residue
655 compared to the melt; over time, the residual mantle evolves to more radiogenic Nd and Hf
656 isotopic compositions than the extracted melts. Both isotope systems are lithophile, refractory,
657 insensitive to redox conditions, and largely immobile during alteration and metamorphism.
658 These properties make them useful for investigating the interplay between the formation and
659 recycling of oceanic and continental crust in driving the geochemical evolution of the mantle.

660 The decoupling of the Nd and Hf isotope systematics (and, thus, deviation from the
661 terrestrial Nd-Hf array) in the early Archean komatiite-basalt systems from the Kaapvaal
662 Craton, such as Schapenburg, Weltevreden, and Komati, have been interpreted to reflect the
663 involvement of primordial magma ocean processes.

664 Based on the combined $^{142,143}\text{Nd}$ and ^{176}Hf systematics, Puchtel et al. (2013) developed a
665 model of formation of the mantle silicate reservoirs that gave rise to the Komati and
666 Weltevreden komatiites *via* crystallization of a primordial magma ocean. According to their
667 model, during magma ocean differentiation, the lower three quarters of the magma column
668 (from depths of ~2900 to ~700 km) were largely dominated by bridgmanite, with subordinate
669 amounts of ferropericlase and Ca-perovskite, Ca-Pv (Trønnes and Frost, 2002; Ito et al., 2004;

670 Caro et al., 2005; Elkins-Tanton, 2008). Puchtel et al. (2013) used an equilibrium
671 crystallization model based on the high-pressure and -temperature partitioning studies of
672 Corgne and Wood (2002; 2004), Corgne et al. (2005), Liebske et al. (2005), and Walter et al.
673 (2004), and assumed a completely molten mantle with a composition corresponding to that of
674 the early depleted reservoir (EDR) of Boyet and Carlson (2006) that crystallized within the
675 first 150 Ma of the Solar System history, i.e., by 4400 Ma.

676 Since the study of Puchtel et al. (2013) has been published, the EDR model of Boyet et al.
677 (2006) has been proven untenable. This model was based on the data available at the time that
678 the accessible Earth has a greater $^{142}\text{Nd}/^{144}\text{Nd}$ ratio than chondrites (Carlson et al., 2007). This
679 ^{142}Nd difference required a higher-than-chondritic Sm/Nd ratio for the accessible Earth. This
680 ratio must have been acquired during global silicate differentiation within the first 30 million
681 years of Solar System formation (Boyet and Carlson, 2006) and implied the formation of a
682 complementary ^{142}Nd -depleted reservoir that is either hidden in the deep Earth, or lost to
683 space by impact erosion (Caro et al., 2008). However, Burkhardt et al. (2016) showed that,
684 compared to chondrites, Earth's building blocks were enriched in ^{142}Nd that was produced by
685 the s-process of nucleosynthesis, which leads to higher $^{142}\text{Nd}/^{144}\text{Nd}$ ratios. After these authors
686 corrected for this effect, the ^{142}Nd composition of chondrites and the accessible Earth were
687 shown to be indistinguishable. The results of Burkhardt et al. (2016), therefore, obviate the
688 need for a hidden-reservoir or ^{142}Nd -superchondritic Earth models and imply a chondritic
689 Sm/Nd ratio for the BSE.

690 In view of the new data of Burkhardt et al. (2016), we have modified the model of Puchtel
691 et al. (2013), as illustrated in **Fig. 4**; the methodology used in these model calculations are
692 available as an **Electronic Supplement**. The composition of the primordial magma ocean,
693 unlike in our previous model, is now represented by that of the chondritic uniform reservoir
694 (CHUR).

695 **Figure 4** shows the time-integrated $^{147}\text{Sm}/^{144}\text{Nd}$ and $^{176}\text{Lu}/^{177}\text{Hf}$ ratios in the sources of
696 the Komati and Weltevreden komatiite systems formed as a result of the 4400 Ma magma
697 ocean differentiation and crystallization event specified above, depending on the relative
698 proportions of fractionating bridgmanite and Ca-Pv. The upper panel of the diagram
699 represents aggregate compositions of the magma ocean cumulates, while the lower panel
700 represents the compositions of the residual liquids. As mentioned in the previous model, the
701 contrasting partitioning behavior of Lu and Hf between bridgmanite and Ca-Pv results in
702 differentiation trends that are highly affected by the relative proportions of these two phases.
703 According to this model, the Komati and Weltevreden mantle domains represent solidification

704 products of a bridgmanite-Ca-Pv cumulate that was derived from ~20% and 12%
705 accumulation of a bridgmanite:Ca-Pv assemblage in the proportions of 93:7 and 80:20,
706 respectively. These proportions and the degrees of magma ocean crystallization are within the
707 range of those envisaged for lower mantle conditions during the Hadean (*e.g.*, Caro et al.,
708 2005). If the modified model of Puchtel et al. (2013) presented here is correct, the mantle
709 plumes that gave rise to the Komati and Weltevreden komatiites must have originated in the
710 lower mantle (**Table 1**).

711 Boyet et al. (2021) obtained a slightly negative average $\mu^{142}\text{Nd}$ value of -4.0 ± 4.1 for a set
712 of Komati drill core samples. As noted above, that study combined their ^{142}Nd results with the
713 ^{143}Nd and ^{176}Hf data of Blichert-Toft et al. (2015) for clinopyroxene separates from the same
714 rocks. In order to explain the negative $\mu^{142}\text{Nd}$ and $\epsilon^{143}\text{Nd}$ values and the corresponding
715 positive $\epsilon^{176}\text{Hf}$ value, Boyet et al. (2021) proposed a four-stage model for the formation of
716 these lavas, whereby the negative $\mu^{142}\text{Nd}$ value and low Hf/Sm ratios developed during the
717 crystallization of a deep magma ocean soon after Earth accretion. The material that ultimately
718 became the source of the komatiites was a residual liquid produced by 50% crystallization of
719 a bridgmanite/ferropericlase/Ca-Pv mineral assemblage in the proportions 79:16:5, which
720 resulted in decoupling of the Nd and Hf isotope systematics. Thus, the model of Boyet et al.
721 (2021) also supports a lower mantle origin for the plume that gave rise to the Komati
722 komatiites.

723 Metal-silicate fractionation processes operating at the high temperatures and pressures
724 characterizing the first ~60 Ma of Solar System history at the base of an early transient
725 magma ocean, or in a partially molten zone at or near the core-mantle boundary (Labrosse et
726 al., 2007), while ^{182}Hf was still extant, have also been argued to be capable of generating
727 coupled ^{182}W and $^{186,187}\text{Os}$ heterogeneities in the mantle (Touboul et al., 2012). To explain the
728 enriched ^{182}W and $^{186,187}\text{Os}$ compositions of the Kostomuksha komatiite system, Touboul et
729 al. (2012) envisioned a lower mantle magma ocean reservoir where silicate melt could
730 potentially equilibrate with metal that represented either the growing core or the metal passing
731 through the molten region on its way to the core. This model is based on experimental data of
732 substantially reduced metal-silicate partitioning for Re and Pt, relative to Os, at high
733 temperatures and pressures (Righter and Drake, 1997; Cottrell and Walker, 2006; Fortenfant
734 et al., 2006; Yokoyama et al., 2009; Brenan and McDonough, 2009), and on the more
735 siderophile behavior of W under the somewhat more reducing conditions that likely existed in
736 the lower mantle during core formation compared to the present-day upper mantle (Wade and

737 Wood, 2005). The model of Touboul et al. (2012) requires the long-term survival of some
738 portion of the mantle in which HSE and MSE were set by high-temperature and -pressure
739 metal-silicate partitioning under reducing conditions. In order to achieve the $^{186, 187}\text{Os}$ and
740 ^{182}W isotopic and elemental characteristics of the Kostomuksha komatiite source, Touboul et
741 al. (2012) envisioned a mantle plume tapping this reservoir and mixing material from it with
742 overlying mantle characterized by Os isotopic compositions and HSE concentrations similar
743 to those in estimates of the BSE of Meisel et al. (2001) and Becker et al. (2006), in the
744 proportions of ~1:1 (**Fig. 5**). If the model of Touboul et al. (2012) is correct, it implies that the
745 plume, which gave rise to the Kostomuksha komatiites, originated in the lowermost mantle.

746 Isotopic heterogeneities involving the HSE-based isotopic systems have also been argued
747 to be related to primordial magma ocean crystallization processes by Puchtel et al. (2014) in
748 their study of the HSE abundances and $^{186, 187}\text{Os}$ compositions of the Komati and Weltevreden
749 komatiite systems considered above. These authors used the experimental partitioning data of
750 Borisov and Palme (1997) and Mallmann and O'Neill (2007) indicating that under the highly
751 reducing conditions that may have existed during crystallization of a primordial magma ocean
752 immediately following the main stage of core formation (Frost et al., 2008), solubility of Pt in
753 silicate melts, unlike the other HSE, may have been low and Pt, hence, would have had a
754 strong tendency to form alloys. Fractionation and subsequent heterogeneous dispersal of Pt
755 alloys within the mantle could have resulted in the formation of both Pt-enriched and -
756 depleted domains. These would then have evolved with supra- and subchondritic Pt/Os ratios,
757 respectively, which over time would have resulted in the decoupling of the ^{186}Os and ^{187}Os
758 systems in these domains (Puchtel et al., 2014).

759 A model of silicate-silicate fractionation during primordial mantle magma ocean
760 crystallization, involving early removal of bridgmanite and Ca-Pv, was also proposed by
761 Puchtel et al. (2016a) to explain the coupled ^{182}W , $^{142,143}\text{Nd}$, and ^{176}Hf isotope systematics of
762 the Schapenburg komatiite source. In their model, the authors recognized that crystal-liquid
763 fractionation in a purely silicate system of a global primordial magma ocean would lead to
764 high Hf/W, Sm/Nd, and Lu/Hf in early-formed cumulates and low Hf/W, Sm/Nd, and Lu/Hf
765 in the residual liquid. If these fractionation processes occurred while ^{182}Hf and ^{146}Sm were
766 still extant, the residual silicate liquid would have developed a coupled deficit in ^{182}W and
767 ^{142}Nd , compared to the ambient mantle, which is what has been observed in the 3.55 Ga
768 Schapenburg komatiites. If the model of Puchtel et al. (2016a) is applicable, it places the
769 mantle domain that served as the sources for the Schapenburg mantle plume in the lowermost
770 mantle.

771 **6.2. Late accretion**

772 The term “late veneer” was first introduced by Turekian and Clark (1969) and later
773 elaborated on by Chou et al. (1978; 1983) to explain the excess of HSE abundances in the
774 terrestrial mantle compared to what would otherwise be expected after core formation on the
775 basis of the low pressure and -temperature metal-silicate experimental partitioning data
776 available at the time (*e.g.*, Kimura et al., 1974). Late accretion is defined as the accretion of
777 0.5-1% (Walker, 2009) of Earth's mass of a chondritic component after cessation of core
778 formation. In earlier studies, it was assumed that this chondritic component was added to the
779 surface of the Earth in the form of relatively small objects to create a thin layer initially
780 coating the entire planet (thus the term “veneer”). It has also been proposed that a slow
781 downward mixing of this putative thin layer into the mantle was responsible for the apparent
782 trend of increasing HSE abundances in Archean komatiites over time (Maier et al., 2009).
783 Studies by Bottke et al. (2002, 2007), however, have concluded that it is unlikely that late
784 accretion in the form of small objects could have achieved an Earth/Moon late accretionary
785 mass influx ratio of ~1200 required on the basis of the Re-Os isotopic and HSE abundance
786 studies of terrestrial (Meisel et al., 2001; Becker et al., 2006; Fischer-Gödde et al., 2011) and
787 lunar (Walker et al., 2004, 2014; Day et al., 2007; Day and Walker, 2015) samples. Bottke et
788 al. (2010) proposed that late accretion to Earth was dominated by addition of a few large
789 projectiles, with a mean diameter of ~2500 km, and that HSE were added to the Moon
790 through the accretion of much smaller bodies, ~250 km in diameter. Projectiles with a
791 diameter of 2500 km hitting the Earth likely have been differentiated into HSE-rich cores and
792 HSE-stripped silicate mantles (Marchi et al., 2018). As a result, mantle domains with low
793 HSE abundances and positive ^{182}W anomalies, on the one hand, and high HSE abundances
794 and negative ^{182}W anomalies, on the other hand, would have been generated. In the absence of
795 modern-style plate tectonics prior to ~2.5 Ga (*e.g.*, Brown and Johnson, 2018), these mantle
796 domains would be expected to survive for extended periods of time before eventually
797 becoming homogenized within the mantle *via* wholesale mantle convection.

798 Heterogeneous distribution of HSE in the early Earth's mantle has been recognized from
799 $^{186,187}\text{Os}$ and HSE abundance studies of komatiites (*e.g.*, Maier et al., 2009; Puchtel et al.,
800 2004a,b, 2005, 2009a,b, 2014, 2016a,b, 2018, 2020, 2022). As noted in **Section 5**, available
801 high-precision ^{187}Os data for komatiitic systems worldwide indicate that most komatiite
802 sources were characterized by initial $\gamma^{187}\text{Os}$ values ranging from only -0.1 to +1.3, implying
803 that these komatiitic systems evolved with long-term Re/Os well within the range of
804 chondritic meteorites (**Fig. 2a**). Only two exceptions have been identified so far, which are

805 the Schapenburg and Kostomuksha komatiite systems. The more limited ^{186}Os dataset
806 indicates a somewhat greater variability outside of the chondritic range, but, nevertheless,
807 suggests that the mantle sources of the late Archean Pyke Hill, Belingwe, and Vetreny
808 komatiite systems evolved with time-integrated Pt/Os within the chondritic range (**Fig. 2b**).
809 By contrast, the high initial $\mu^{186}\text{Os}$ and $\gamma^{187}\text{Os}$ values in the mantle source of the Kostomuksha
810 komatiites require long-term suprachondritic Pt/Os and Re/Os ratios. Originally, these
811 coupled $^{186,187}\text{Os}$ enrichments were interpreted to be the result of core-mantle interaction
812 processes (Puchtel et al., 2005). However, the ^{182}W data obtained by Touboul et al. (2012) for
813 these komatiites rendered this interpretation implausible and these authors instead proposed
814 that the combined $^{186,187}\text{Os}$ and ^{182}W systematics were the result of metal-silicate fractionation
815 in a primordial magma ocean, as discussed earlier. Additional contrasts are the Komati and
816 Weltevreden (Puchtel et al., 2014) and the Lapland (Puchtel et al., 2020) komatiite systems,
817 which evolved with non-chondritic time-integrated Pt/Os ratios and chondritic time-integrated
818 Re/Os ratios, thereby displaying decoupling of the ^{186}Os and ^{187}Os systematics. For the
819 Komati and Weltevreden komatiite systems, this decoupled behavior has been interpreted to
820 be the result of fractionation of Pt-Fe alloys in a primordial magma ocean during the first 150
821 Ma of Earth history, followed by slow homogenization of the crystallized post-magma ocean
822 mantle domains characterized by fractionated Pt/Os ratios (Puchtel et al., 2014). For the
823 Lapland komatiite system, derivation from a mantle domain characterized by an excess of late
824 accreted, differentiated planetesimal core metal, the so-called “grainy” late accretion (Walker,
825 2016), were considered to be one of the two plausible models for explaining the decoupled
826 ^{186}Os and ^{187}Os systematics (Puchtel et al., 2020).

827 On the basis of variable Pt and Ru contents in komatiites of various ages, Maier et al.
828 (2009) argued for a gradual increase in HSE abundances in the presumed deep mantle sources
829 of komatiites between ~3.5 and ~2.9 Ga due to slow downward mixing of a “late veneer” of
830 chondritic materials. However, the $^{186,187}\text{Os}$ and ^{182}W isotopic and HSE abundance studies of
831 Puchtel et al. (2020; 2022, and references therein) of the best preserved early Archean to early
832 Proterozoic komatiite systems worldwide revealed a somewhat more complex picture. As
833 attested to by the plot of the calculated total HSE abundances in the sources of these komatiite
834 systems as percent of those in the estimates of the modern BSE of Becker et al. (2006) versus
835 age (**Fig. 3**), this trend has been argued unlikely to be the result of simple “slow downward
836 mixing of a late veneer of chondritic materials”, although a broad trend of increasing HSE
837 abundances in komatiite sources over time is apparent (*e.g.*, Puchtel et al., 2016a, 2018, 2020,
838 2022). The argument is two-fold. First, as is evident from **Fig. 3**, the total HSE abundances in

839 the sources of some late Archean komatiite systems were even lower than those in some early
840 Archean komatiite systems. Second, for some of the komatiite systems considered here, *e.g.*,
841 the Schapenburg and Kostomuksha komatiites, the calculated total HSE abundances were
842 shown to be inconsistent with the proportion of late accreted materials estimated to have been
843 added to their sources based on the $^{186,187}\text{Os}$ and ^{182}W data (Touboul et al., 2012; Puchtel et
844 al., 2016a).

845 These observations are illustrated in **Fig. 6**, where the $\mu^{182}\text{W}$ values of komatiite systems
846 are plotted against the calculated total HSE abundances in their mantle sources normalized to
847 those in the estimates for the modern BSE of Becker et al. (2006). This proportion
848 corresponds to the fraction of the total HSE budget of the modern BSE added during late
849 accretion, assuming an essentially HSE-free BSE immediately following core formation.
850 According to this model, the HSE budgets, taking into account their respective uncertainties,
851 of those komatiitic systems that plot within the segment constrained by the blue lines in **Fig.**
852 **6**, are consistent with having been established *via* addition of late accreted materials to their
853 mantle source regions. By contrast, the HSE budgets of the komatiite systems that plot outside
854 this segment are presumed to have been affected by additional primordial processes, such as
855 metal-silicate (*e.g.*, the Kostomuksha komatiites: Touboul et al., 2012) or silicate-silicate
856 (*e.g.*, the Schapenburg komatiites: Puchtel et al., 2016a) fractionation in a primordial magma
857 ocean within the first 60 Ma of Solar System history. Furthermore, the combined $^{187,186}\text{Os}$ -
858 ^{182}W and HSE abundance data for the Lapland komatiite system (**Fig. 6**) are consistent with
859 involvement of fractionated metal derived from cores of differentiated planetesimals during
860 late accretion processes and formation of Os-W isotope and HSE abundance heterogeneities
861 in the early mantle (Puchtel et al., 2020).

862 It has been argued that the impactors that created the largest impact basins on the Moon,
863 Mars, and presumably also the Earth, were hundreds of km in diameter (Ryder, 2002; Strom
864 et al., 2005; Bottke et al., 2010) and possibly dominated by differentiated planetesimals.
865 Impacts of such bodies would be capable of generating large ^{182}W and HSE anomalies in
866 portions of the mantle as a result of such “grainy” late accretion (Walker, 2016; Marchi et al.,
867 2018; 2020). Cores of differentiated planetesimals would have up to two orders of magnitude
868 higher W abundances, and up to 350 ppm less radiogenic $^{182}\text{W}/^{184}\text{W}$, than the modern BSE
869 (Kleine et al., 2002, 2004; Schoenberg et al., 2002; Yin et al., 2002). Hence, any mantle
870 domain to which an excess of this material was added would be ^{182}W -depleted and would also
871 be expected to be enriched in HSE, compared to BSE, as is observed for the Lapland
872 komatiite system (Puchtel et al., 2020). On the other hand, the mantle domain to which less of

873 a late accretionary HSE component was added, *e.g.*, in the form of the HSE-stripped silicate
874 mantles of differentiated planetesimals, would be ^{182}W -enriched, compared to those mantle
875 domains to which a full HSE complement of late accretionary material was added, and would
876 also be depleted in HSE relative to BSE. A typical example of a komatiite system derived
877 from such a mantle domain is the Boston Creek komatiites (Puchtel et al., 2018).

878 Using the data for the komatiite systems, for which late accretion has been argued to be
879 the main cause for the observed ^{182}W versus source HSE abundance relationships (**Fig. 6**),
880 and assuming that the ^{182}W excesses were due entirely to a deficit of late accreted materials in
881 their mantle sources, Puchtel et al. (2022) estimated $\mu^{182}\text{W}$ of the pre-late accretionary BSE to
882 be $+17\pm 7$ (**Fig. 6**). This estimate is consistent with the ^{182}W excess in the pre-late accretion
883 BSE of $+18\pm 9$ ppm obtained by Kleine and Walker (2017) using an independent approach
884 and to the estimates for the ^{182}W composition of the pre-late accretionary Moon of $+25\pm 5$
885 ppm (Kruijer et al., 2015; Touboul et al., 2015; Kruijer and Kleine, 2017). These similarities
886 provide further support to the hypothesis that the Earth and the Moon formed from material
887 with identical W isotopic compositions (Kleine and Walker, 2017), in concert with earlier
888 observations of similarity of O, Si, and Ti isotopic compositions between the Earth and the
889 Moon (*e.g.*, Dauphas et al., 2014), as well as additional evidence that the Moon likely formed
890 mainly from terrestrial, rather than impactor, material.

891 **6.3. Core-mantle boundary processes**

892 Core-mantle exchange is yet another process that may have been responsible for creating
893 large ^{182}W and $^{186,187}\text{Os}$ isotope and HSE abundance heterogeneities in the mantle. Originally,
894 the idea was proposed by Walker et al. (1995) based on their studies of the Re, Pt, and Os
895 partitioning behavior in group IIAB magmatic iron meteorites. Walker et al. (1995) noted that
896 during magmatic differentiation, solid metal – liquid metal partition coefficients decrease in
897 the order $D_{\text{Os}} > D_{\text{Re}} > D_{\text{Pt}}$, so that after crystallization of the inner core, the liquid outer core
898 would end up with supra-chondritic Re/Os and Pt/Os and, given enough time, would develop
899 coupled $^{186,187}\text{Os}$ enrichments. Walker et al. (1997) observed a coupled radiogenic $^{186,187}\text{Os}$
900 signature in the Noril'sk sulfide ores, which they interpreted as having originated from
901 interaction of the starting 251 Ma Siberian superplume (*e.g.*, Campbell, 2007) with the liquid
902 outer core at the CMB.

903 The concept of core-mantle interaction was further elaborated upon by Brandon et al.
904 (1998, 1999, 2003) and Puchtel et al. (2005) in their studies of plume-derived ocean island
905 basalts and komatiites. These authors proposed that the type of correlation between the initial

906 $\mu^{186}\text{Os}$ and $\gamma^{187}\text{Os}$ values observed in plume-derived Hawaiian picrites and Gorgona Island
907 and Kostomuksha komatiites is unique to mixtures with fractionated liquid outer core metal
908 (Pt/Re \sim 100), whereas common crustal materials have Pt/Re $<$ 30.

909 The major drawback of the original core-mantle interaction model stems from the fact that
910 the onset of inner core crystallization is poorly constrained, ranging from $<$ 1.0 to 3.5 Ga given
911 the uncertainties in estimates of present-day heat flux at the CMB which vary from 3 to 10
912 TW (see review in Nakagawa, 2020, and references therein), as well as currently insufficient
913 knowledge of the partition coefficients of radioactive elements (*e.g.*, K) under the CMB
914 conditions. Another issue concerns the fact that the core-mantle interaction model of Walker
915 et al. (1995) and Brandon et al. (1998, 1999) calls for physical addition of \sim 1% of the outer
916 core liquid metal to the silicate lower mantle. Because the liquid outer core has up to three
917 orders of magnitude higher HSE abundances compared to the mantle, the $^{186}, ^{187}\text{Os}$
918 composition of the resulting hybrid mantle source would be dominated by that of the outer
919 core, and this source would also have had an order of magnitude higher HSE abundances
920 compared to those in the BSE. Most OIB, including Hawaiian picrites, are sulfur-saturated
921 melts and likely to have lost a significant part of their HSE inventory to either immiscible
922 sulfide liquid fractionation or to retaining residual sulfide in their melting source regions (*e.g.*,
923 Shirey and Walker, 1998; Bennett et al., 2000; Jamais et al., 2008; Ireland et al., 2009). Such
924 loss of HSE during magma generation and ascent would not be the case for komatiites,
925 however, which are strongly sulfur-undersaturated magmas and, therefore, reliably record the
926 HSE abundances in their mantle source regions upon emplacement. Yet, those komatiites for
927 which input from the outer core has been advocated to explain their coupled $^{186,187}\text{Os}$
928 enrichments, *e.g.*, Gorgona Island (Brandon et al., 2003) and Kostomuksha (Puchtel et al.,
929 2005) komatiites, have calculated HSE abundances in their mantle source regions similar to
930 those in estimates for the modern BSE.

931 To reconcile the $^{186,187}\text{Os}$ and HSE abundance data for the Kostomuksha komatiites with
932 this apparent inconsistency, Puchtel and Humayun (2000) proposed a mechanism of core-
933 mantle interaction *via* isotopic exchange at the core-mantle interface, without any significant
934 mass transfer from the core to the mantle. This idea has been further advanced by Humayun
935 (2011). The mechanism of core-mantle interaction of Humayun (2011) requires the outer core
936 liquid to be trapped in a cumulate pile of Fe-rich non-metallic precipitates (FeO, FeS, Fe₃Si)
937 at the top of the core, then undergo fractional crystallization by precipitating solid metal
938 grains and leaving behind the residual metallic liquid. The residual liquid is then incorporated
939 into the base of the mantle, where it subsequently may be entrained by mantle plumes.

940 Based on the discovery of negative $\mu^{182}\text{W}$ values in some modern ocean island basalts,
941 Mundl et al. (2017), Rizo et al. (2019), and Mundl-Petermeier et al. (2019, 2020) have also
942 argued for some form of core-mantle exchange/equilibration in order to transfer the inferred
943 negative $\mu^{182}\text{W}$ value of the core of -220 to plumes rising from the CMB. Although the
944 $^{186,187}\text{Os}$ and ^{182}W data obtained on the same samples are still limited, all Hawaiian lavas with
945 negative $\mu^{182}\text{W}$ (ranging between -7.8 and -20.2) are also characterized by positive $\mu^{186}\text{Os}$
946 (ranging between $+18.6$ and $+62.8$) and positive $\gamma^{187}\text{Os}$ (ranging between $+2.0$ and $+7.2$).
947 Furthermore, Puchtel et al. (2020) obtained a negative $\mu^{182}\text{W}$ value of -10 for the Lapland
948 komatiites, which is within the range of the $\mu^{182}\text{W}$ values obtained for Hawaii, and proposed
949 that Lapland komatiites could be early Proterozoic equivalents of Hawaiian picrites. A core-
950 mantle interaction process, as put forward by Puchtel et al. (2020), would be expected to have
951 decreased the ^{182}W value in the Lapland komatiite source relative to the ambient mantle, and
952 also have increased the HSE abundances in this source over ambient mantle levels, which is
953 consistent with the observations (**Fig. 6**). That study further proposed that if the residual metal
954 in the model of Humayun (2011) had a composition similar to that of fractionated iron
955 meteorites, its entrainment into the mantle plume that gave rise to the Lapland komatiites
956 could explain the decoupled $^{186,187}\text{Os}$ systematics of these komatiites.

957 **6.4. Crustal recycling processes**

958 Yet another important mechanism for creating mantle chemical heterogeneities is
959 recycling of Earth's mantle lithosphere, oceanic crust, and sedimentary layers back into the
960 mantle (Hofmann and White, 1982; Shirey and Hanson, 1986; Chase and Patchett, 1988;
961 Campbell and Griffiths, 1992; Hart et al., 1992; Carlson, 1994; Roy-Barman and Allègre,
962 1995; Widom, 1997; Lassiter and Hauri, 1998; Blichert-Toft et al., 1999; Lassiter, 2006). This
963 recycling may occur via subduction – a process by which one tectonic plate moves under
964 another and sinks into the mantle as the plates converge; subduction is the driving force
965 behind modern plate tectonics. The subducted material may age in the mantle for hundreds of
966 millions of years until entrained in mantle plumes. Although there is little agreement on the
967 timing of the onset or even existence of modern-style plate tectonics in the Hadean and
968 Archean (e.g., Brown, 2007; Shirey et al., 2008; Gerya, 2014; Sizova et al., 2015; Johnson et
969 al., 2017; Bédard, 2018), several lines of geochemical evidence put forward by Shirey et al.
970 (2008) require that some version of modern-style plate tectonics already operated as far back
971 in Earth history as 3.5 billion years ago, followed by a transition from the stagnant-lid to
972 mobile-lid plate tectonic regimes sometime in the late Archean (O'Neill and Debaille, 2014).

973 Crustal recycling, e.g., in the form of subduction of pelagic sediments into the mantle,
974 may also cause decoupling of Nd and Hf isotope systematics of lavas from the Nd-Hf mantle
975 array, as has been argued to be the case for a suite of drill core Komati komatiite samples
976 (Blichert-Toft et al., 2015). This is due to the fact that the Lu/Hf ratio is strongly fractionated
977 relative to Sm/Nd in the Earth's sedimentary system (Patchett et al., 1984). This is caused by
978 high resistance to chemical weathering of the mineral zircon, which contains most of the Hf
979 budget of continental crustal rocks. During weathering of continental crustal rocks, they break
980 down into zircon-bearing sandy sediments with very low Lu/Hf and fine-grained clay material
981 with up to three times the chondritic Lu/Hf ratio. During sediment transport via turbidity
982 currents, sandy sediments stay on or near the continent, while the pelagic material is carried
983 out onto the ocean floor, where it may eventually be subducted into the mantle.

984 **7. The Nd-Hf-Os isotope paradox and its implications for early Earth history**

985 As noted above, there is evidence for decoupling between the radiogenic lithophile ^{143}Nd
986 and ^{176}Hf systems in certain komatiites mantle sources, but there is also apparent decoupling
987 between these lithophile isotope systems and the highly siderophile ^{187}Os system in some
988 komatiite mantle sources. The majority of the Archean and Proterozoic komatiite systems are
989 characterized by variable, and generally strong, long-term depletions in more incompatible
990 lithophile trace elements relative to less incompatible elements, e.g., Nd versus Sm and Hf
991 versus Lu (**Fig. 1**), yet they retain chondritic time-integrated Re/Os (**Fig. 2**). These komatiite
992 mantle sources must have experienced relatively early melt depletion events that fractionated
993 the Sm/Nd and Lu/Hf ratios to suprachondritic values high enough to bring the ^{143}Nd and
994 ^{176}Hf compositions to the variably positive $\epsilon^{143}\text{Nd}$ and $\epsilon^{176}\text{Hf}$ values. Since Re is generally
995 moderately to highly incompatible during mantle melting, whereas Os is moderately to highly
996 compatible (e.g., Barnes et al., 1985; Mallmann and O'Neill, 2007), these melt extraction
997 events should have also decreased the Re/Os ratio in the komatiite-basalt mantle sources. This
998 would have resulted in retardation of ^{187}Os ingrowth and, thus, evolution of the sources to
999 variably negative $\gamma^{187}\text{Os}$ values. However, such isotopic relationships are not observed in the
1000 global komatiite record.

1001 Puchtel et al. (2022) named this phenomenon the Nd-Hf-Os isotope paradox, to which
1002 Puchtel et al. (2020, 2022) offered a solution by developing a model whereby the komatiite-
1003 basalt mantle sources underwent early (~100 Ma into Solar System history), low-degree ($F =$
1004 1.5-2.0%) partial melting and melt extraction events that would have sufficiently fractionated
1005 the Sm/Nd and Lu/Hf ratios in the mantle sources, but would have had little effect on the

1006 Re/Os ratio due to the significantly lower incompatibility of Re compared to Nd and Hf
1007 during low-degrees of partial mantle melting.

1008 Because this depleted reservoir is apparently persistent throughout the Archean and is
1009 globally distributed, it requires early formation and subsequent complete isolation of a
1010 complementary basaltic crust enriched in incompatible lithophile trace elements. Calculations
1011 by Puchtel et al. (2022) indicate that such crust formed as a result of 1.5-2.0% batch melting
1012 of a BSE-like mantle would contain 31-27 ppm Nd, 7.1-6.5 ppm Sm, 0.62-0.59 ppm Lu, and
1013 5.2-4.7 ppm Hf, and would have $^{147}\text{Sm}/^{144}\text{Nd} = 0.140\text{-}0.145$ and $^{176}\text{Lu}/^{177}\text{Hf} = 0.0166\text{-}0.0174$
1014 (compared to 0.1967 and 0.0336 in the BSE, respectively). Based on these estimates of Sm
1015 and Nd concentrations in the early crust, the mass of this reservoir must have represented
1016 $\leq 2.0\%$ of the mass of the BSE, which is consistent with this reservoir being the size of the D"
1017 layer. The existence of such crust has been previously advocated for by Galer and Goldstein
1018 (1991). Alternatively, this earliest mafic crust could have served as the source of the oldest
1019 tonalite-trondhjemite-granodiorite (TTG) complexes (Carlson et al., 2019), such as those from
1020 the Nuvvuagittuq Greenstone Belt in Québec (O'Neil et al., 2008, 2016) or the Vodla Block
1021 TTG complex in the Fennoscandian Shield (Puchtel et al., 2016b).

1022 The residence time of this early mafic crust in the mantle is difficult to constrain. The
1023 available komatiite-basalt record would require its isolation through at least the late Archean,
1024 *i.e.*, when the ^{142}Nd anomalies were still present in the mantle (Debaille et al., 2013).
1025 However, there is no evidence that this crust was stored in the mantle until the present day,
1026 based on the generally chondritic ^{138}Ce , $^{142,143}\text{Nd}$, and ^{176}Hf composition estimates for the
1027 BSE (Jackson and Carlson, 2012; Horan et al., 2018; Willig and Stracke, 2019; Willig et al.,
1028 2020; Hyung and Jacobsen, 2020).

1029 **8. Komatiite constraints on early mixing rates of the terrestrial mantle**

1030 It has been proposed that the mixing rates of the mantle, or the average time of mantle
1031 homogenization, can be evaluated through studies of short-lived radiogenic isotope
1032 systematics and HSE abundances in mantle-derived rocks (*e.g.*, Jacobsen and Yu, 2015;
1033 Carlson et al., 2019; Hyung and Jacobsen, 2020; Tusch et al., 2021; Puchtel et al., 2022).
1034 Isotopic variations due to the decay of the now extinct ^{146}Sm and ^{182}Hf nuclides recorded
1035 processes in the Earth that fractionated Sm/Nd and Hf/W ratios between different terrestrial
1036 reservoirs at the times when these parent nuclides were still alive. When these events occurred
1037 during the first ~ 600 and ~ 60 Ma of Earth history, respectively, the differentiation processes
1038 resulted in formation of ^{142}Nd and ^{182}W anomalies in these terrestrial reservoirs. Due to the

1039 protracted, violent accretion history of the Earth accompanied by vigorous convective mixing
1040 during the Hadean and Archean eons, these reservoirs and, thus, the isotopic anomalies they
1041 hosted, were gradually erased from the geological record. Hence, tracing the variations in the
1042 magnitude of these isotopic anomalies over geological time can be used to determine the
1043 mixing rates of the terrestrial mantle (*e.g.*, Jacobsen and Yu, 2015; Hyung and Jacobsen,
1044 2020).

1045 Early mantle convection models (*e.g.*, Blichert-Toft and Albarède, 1994; Coltice and
1046 Schmalzl, 2006) concluded that the mixing times in the hot Hadean and Archean mantle were
1047 10 times faster than today, and that any large-scale primordial chemical and isotopic
1048 heterogeneities in the mantle would have been erased within ~100 Ma of their creation.
1049 However, during the past two decades, numerous ^{142}Nd and ^{182}W anomalies have been
1050 discovered in the terrestrial mantle-derived rock record (**Fig. 7**). The largest ^{142}Nd anomalies
1051 ($\mu^{142}\text{Nd}$ up to +20 ppm and down to -20 ppm) have been reported for Eo- to Paleoarchean
1052 supracrustal rocks from the Isua Greenstone Belt, Greenland (Boyet et al., 2003; Caro et al.,
1053 2006; Bennett et al., 2007; Rizo et al., 2011; 2012; 2013; O'Neil et al., 2016), the
1054 Nuvvuagittuq Greenstone Belt, Québec (O'Neil et al., 2008; 2012; Roth et al., 2013), the
1055 Acasta Gneiss Complex, Canada (Roth et al., 2014; Reimink et al., 2018), and the Barberton
1056 Greenstone Belt, Kaapvaal Craton, South Africa (Puchtel et al., 2016a; Boyet et al., 2021).
1057 These isotopic anomalies must have been created before ~4.0 Ga by silicate-silicate
1058 differentiation and, thus, have survived for >1.0 Ga, implying much slower mixing times of
1059 the mantle for ^{142}Nd than was predicted by the early mantle convection models. Following
1060 these discoveries, more recent mantle convection models argue for complete homogenization
1061 of the mantle by the end of the Archean (*e.g.*, Rosas and Korenaga, 2018; Korenaga, 2021).
1062 Only few terrestrial samples with ages between 3.0 and 2.7 Ga have $\mu^{142}\text{Nd}$ values deviating
1063 from the terrestrial standard by more than ± 5 ppm, the only known exception being 2.72 Ga
1064 tholeiites from the Abitibi Greenstone Belt, Canada (Debaille et al., 2013). Although there is a
1065 significant gap in the mafic-ultramafic rock record for ^{142}Nd data between ~2.7 Ga and the
1066 present day, it indeed appears that ^{142}Nd anomalies largely disappeared by the end of the
1067 Archean (**Fig. 7**). As a result, on the basis of the now much larger ^{142}Nd record and using a
1068 mathematical mantle mixing box model, Hyung and Jacobsen (2020) concluded that the
1069 relationships in **Fig. 7** are consistent with mantle mixing rates of ~400 Ma that operated since
1070 the early Hadean. These authors further argued that such fast mixing rates are consistent with
1071 Earth's thermal and chemical evolution having been largely regulated by plate tectonics for
1072 most of its history.

1073 Nonetheless, recent studies have shown that some modern plume-derived OIB (**Fig. 7**)
1074 have ^{142}Nd compositions resolved, albeit marginally, from the terrestrial standard (*e.g.*, Horan
1075 et al., 2018; Peters et al., 2018), indicating that some ^{142}Nd isotopic signatures dating back to
1076 Earth's earliest differentiation events may still be preserved in deepest parts of the modern
1077 mantle.

1078 In contrast to the earliest ^{142}Nd record, mostly positive ^{182}W anomalies, of up to $\sim+20$
1079 ppm, have been reported for mafic-ultramafic rocks ranging in age from 4.0 to 2.7 Ga (**Fig.**
1080 **7b**). The only exceptions are komatiites from the Schapenburg system (Puchtel et al., 2016a),
1081 which have a negative ^{182}W anomaly of -8 ppm. On the other hand, some recent and modern
1082 OIB, such as Hawaii, Samoa, Iceland, Galapagos, Heard, Pitcairn (Mundl et al., 2017; Mundl-
1083 Petermeier et al., 2019, 2020), and Kerguelen and Reunion (Rizo et al., 2019) are
1084 characterized by negative ^{182}W anomalies down to -25 ppm, although the volumetrically
1085 dominant signature in OIB is most likely $^{182}\text{W} = 0$. The very limited data available (Puchtel et
1086 al., 2016b, 2020) provide a hint that there may be a transition at ~ 2.5 Ga from mostly positive
1087 $\mu^{182}\text{W}$ -dominated to no-anomaly $\mu^{182}\text{W}$ -dominated mantle (**Fig. 7b**). With the relatively
1088 young 2.05 Ga Lapland komatiites already registering a negative ^{182}W anomaly of -10 ppm
1089 (Puchtel et al., 2020), and some OIB sources registering negative ^{182}W anomalies down to $-$
1090 25 ppm, this transition may indicate the combined effects of the onset of modern-style plate
1091 tectonics and core-mantle interaction taking over as the main driving forces controlling the W
1092 isotopic composition of the deep plume mantle sources (*e.g.*, Rizo et al., 2019; Carlson et al.,
1093 2019).

1094 The different behavior of the two short-lived isotopic systems in the mantle may be
1095 possible to reconcile when the mechanisms behind the origin of ^{142}Nd and ^{182}W anomalies are
1096 considered. Because both Sm and Nd are uniformly strongly lithophile elements under the
1097 redox conditions applicable to Earth's formation, ^{142}Nd anomalies are solely the result of
1098 primordial silicate-silicate planetary differentiation (*e.g.*, Boyet and Carlson, 2005). No new
1099 ^{142}Nd anomalies could have been created in the BSE after ~ 4.0 Ga, when ^{146}Sm became
1100 extinct. In contrast to the ^{146}Sm - ^{142}Nd system, Hf is strongly lithophile, while W is
1101 moderately siderophile. Hafnium, therefore, can be fractionated from W during metal-silicate
1102 differentiation, such as that which occurred during planetary core segregation. During silicate-
1103 silicate differentiation, W is more incompatible than Hf, which can result in fractionation of
1104 Hf from W in purely silicate systems. Both processes are considered to be capable of creating
1105 ^{182}W anomalies within the first 60 Ma of Earth's history, while ^{182}Hf was still extant. The
1106 additional processes that are thought to be capable of introducing ^{182}W heterogeneities to the

1107 mantle and to which the ^{142}Nd system was insensitive, were late accretion and core-mantle
1108 interaction, as discussed in **Section 6**. As a result of the combination of all these factors in
1109 variable, and generally unconstrained, proportions, the use of the ^{182}Hf - ^{182}W isotopic system
1110 for tracing mixing times of the mantle appears to be of lesser value than the ^{146}Sm - ^{142}Nd
1111 systematics.

1112 Mantle mixing rates in terms of HSE have been studied *via* tracing the changes in HSE
1113 abundances in the mantle over the span of geological time (*e.g.*, Maier et al., 2009; Puchtel et
1114 al., 2018, 2020, 2022). Because the lunar highland crust, which was formed at ~ 4.4 Ga (*e.g.*,
1115 Borg et al., 2014), is only negligibly contaminated by meteoritic material (*e.g.*, Day et al.,
1116 2010), late accretion must have been largely complete prior to 4.4 Ga, *i.e.*, within the first
1117 ~ 150 Ma of the Solar System history. Puchtel et al. (2022) used the estimated HSE
1118 abundances in the sources of the Archean and Proterozoic komatiite systems plotted in **Fig. 3**
1119 as a function of their ages and *Isoplot* regression analysis to calculate the average time by
1120 which the late accreted materials would have been completely homogenized within the
1121 mantle, and found 2.5 ± 0.2 Ga. These data require that survival times of the late accreted
1122 planetesimals within the mantle, before complete homogenization, were on average 1.9 ± 0.2
1123 Ga (*i.e.*, the time interval between 4.4 and 2.5 Ga), thus constraining the average mixing rates
1124 of the terrestrial mantle in terms of siderophile element abundances in the Hadean and the
1125 Archean. This period in time coincides with the timing of onset of modern-style plate
1126 tectonics on Earth, as argued by some (Brown, 2007; Brown and Johnson, 2018), and with the
1127 near-complete disappearance of all ^{142}Nd and positive ^{182}W anomalies in the mantle (Carlson
1128 et al., 2019; Reimink et al., 2020, Tusch et al., 2021).

1129 It is possible that some inefficient mixing could be due to early Earth tectonic regimes
1130 differing from those of modern-style plate tectonics (O'Neill and Debaille, 2014). A stagnant-
1131 lid, or episodic, subduction regime in the Hadean is consistent with the persistence of short-
1132 lived isotopic anomalies and compositional heterogeneities, although more recent modeling
1133 indicates that such mantle heterogeneities can survive for billions of years, even under a
1134 mobile-lid tectonic regime (Foley and Rizo, 2017).

1135 **9. The diverse nature of komatiite sources reflects on the complexity of the terrestrial** 1136 **mantle**

1137 As is evident from the chemical and isotopic data summarized in **Tables 1** and **2** and
1138 discussed throughout this review, komatiite mantle sources were characterized by extreme
1139 diversity throughout the Archean and early Proterozoic in terms of both trace- and HSE

1140 abundances and radiogenic isotope systematics. Early Archean komatiites were likely derived
1141 from lower mantle domains that were created very early in Earth history as a result of deep-
1142 seated magma ocean crystallization processes. These mantle domains were characterized by
1143 highly variable, and often strong, long-term depletions in the highly incompatible lithophile
1144 trace elements and generally large deficits in the late accreted component, as attested to by
1145 their HSE abundance and ^{182}W systematics.

1146 The late Archean and Proterozoic komatiites show evidence in their mantle sources for
1147 limited variability of long-term depletions in highly incompatible lithophile trace elements as
1148 a result of prior melt extractions. With the exception of the Kostomuksha and possibly
1149 Lapland systems, these komatiites were derived from mantle plumes that originated in the
1150 upper mantle, most likely in the MTZ. These komatiite sources were characterized by smaller
1151 deficits to excesses in the late accreted component, as testified to by their HSE abundance and
1152 ^{182}W systematics.

1153 Finally, our compilation of the geochemical data relevant to the mantle sources of
1154 Archean and early Proterozoic komatiites reveals that none of the projected sources were
1155 similar in composition to estimates for the BSE. The komatiite systems considered here,
1156 which span wide geographical and temporal distributions, further demonstrate that no single
1157 petrogenetic model can account for all the diverse chemical compositions of komatiites.

1158 **10. Conclusions**

1159 Komatiites, due to their unique properties and, with a few exceptions, very old ages, are
1160 among the best samples to constrain the evolution of the chemical composition of the early
1161 Earth's mantle. Isotopic and elemental signatures created in early-formed silicate reservoirs
1162 *via* radioactive decay of short- and long-lived nuclides, including $^{146,147}\text{Sm}$, ^{176}Lu , ^{182}Hf ,
1163 ^{187}Re , and ^{190}Pt , have been sampled by komatiitic magmas and preserved in the geological
1164 rock record. These signatures have been used here to constrain the nature and timing of
1165 formation of these, by now largely vanished, mantle reservoirs.

1166 The komatiites considered in the present review are interpreted to have been derived from
1167 anhydrous melting in mantle plumes that were initiated in both the lower and upper mantle,
1168 although, in contrast to modern plumes, all evidence for the depths of ancient mantle plume
1169 initiation is circumstantial in nature.

1170 The data for the existing 3.6-2.0 Ga komatiite record provide robust evidence for the
1171 presence of remarkably ancient isotopic and chemical heterogeneities in the mantle at that
1172 time interval in Earth history. These heterogeneities have been shown here to reflect the

1173 combined effects of (i) the co-existence of diverse post-magma ocean silicate domains
1174 characterized by variably-fractionated lithophile and siderophile element abundances; (ii) the
1175 presence of distinct reservoirs representing mantles and cores of large, differentiated
1176 planetesimals delivered to Earth during late accretion; and (iii) isotopic exchange across the
1177 core-mantle boundary.

1178 The near-complete disappearance of resolvable ^{142}Nd anomalies and of decoupled ^{143}Nd -
1179 ^{176}Hf isotopic signatures in the mafic-ultramafic rock record by ~ 2.5 Ga indicates that the
1180 earliest silicate reservoirs, formed as a result of primordial magma ocean crystallization, had
1181 been largely destroyed by that time through vigorous, convective mantle mixing, implying
1182 mixing rates of the mantle on the order of ~ 1.5 Ga. The shift from mostly positive ^{182}W
1183 offsets in the pre-2.5 Ga mantle sources of mafic-ultramafic lavas to no ^{182}W offsets at ~ 2.5
1184 Ga, as well as disappearance of HSE abundance anomalies at ~ 2.5 Ga, may indicate the
1185 combined effects of the onset of modern-style plate tectonics and core-mantle interaction that
1186 took over as the main driving force of creating ^{182}W isotopic heterogeneities in the mantle.

1187 This review further emphasizes the great compositional complexity of early Archean to
1188 early Proterozoic komatiite mantle sources in terms of both lithophile and siderophile element
1189 abundances and isotope systematics; apparently, none of these sources were similar in
1190 composition to that of the BSE. Obviously, no single petrogenetic model can fully account for
1191 the chemical and isotopic diversity of komatiites.

1192 **Acknowledgements**

1193 This work was supported by NSF Petrology and Geochemistry grant EAR 1754186 to
1194 ISP. We are grateful to Al Hofmann and Maud Boyet for thorough and constructive reviews
1195 of the initial version of this manuscript and to Catherine Chauvel for editorial handling. This
1196 work greatly benefitted from close collaborations with Carl Anhaeusser, Nick Arndt, Gary
1197 Byerly, Eero Hanski, Al Hofmann, Munir Humayun, Vyacheslav and Victoria Kulikov, Mike
1198 Leshner, Marek Locmelis, Euan Nisbet, and Andi Mundl-Petermeier.

1199

1200

References

- 1201 Abbott, D., 1996. Plumes and hotspots as sources of greenstone belts. *Lithos* 37 (2-3): 113-
1202 127.
- 1203 Abe, Y., 1997. Thermal and chemical evolution of the terrestrial magma ocean. *Physics of the*
1204 *Earth and Planetary Interiors* 100 (1-4): 27-39.
- 1205 Agee, C.B. and Walker, D., 1988. Static compression and olivine flotation in ultrabasic
1206 silicate liquid. *Journal of Geophysical Research* 93 (B4): 3437-3449.
- 1207 Albarède, F., Blichert-Toft, J., Vervoort, J. D., Gleason, J. D., Rosing, M., 2000. Hf-Nd
1208 isotope evidence for a transient dynamic regime in the early terrestrial mantle. *Nature* **404**
1209 (6777): 488-490.
- 1210 Allègre, C.J., 1982. Genesis of Archaean komatiites in a wet ultramafic subducted plate. In:
1211 Arndt, N.T. and Nisbet, E.G. (Eds.), *Komatiites*, George Allen and Unwin, London, pp.
1212 495-500.
- 1213 Andreasen, R., Sharma, M., Subbarao, K.V., and Viladkar, S.G., 2008. Where on Earth is the
1214 enriched Hadean reservoir? *Earth and Planetary Science Letters* 266 (1-2): 14-28.
- 1215 Archer, G.J., Brennecka, G.A., Gleißner, P., Stracke, A., Becker, H., and Kleine, T., 2019.
1216 Lack of late-accreted material as the origin of ¹⁸²W excesses in the Archean mantle:
1217 Evidence from the Pilbara Craton, Western Australia. *Earth and Planetary Science Letters*,
1218 528: 115841.
- 1219 Arevalo, R., McDonough, W. F., 2008. Tungsten geochemistry and implications for
1220 understanding the Earth's interior. *Earth and Planetary Science Letters* **272** (3-4): 656-665.
- 1221 Armstrong, R. L., 1981. Radiogenic isotopes: the case for crustal recycling on a near-steady-
1222 state no-continental-growth. *Philosophical Transactions of the Royal Society of London*
1223 **A301**: 443-472.
- 1224 Arndt, N.T., 1994. Archaean Komatiites. In: Condie, K.C. (Ed.). *Archaean Crustal Evolution*,
1225 Elsevier, Amsterdam, pp. 11-44.
- 1226 Arndt, N.T. and Nisbet, E.G., 1982. *Komatiites*. Allen and Unwin, London, 582 pp.
- 1227 Arndt, N.T., Leshner, C.M., and Barnes, S.J., 2008. *Komatiite*. Cambridge University Press,
1228 Cambridge, UK, 467 pp.
- 1229 Arndt, N.T., Naldrett, A.J., Pyke, D.R., 1977. Komatiitic and iron-rich tholeiitic lavas of
1230 Munro Township, northeast Ontario. *Journal of Petrology* **18**: 319-369.
- 1231 Arndt, N.T., 1977. Ultrabasic magmas and high-degree melting of the mantle. *Contributions*
1232 *to Mineralogy and Petrology* 64 (2): 205-221.
- 1233 Arndt, N.T., Ginibre, C., Chauvel, C., Albarède, F., Cheadle, M., Herzberg, C., Jenner, G.,
1234 and Lahaye, Y., 1998. Were komatiites wet? *Geology* 26 (8): 739-742.
- 1235 Arndt, N., Bruzak, G., and Reischmann, T., 2001. The oldest continental and oceanic
1236 plateaus: Geochemistry of basalts and komatiites of the Pilbara Craton, Australia.
1237 *Geological Society of America Special Paper* 352: 359-387.
- 1238 Asafov, E.V., Sobolev, A.V., Gurenko, A.A., Arndt, N.T., Batanova, V.G., Portnyagin, M.V.,
1239 Garbe-Schönberg, D., and Krashennnikov, S.P., 2018. Belingwe komatiites (2.7 Ga)
1240 originate from a plume with moderate water content, as inferred from inclusions in
1241 olivine. *Chemical Geology* 478: 39-59.

- 1242 Ballmer, M.D., Schumacher, L., Lekic, V., Thomas, C., and Ito, G., 2016. Compositional
 1243 layering within the large low shear-wave velocity provinces in the lower mantle.
 1244 *Geochemistry, Geophysics, Geosystems* 17 (12): 5056-5077.
- 1245 Bao, X., Lithgow-Bertelloni, C.R., Jackson, M.G., and Romanowicz, B., 2022. On the relative
 1246 temperatures of Earth's volcanic hotspots and mid-ocean ridges. *Science* 373 (6576): 57-
 1247 61.
- 1248 Barnes, S.-J., Naldrett, A.J., Gorton, M.P., 1985. The origin of the fractionation of platinum-
 1249 group elements in terrestrial magmas. *Chemical Geology* 53 (3-4): 303-323.
- 1250 Barnes, S.J. and Van Kranendonk, M.J., 2014. Archean andesites in the east Yilgarn craton,
 1251 Australia: Products of plume-crust interaction? *Lithosphere* 6 (2): 80-92.
- 1252 Barnes, S.J., Mole, D., Wyche, S., and Dering, G., 2016. Komatiites and associated rocks of
 1253 the Kalgoorlie–Leonora region. *Geological Survey of Western Australia Record* 2016/12,
 1254 70 pp.
- 1255 Becker, H., Horan, M.F., Walker, R.J., Gao, S., Lorand, J.-P., and Rudnick, R.L., 2006.
 1256 Highly siderophile element composition of the Earth's primitive upper mantle: Constraints
 1257 from new data on peridotite massifs and xenoliths. *Geochimica et Cosmochimica Acta* 70
 1258 (17): 4528-4550.
- 1259 Bédard, J.H., 2018. Stagnant lids and mantle overturns: Implications for Archaean tectonics,
 1260 magmagenesis, crustal growth, mantle evolution, and the start of plate tectonics.
 1261 *Geoscience Frontiers* 9 (1): 19-49.
- 1262 Bennett, V.C., Esat, T.M., and Norman, M.D., 1996. Two mantle-plume components in
 1263 Hawaiian picrites inferred from correlated Os-Pb isotopes. *Nature* **381** (6579): 221-224.
- 1264 Bennett, V.C., Norman, M.D., and Garcia, M.O., 2000. Rhenium and platinum group element
 1265 abundances correlated with mantle source components in Hawaiian picrites: sulphides in
 1266 the plume. *Earth and Planetary Science Letters* 183 (3-4): 513-526.
- 1267 Bennett, V.C., Brandon, A.D., and Nutman, A.P., 2007. Coupled ¹⁴²Nd-¹⁴³Nd isotopic
 1268 evidence for Hadean mantle dynamics. *Science* 318 (5858): 1907-1910.
- 1269 Bercovici, D. and Karato, S., 2003. Whole-mantle convection and the transition-zone water
 1270 filter. *Nature* 425 (6953): 39-44.
- 1271 Berry, A.J., Danyushevsky, L.V., O'Neill, H.S.C., Newville, M., and Sutton, S.R., 2008.
 1272 Oxidation state of iron in komatiitic melt inclusions indicates hot Archaean mantle.
 1273 *Nature* 455 (7215): 960-963.
- 1274 Bickle, M.J., 1982. The magnesium contents of komatiitic liquids. In: *Komatiites*. George
 1275 Allen and Unwin, London, pp. 479-494.
- 1276 Bickle, M.J., 1986. Implications of melting for stabilisation of lithosphere and heat loss in the
 1277 Archaean. *Earth and Planetary Science Letters* 80 (3-4): 314-324.
- 1278 Bina, C.R. and Helffrich, G., 1994. Phase transition Clapeyron slopes and transition zone
 1279 seismic discontinuity topography. *Journal of Geophysical Research* 99 (B8): 15853-
 1280 15860.
- 1281 Blichert-Toft, J. and Albarède, F., 1994. Short-lived chemical heterogeneities in the Archaean
 1282 mantle with implications for mantle convection. *Science* 263: 1593-1596.
- 1283 Blichert-Toft, J. and Arndt, N.T., 1999. Hf isotope compositions of komatiites. *Earth and*
 1284 *Planetary Science Letters* 171(3): 439-451.

- 1285 Blichert-Toft, J., Frey, F.A., and Albarède, F., 1999. Hf isotope evidence for pelagic
1286 sediments in the source of Hawaiian basalts. *Science* **285**: 879-882.
- 1287 Blichert-Toft, J. and Puchtel, I.S., 2010. Depleted mantle sources through time: Evidence
1288 from Lu-Hf and Sm-Nd isotope systematics of Archean komatiites. *Earth and Planetary*
1289 *Science Letters* 297 (3-4): 598-606.
- 1290 Blichert-Toft, J., Arndt, N.T., Wilson, A., and Coetsee, G., 2015. Hf and Nd isotope
1291 systematics of early Archean komatiites from surface sampling and ICDP drilling in the
1292 Barberton Greenstone Belt, South Africa. *American Mineralogist* 100: 2396-2411.
- 1293 Borg, L.E., Gaffney, A.M., and Shearer, C.K., 2014. A review of lunar chronology revealing
1294 a preponderance of 4.34–4.37 Ga ages. *Meteoritics and Planetary Science* **50** (4): 715-732.
- 1295 Borisov, A. and Palme, H., 1997. Experimental determination of the solubility of platinum in
1296 silicate melts. *Geochimica et Cosmochimica Acta* 61 (20): 4349-4357.
- 1297 Botke, W.F., Morbidelli, A., Jedicke, R., Petit, J.-M., Levison, H.F., Michel, P., Metcalfe,
1298 T.S., 2002. Debiased Orbital and Absolute Magnitude Distribution of the Near-Earth
1299 Objects. *Icarus* 156 (2): 399-433.
- 1300 Botke, W.F., Levison, H.F., Nesvorny, D., Dones, L., 2007. Can planetesimals left over from
1301 terrestrial planet formation produce the lunar Late Heavy Bombardment? *Icarus* 190 (1):
1302 203-223.
- 1303 Botke, W.F., Walker, R.J., Day, J.M.D., Nesvorny, D., and Elkins-Tanton, L., 2010.
1304 Stochastic Late Accretion to Earth, the Moon, and Mars. *Science* 330 (6010): 1527-1530.
- 1305 Bouvier, A., Vervoort, J.D., and Patchett, P.J., 2008. The Lu-Hf and Sm-Nd isotopic
1306 composition of CHUR: Constraints from unequilibrated chondrites and implications for
1307 the bulk composition of terrestrial planets. *Earth and Planetary Science Letters* 273 (1-2):
1308 48-57.
- 1309 Boyet, M., Blichert-Toft, J., Rosing, M., Storey, M., Télouk, P., and Albarède, F., 2003. ¹⁴²Nd
1310 evidence for early Earth differentiation. *Earth and Planetary Science Letters* 214 (3-4):
1311 427-442.
- 1312 Boyet, M., and Carlson, R.W., 2005. ¹⁴²Nd evidence for early (>4.53 Ga) global
1313 differentiation of the silicate Earth. *Science* **309** (5734): 576-581.
- 1314 Boyet, M., and Carlson, R.W., 2006. A new geochemical model for the Earth's mantle
1315 inferred from ¹⁴⁶Sm-¹⁴²Nd systematics. *Earth and Planetary Science Letters* 250 (1-2):
1316 254-268.
- 1317 Boyet, M., Garçon, M., Arndt, N.T., Carlson, R. W., and Konc, Z., 2021. Residual liquid from
1318 deep magma ocean crystallization in the source of komatiites from the ICDP drill core in
1319 the Barberton Greenstone Belt. *Geochimica et Cosmochimica Acta* 304: 141-159.
- 1320 Brenan, J.M. and McDonough, W.F., 2009. Core formation and metal-silicate fractionation of
1321 osmium and iridium from gold. *Nature Geoscience* 2: 798-801.
- 1322 Brown, M. and Johnson, T., 2018. Secular change in metamorphism and the onset of global
1323 plate tectonics. *American Mineralogist* 103 (2): 181-196.
- 1324 Brown, M., 2007. Metamorphism, Plate Tectonics, and the Supercontinent Cycle. *Earth*
1325 *Science Frontiers* 14 (1): 1-18.
- 1326 Brown, S.M., Elkins-Tanton, L.T., and Walker, R.J., 2014. Effects of magma ocean
1327 crystallization and overturn on the development of ¹⁴²Nd and ¹⁸²W isotopic

- 1328 heterogeneities in the primordial mantle. *Earth and Planetary Science Letters* 408: 319-
1329 330.
- 1330 Bowring, S. A., Housh, T., 1995. The Earth's early evolution. *Science* **269** (5230): 1535-1540.
- 1331 Boyet, M., Blichert-Toft, J., Rosing, M., Storey, M., Télouk, P., Albarède, F., 2003. ^{142}Nd
1332 evidence for early Earth differentiation. *Earth and Planetary Science Letters* **214**: 427-442.
- 1333 Brandon, A.D., Walker, R.J., Morgan, J.W., Norman, M.D., and Prichard, H.M., 1998.
1334 Coupled ^{186}Os and ^{187}Os evidence for core-mantle interaction. *Science* 280 (5369): 1570-
1335 1573.
- 1336 Brandon, A.D., Norman, M.D., Walker, R.J., and Morgan, J.W., 1999. ^{186}Os - ^{187}Os
1337 systematics of Hawaiian picrites. *Earth and Planetary Science Letters* 174 (1-2): 25-42.
- 1338 Brandon, A.D., Walker, R.J., Puchtel, I.S., Becker, H., Humayun, M., and Revillon, S., 2003.
1339 ^{186}Os - ^{187}Os systematics of Gorgona Island komatiites: Implications for early growth of the
1340 inner core. *Earth and Planetary Science Letters* 206 (3-4): 411-426.
- 1341 Brandon, A.D., Humayun, M., Puchtel, I.S., and Zolensky, M., 2005. Re-Os isotopic
1342 systematics and platinum group element composition of the Tagish Lake carbonaceous
1343 chondrite. *Geochimica et Cosmochimica Acta* **69** (6): 1619-1631.
- 1344 Brandon, A.D., Walker, R.J., and Puchtel, I.S., 2006. Platinum-osmium isotope evolution of
1345 the Earth's mantle: Constraints from chondrites and Os-rich alloys. *Geochimica et*
1346 *Cosmochimica Acta* 70 (8): 2093-2103.
- 1347 Burkhardt, C., Borg, L.E., Brennecka, G.A., Shollenberger, Q.R., Dauphas, N., and Kleine,
1348 T., 2016. A nucleosynthetic origin for the Earth's anomalous ^{142}Nd composition. *Nature*
1349 537: 394-398.
- 1350 Byerly, B.L., Kareem, K., Bao, H., and Byerly, G.R., 2017. Early Earth mantle heterogeneity
1351 revealed by light oxygen isotopes of Archaean komatiites. *Nature Geoscience* 10: 871-
1352 876.
- 1353 Campbell, I.H., Griffiths, R.W., and Hill, R.I., 1989. Melting in an Archaean mantle plume:
1354 head it's basalts, tails it's komatiites. *Nature* 339 (6227): 697-699.
- 1355 Campbell, I.H. and Hill, R.I., 1988. A two stage model for the formation of the granite-
1356 greenstone terrains of the Kalgoorlie-Norseman area, Western Australia. *Earth and*
1357 *Planetary Science Letters* 90 (1): 11-25.
- 1358 Campbell, I.H. and Griffiths, R.W., 1990. Implications of mantle plume structure for the
1359 evolution of flood basalts. *Earth and Planetary Science Letters* 99 (1-2): 79-93.
- 1360 Campbell, I.H. and Griffiths, R.W., 1992. The changing nature of mantle hotspots through
1361 time: Implications for the chemical evolution of the mantle. *Journal of Geology* 92 (5):
1362 497-523.
- 1363 Campbell, I.H. and Griffiths, R.W., 1993. The evolution of the mantle's chemical structure.
1364 *Lithos* 30 (3): 389-399.
- 1365 Campbell, I.H., 2007. Testing the plume theory. *Chemical Geology* 241 (3-4): 153-176.
- 1366 Campbell, I.H. and Griffiths, R.W., 2014. Did the formation of D" cause the Archaean-
1367 Proterozoic transition? *Earth and Planetary Science Letters* 388: 1-8.
- 1368 Canil, D., 1997. Vanadium partitioning and the oxidation state of Archaean komatiite
1369 magmas. *Nature* 389 (6653): 842-845.

- 1370 Canil, D., 1999. Vanadium partitioning between orthopyroxene, spinel and silicate melt and
1371 the redox states of mantle source regions for primary magmas. *Geochimica et*
1372 *Cosmochimica Acta* 63 (3-4): 557-572.
- 1373 Canil, D., 2002. Vanadium in peridotites, mantle redox and tectonic environments: Archean
1374 to present. *Earth and Planetary Science Letters* 195 (1-2): 75-90.
- 1375 Canil, D. and Fedortchouk, Y., 2001. Olivine-liquid partitioning of vanadium and other trace
1376 elements, with applications to modern and ancient picrites. *Canadian Mineralogist* 39:
1377 319-330.
- 1378 Canup, R.M., 2012. Forming a Moon with an Earth-like Composition via a Giant Impact.
1379 *Science* 338 (6110): 1052-1055.
- 1380 Carlson, R.W., 1994. Mechanisms of Earth differentiation: consequences for the chemical
1381 structure of the mantle. *Review of Geophysics* 32 (4): 337-361.
- 1382 Carlson, R.W., Boyet, M., and Horan, M., 2007. Chondrite barium, neodymium, and
1383 samarium isotopic heterogeneity and early earth differentiation. *Science* 316 (5828):
1384 1175-1178.
- 1385 Carlson, R. W., Boyet, M., O'Neil, J., Rizo, H., and Walker, R. J., 2015. Early Differentiation
1386 and Its Long-Term Consequences for Earth Evolution. In: *The Early Earth*. Hoboken,
1387 New Jersey, John Wiley & Sons, Inc.: 143-172.
- 1388 Carlson, R.W., Garçon, M., O'Neil, J., Reimink, J., and Rizo, H., 2019. The nature of Earth's
1389 first crust. *Chemical Geology* 530: 119321.
- 1390 Caro, G., Bourdon, B., Birck, J.-L., and Moorbath, S., 2003. ^{146}Sm - ^{142}Nd evidence from Isua
1391 metamorphosed sediments for early differentiation of the Earth's mantle. *Nature* 423
1392 (6938): 428-432.
- 1393 Caro, G., Bourdon, B., Wood, B.J., and Corgne, A., 2005. Trace-element fractionation in
1394 Hadean mantle generated by melt segregation from a magma ocean. *Nature* 436 (7048):
1395 246-249.
- 1396 Caro, G., Bourdon, B., Birck, J.-L., and Moorbath, S., 2006. High-precision $^{142}\text{Nd}/^{144}\text{Nd}$
1397 measurements in terrestrial rocks: Constraints on the early differentiation of the Earth's
1398 mantle. *Geochimica et Cosmochimica Acta* 70 (1): 164-191.
- 1399 Caro, G., Bourdon, B., Halliday, A.N., and Quitte, G., 2008. Super-chondritic Sm/Nd ratios in
1400 Mars, the Earth and the Moon. *Nature* 452 (7185): 336-339.
- 1401 Caro, G., 2011. Early Silicate Earth Differentiation. *Annual Review of Earth and Planetary*
1402 *Sciences* 39 (1): 31-58.
- 1403 Caro, G., Morino, P., Mojzsis, S.J., Cates, N.L., and Bleeker, W., 2017. Sluggish Hadean
1404 geodynamics: Evidence from coupled $^{146,147}\text{Sm}$ - $^{142,143}\text{Nd}$ systematics in Eoarchean
1405 supracrustal rocks of the Inukjuak domain (Québec). *Earth and Planetary Science Letters*
1406 457: 23-37.
- 1407 Cawthorn, R.G, 1975. Degrees of melting in mantle diapirs and the origin of ultrabasic
1408 liquids. *Earth and Planetary Science Letters* 27 (1): 113-120.
- 1409 Chase, C.G., Patchett, P.J., 1988. Stored mafic/ultramafic crust and early Archaean mantle
1410 differentiation. *Earth and Planetary Science Letters* 91 (1-2): 66-72.
- 1411 Chou, C.-L., 1978. Fractionation of siderophile elements in the earth's upper mantle.
1412 *Proceedings of the 9th Lunar and Planetary Science Conference*, pp. 219-230.

- 1413 Chou, C.-L., Shaw, D.M., Crocket, J.H., 1983. Siderophile trace elements in the Earth's
1414 oceanic crust and upper mantle. *Journal of Geophysical Research* 88 (S2): A507-A518.
- 1415 Coltice, N. and Schmalzl, J., 2006. Mixing times in the mantle of the early Earth derived from
1416 2-D and 3-D numerical simulations of convection. *Geophysical Research Letters* 33 (23):
1417 L23304.
- 1418 Condie, K.C., 1975. Mantle-plume model for the origin of Archaean greenstone belts based
1419 on trace element distributions. *Nature* 258 (5534): 413-414.
- 1420 Condie, K.C., 1981. *Archaean greenstone belts*. Elsevier, Amsterdam, 434 pp.
- 1421 Condie, K.C., 1994. Greenstones through time. In: Condie, K.C. (Ed.). *Archean Crustal*
1422 *Evolution*. Elsevier, Amsterdam, pp. 85-120.
- 1423 Condie, K.C., 2005. High field strength element ratios in Archean basalts: a window to
1424 evolving sources of mantle plumes? *Lithos* 79 (3-4): 491-504.
- 1425 Cooper, L.B., Ruscitto, D.M., Plank, T., Wallace, P.J., Syracuse, E.M., and Manning, C.E.,
1426 2012. Global variations in H₂O/Ce: 1. Slab surface temperatures beneath volcanic arcs.
1427 *Geochemistry Geophysics Geosystems* 13 (3): Q03024.
- 1428 Corgne, A. and Wood, B.J., 2002. CaSiO₃ and CaTiO₃ perovskite-melt partitioning of trace
1429 elements: Implications for gross mantle differentiation. *Geophysical Research Letters* 29
1430 (19): 39.1-39.4.
- 1431 Corgne, A. and Wood, B.J., 2004. Trace element partitioning between majoritic garnet and
1432 silicate melt at 25 GPa. *Physics of the Earth and Planetary Interiors* 143: 407-419.
- 1433 Corgne, A., Liebske, C., Wood, B.J., Rubie, D.C., and Frost, D.J., 2005. Silicate perovskite-
1434 melt partitioning of trace elements and geochemical signature of a deep perovskitic
1435 reservoir. *Geochimica et Cosmochimica Acta* 69 (2): 485-496.
- 1436 Cottrell, E. and Walker, D., 2006. Constraints on core formation from Pt partitioning in mafic
1437 silicate liquids at high temperatures. *Geochimica et Cosmochimica Acta* 70 (6): 1565-
1438 1580.
- 1439 Courtillot, V., Davaille, A., Besse, J., and Stock, J., 2003. Three distinct types of hotspots in
1440 the Earth's mantle. *Earth and Planetary Science Letters* 205 (3): 295-308.
- 1441 Crocket, J.H., Fleet, M.E., and Stone, W.E., 1997. Implications of composition for
1442 experimental partitioning of platinum-group elements and gold between sulfide liquid and
1443 basalt melt: The significance of nickel content. *Geochimica et Cosmochimica Acta* 61
1444 (19): 4139-4149.
- 1445 Dale, C.W., Kruijer, T.S., and Burton, K.W., 2017. Highly siderophile element and ¹⁸²W
1446 evidence for a partial late veneer in the source of 3.8 Ga rocks from Isua, Greenland.
1447 *Earth and Planetary Science Letters* 458: 394-404.
- 1448 Dauphas, N., Burkhardt, C., Warren, P. H., Fang-Zhen, T., 2014. Geochemical arguments for
1449 an Earth-like Moon-forming impactor. *Philosophical Transactions of the Royal Society*:
1450 **372** (2024): 20130244.
- 1451 Day, J.M.D., Walker, R.J., James, O.B., and Puchtel, I.S., 2010. Osmium isotope and highly
1452 siderophile element systematics of the lunar crust. *Earth and Planetary Science Letters*
1453 289 (3-4): 595-605.
- 1454 Day, J.M.D., 2013. Hotspot volcanism and highly siderophile elements. *Chemical Geology*
1455 341: 50-74.

- 1456 Day, J.M.D., Pearson, D.G., Taylor, L.A., 2007. Highly siderophile element constraints on
1457 accretion and differentiation of the Earth-Moon system. *Science* 315 (5809): 217-219.
- 1458 Day, J.M.D. and Walker, R.J., 2015. Highly siderophile element depletion in the Moon. *Earth*
1459 *and Planetary Science Letters* 423: 114-124.
- 1460 Day, J.M.D., Brandon, A.D., and Walker, R.J., 2016. Highly Siderophile Elements in Earth,
1461 Mars, the Moon, and Asteroids. *Reviews in Mineralogy and Geochemistry* 81 (1): 161-
1462 238.
- 1463 Debaille, V., O'Neill, C., Brandon, A.D., Haenecour, P., Yin, Q.-Z., Mattielli, N., and
1464 Treiman, A.H., 2013. Stagnant-lid tectonics in early Earth revealed by ¹⁴²Nd variations in
1465 late Archean rocks. *Earth and Planetary Science Letters* 373: 83-92.
- 1466 DePaolo, D. J., 1980. Crustal growth and mantle evolution: inferences from models of
1467 element transport and Nd and Sr isotopes. *Geochimica et Cosmochimica Acta* **44** (8):
1468 1185-1196.
- 1469 DePaolo, D.J. and Wasserburg, G.J., 1976. Nd isotopic variations and petrogenetic models.
1470 *Geophysical Research Letters* 3 (5): 249-252.
- 1471 Desrochers, J.-P., Hubert, C., Ludden, J.N., and Pilote, P., 1993. Accretion of Archean
1472 oceanic plateau fragments in the Abitibi greenstone belt, Canada. *Geology* **21** (5): 451-
1473 454.
- 1474 De Wit, M.J. and Ashwal, L.D., 1997. *Greenstone Belts*. Clarendon Press, Oxford, 809 pp.
- 1475 Dostal, J. and Mueller, W.U., 2013. Deciphering an Archean mantle plume: Abitibi
1476 greenstone belt, Canada. *Gondwana Research* 23 (2): 493-505.
- 1477 Drake, M. J., 2000. Accretion and primary differentiation of the Earth: A personal journey.
1478 *Geochimica et Cosmochimica Acta* **64** (14): 2363-2370.
- 1479 Dupré, B., Chauvel, C., and Arndt, N.T., 1984. Pb and Nd isotopic study of two Archean
1480 komatiitic flows from Alexo, Ontario. *Geochimica et Cosmochimica Acta* **48** (10): 1965-
1481 1972.
- 1482 Dziewonski, A.M., Hager, B.H., and O'Connell, R.J., 1977. Large-scale heterogeneities in the
1483 lower mantle. *Journal of Geophysical Research* 82 (2): 239-255.
- 1484 Elkins-Tanton, L.T., Parmentier, E.M., and Hess, P.C., 2003. Magma ocean fractional
1485 crystallization and cumulate overturn in terrestrial planets: Implications for Mars.
1486 *Meteoritics & Planetary Science* 38 (12): 1753-1771.
- 1487 Elkins-Tanton, L.T., 2008. Linked magma ocean solidification and atmospheric growth for
1488 Earth and Mars. *Earth and Planetary Science Letters* 271 (1-4): 181-191.
- 1489 Elkins-Tanton, L.T., 2012. Magma Oceans in the Inner Solar System. *Annual Review of*
1490 *Earth and Planetary Sciences* 40 (1): 113-139.
- 1491 Farnetani, C.G. and Richards, M.A., 1995. Thermal entrainment and melting in mantle
1492 plumes. *Earth and Planetary Science Letters* 136 (4): 251-267.
- 1493 Farnetani, C.G., 1997. Excess temperature of mantle plumes: the role of chemical
1494 stratification across "D". *Geophysical Research Letters* 24 (13): 1583-1586.
- 1495 Fischer-Gödde, M., Becker, H., and Wombacher, F., 2010. Rhodium, gold and other highly
1496 siderophile element abundances in chondritic meteorites. *Geochimica et Cosmochimica*
1497 *Acta* **74** (1): 356-379.

- 1498 Fischer-Gödde, M., Becker, H., Wombacher, F., 2011. Rhodium, gold and other highly
1499 siderophile elements in orogenic peridotites and peridotite xenoliths. *Chemical Geology*
1500 280 (3-4): 365-383.
- 1501 Fletcher, M. and Wyman, D.A., 2015. Mantle plume-subduction zone interactions over the
1502 past 60 Ma. *Lithos* 233: 162-173.
- 1503 Foley, S.F., Barth, M.G., and Jenner, G.A., 2000. Rutile/melt partition coefficients for trace
1504 elements and an assessment of the influence of rutile on the trace element characteristics
1505 of subduction zone magmas. *Geochimica et Cosmochimica Acta* 64 (5): 933-938.
- 1506 Foley, B.J. and Rizo, H., 2017. Long-term preservation of early formed mantle heterogeneity
1507 by mobile lid convection: Importance of grainsize evolution. *Earth and Planetary Science*
1508 *Letters* 475: 94-105.
- 1509 Fortenfant, S.S., Gunther, D., Dingwell, D.B., and Rubie, D.C., 2003. Temperature
1510 dependence of Pt and Rh solubilities in a haplobasaltic melt. *Geochimica et*
1511 *Cosmochimica Acta* 67 (1): 123-131.
- 1512 French, S.W. and Romanowicz, B., 2015. Broad plumes rooted at the base of the Earth's
1513 mantle beneath major hotspots. *Nature* 525 (7567): 95-99.
- 1514 Frost, D. J., Mann, U., Asahara, Y., Rubie, D. C., 2008. The redox state of the mantle during
1515 and just after core formation. *Philosophical Transactions of the Royal Society* **366** (1883):
1516 4315-4337.
- 1517 Galer, S. J. G., Goldstein, S. L., O'Nions, R. K., 1989. Limits on chemical and convective
1518 isolation in the Earth's interior. *Chemical Geology* **75** (4): 257-290.
- 1519 Galer, S. J. G., Goldstein, S. L., 1991. Early mantle differentiation and its thermal
1520 consequences. *Geochimica et Cosmochimica Acta* **55** (1-2): 227-239.
- 1521 Gerya, T., 2014. Precambrian geodynamics: Concepts and models. *Gondwana Research* 25
1522 (2): 442-463.
- 1523 Gangopadhyay, A. and Walker, R.J., 2003. Re-Os systematics of the ca. 2.7 Ga komatiites
1524 from Alexo, Ontario, Canada. *Chemical Geology* 196 (1-4): 147-162.
- 1525 Goldstein, S.L., O'Nions, R.K., and Hamilton, P.J., 1984. A Sm-Nd Isotopic Study of
1526 Atmospheric Dusts and Particulates from Major River Systems. *Earth and Planetary*
1527 *Science Letters* 70 (2): 221-236.
- 1528 Goldstein, S.L., Galer, S.J.G., 1992. On the trail of early mantle differentiation: $^{142}\text{Nd}/^{144}\text{Nd}$
1529 ratios of early Archean rocks. *Eos* **73** (30): 323.
- 1530 Green, D.H., 1975. Genesis of Archean peridotitic magmas and constraints on Archean
1531 geothermal gradients and tectonics. *Geology* 3 (1): 15-18.
- 1532 Green, D.H., 1981. Petrogenesis of Archean ultramafic magmas and implications for Archean
1533 tectonics. In: *Precambrian Plate Tectonics*, Kröner, A. (Ed.), Elsevier, Amsterdam, pp.
1534 469-480.
- 1535 Grove, T.L., de Wit, M.J., and Dann, J., 1997. Komatiites from the Komati type section,
1536 Barberton, South Africa. In: de Wit, M.J. and Ashwal, L.D. (Eds.). *Greenstone Belts*.
1537 Oxford Science Publications, Oxford, pp. 422-437.
- 1538 Grove, T.L. and Parman, S.W., 2004. Thermal evolution of the Earth as recorded by
1539 komatiites. *Earth and Planetary Science Letters* 219 (3-4): 173-187.

- 1540 Hamilton, P.J., O'Nions, R.K., Bridgwater, D., and Nutman, A.P., 1983. Sm-Nd studies of
1541 Archaean metasediments and metavolcanics from West Greenland and their implications
1542 for the Earth's early history. *Earth and Planetary Science Letters* 62 (2): 263-272.
- 1543 Harper, C.L. and Jacobsen, S.B., 1992. Evidence from coupled ^{147}Sm - ^{143}Nd and ^{146}Sm - ^{142}Nd
1544 systematics for very early (4.5-Gyr) differentiation of the Earth's mantle. *Nature* 360
1545 (6406): 728-732.
- 1546 Harper, C.L. and Jacobsen, S.B., 1996. Evidence for ^{182}Hf in the early Solar System and
1547 constraints on the timescale of terrestrial accretion and core formation. *Geochimica et*
1548 *Cosmochimica Acta* 60 (7): 1131-1153.
- 1549 Hart, S. R., Brooks, S., 1977. The geochemistry and evolution of Early Precambrian mantle.
1550 *Contributions to Mineralogy and Petrology* 61 (2): 109-128.
- 1551 Hart, S. R., Zindler, A., 1986. In search of a bulk-earth composition. *Chemical Geology* 57
1552 (3-4): 247-267.
- 1553 Hart, S.R., Hauri, E.H., Oschmann, L.A., and Whitehead, J.A., 1992. Mantle plumes and
1554 entrainment: isotopic evidence. *Science* 256 (5056): 517-520.
- 1555 Hauri, E.H., Gaetani, G.A., and Green, T.H., 2006. Partitioning of water during melting of the
1556 Earth's upper mantle at H_2O -undersaturated conditions. *Earth and Planetary Science Letters* 248 (3-4): 715-734.
- 1557 He, Y., Wen, L., Capdeville, Y., and Zhao, L., 2015. Seismic evidence for an Iceland thermo-
1558 chemical plume in the Earth's lowermost mantle. *Earth and Planetary Science Letters* 417:
1559 19-27.
- 1560 Herzberg, C.T. and Ohtani, E., 1988. Origin of komatiite at high pressures. *Earth and*
1561 *Planetary Science Letters* 88 (3-4): 321-329.
- 1562 Herzberg, C.T., 1992. Depth and degree of melting of komatiites. *Journal of Geophysical*
1563 *Research* 97 (B4): 4521-4540.
- 1564 Herzberg, C.T., 1995. Generation of plume magmas through time: an experimental
1565 perspective. *Chemical Geology* 126 (1): 1-16.
- 1566 Herzberg, C. and O'Hara, M.J., 2002. Plume-associated ultramafic magmas of Phanerozoic
1567 age. *Journal of Petrology* 43 (10): 1857-1883.
- 1568 Herzberg, C., Asimow, P.D., Arndt, N.T., Niu, Y.L., Leshner, C.M., Fitton, J.G., Cheadle,
1569 M.J., and Saunders, A.D., 2007. Temperatures in ambient mantle and plumes: Constraints
1570 from basalts, picrites, and komatiites. *Geochemistry Geophysics Geosystems* 8: Q02006.
- 1571 Herzberg, C. and Gazel, E., 2009. Petrological evidence for secular cooling in mantle plumes.
1572 *Nature* 458 (7238): 619-622.
- 1573 Herzberg, C., Condie, K., and Korenaga, J., 2010. Thermal history of the Earth and its
1574 petrological expression. *Earth and Planetary Science Letters* 292 (1-2): 79-88.
- 1575 Hickman, A. and Kranendonk, M.V., 2012. Early Earth Evolution: Evidence from the 3.5-1.8
1576 Ga Geological History of the Pilbara Region of Western Australia. *Episodes* 35 (1): 283-
1577 297.
- 1578 Hirschmann, M.M., 2018. Comparative deep Earth volatile cycles: The case for C recycling
1579 from exosphere/mantle fractionation of major (H_2O , C, N) volatiles and from $\text{H}_2\text{O}/\text{Ce}$,
1580 CO_2/Ba , and CO_2/Nb exosphere ratios. *Earth and Planetary Science Letters* 502: 262-273.
- 1581 Hoffmann, J.E., Münker, C., Polat, A., Rosing, M.T., and Schulz, T., 2011. The origin of
1582 decoupled Hf-Nd isotope compositions in Eoarchean rocks from southern West
1583 Greenland. *Geochimica et Cosmochimica Acta* 75 (21): 6610-6628.

1584 Hoffmann, J.E. and Wilson, A.H., 2017. The origin of highly radiogenic Hf isotope
1585 compositions in 3.33 Ga Comondale komatiite lavas (South Africa). *Chemical Geology*
1586 455: 6-21.

1587 Hofmann, A.W. and Hart, S., 1978. An assessment of local and regional isotopic equilibrium
1588 in the mantle. *Earth and Planetary Science Letters* 38 (1): 44-62.

1589 Hofmann, A.W. and White, W.M., 1982. Mantle plumes from ancient oceanic crust. *Earth*
1590 *and Planetary Science Letters* 57 (2): 421-436.

1591 Hofmann, A.W., Jochum, K.P., Seufert, M., and White, W.M., 1986. Nb and Pb in oceanic
1592 basalts: New constraints on mantle evolution. *Earth and Planetary Science Letters* 79 (1-
1593 2): 33-45.

1594 Hofmann, A.W., 1988. Chemical differentiation of the Earth: The relationship between
1595 mantle, continental crust and oceanic crust. *Earth and Planetary Science Letters* 90 (3):
1596 297-314.

1597 Horan, M.F., Walker, R.J., Morgan, J.W., Grossman, J.N., and Rubin, A.E., 2003. Highly
1598 siderophile elements in chondrites. *Chemical Geology* **196** (1-4): 5-20.

1599 Horan, M.F., Carlson, R.W., Walker, R.J., Jackson, M., Garçon, M., and Norman, M., 2018.
1600 Tracking Hadean processes in modern basalts with ¹⁴²Neodymium. *Earth and Planetary*
1601 *Science Letters* 484: 184-191.

1602 Humayun, M., 2011. A model for osmium isotopic evolution of metallic solids at the core-
1603 mantle boundary. *Geochemistry Geophysics Geosystems* 12 (3): 1-23.

1604 Huppert, H.E., Sparks, R.S.J., Turner, J.S., and Arndt, N.T., 1984. Emplacement and cooling
1605 of komatiite lavas. *Nature* 309 (5963): 19-22.

1606 Huppert, H.E. and Sparks, R.S.J., 1985. Cooling and contamination of mafic and ultramafic
1607 magmas during ascent through continental crust. *Earth and Planetary Science Letters* 74
1608 (4): 371-386.

1609 Hyung, E. and Jacobsen, S.B., 2020. The ¹⁴²Nd/¹⁴⁴Nd variations in mantle-derived rocks
1610 provide constraints on the stirring rate of the mantle from the Hadean to the present.
1611 *Proceedings of the National Academy of Sciences*: 117 (26): 14738-14744.

1612 Ireland, T.J., Walker, R.J., and Garcia, M.O., 2009. Highly siderophile element and ¹⁸⁷Os
1613 isotope systematics of Hawaiian picrites: Implications for parental melt composition and
1614 source heterogeneity. *Chemical Geology* 260 (1-2): 112-128.

1615 Ito, E., Kubo, A., Katsura, T., Walter, M.J., 2004. Melting experiments of mantle materials
1616 under lower mantle conditions with implications for magma ocean differentiation. *Physics*
1617 *of the Earth and Planetary Interiors* 143: 397-406.

1618 Jackson, M.G. and Carlson, R.W., 2012. Homogeneous superchondritic ¹⁴²Nd/¹⁴⁴Nd in the
1619 mid-ocean ridge basalt and ocean island basalt mantle. *Geochemistry Geophysics*
1620 *Geosystems* 13 (6): Q06011.

1621 Jacobsen, S.B., and Wasserburg, G.J., 1980. Sm-Nd isotopic evolution of chondrites. *Earth*
1622 *and Planetary Science Letters* 50 (1): 139-155.

1623 Jacobsen, S. B., 1988. Isotopic and chemical constraints on mantle-crust evolution.
1624 *Geochimica et Cosmochimica Acta* **52** (6): 1341-1350.

1625 Jacobsen, S.B. and Yu, G., 2015. Extinct isotope heterogeneities in the mantles of Earth and
1626 Mars: Implications for mantle stirring rates. *Meteoritics & Planetary Science* 50 (4): 555-
1627 567.

- 1628 Jahn, B.-M., Gruau, G., and Glikson, A.Y., 1982. Komatiites of the Onverwacht Group, South
1629 Africa: REE geochemistry, Sm-Nd age and mantle evolution. *Contributions to Mineralogy
1630 and Petrology* 80 (1): 25-40.
- 1631 Jamais, M., Lassiter, J.C., and Brüggmann, G., 2008. PGE and Os-isotopic variations in lavas
1632 from Kohala Volcano, Hawaii: Constraints on PGE behavior and melt/crust interaction.
1633 *Chemical Geology* 250 (1-4): 16-28.
- 1634 Jenner, F.E. and O'Neill, H.St.C.C.Q., 2012. Major and trace analysis of basaltic glasses by
1635 laser-ablation ICP-MS. *Geochemistry, Geophysics, Geosystems* 13 (3): Q03003.
- 1636 Jochum, K.P., Arndt, N.T., and Hofmann, A.W., 1991. Nb-Th-La in komatiites and basalts:
1637 constraints on komatiite petrogenesis and mantle evolution. *Earth and Planetary Science
1638 Letters* 107 (2): 272-289.
- 1639 Johnson, T.E., Brown, M., Gardiner, N.J., Kirkland, C.L., and Smithies, R.H., 2017. Earth's
1640 first stable continents did not form by subduction. *Nature* 543 (7644): 239-242.
- 1641 Kato, T., Ringwood, A.E., and Irifune, T., 1988. Experimental determination of element
1642 partitioning between silicate perovskite, garnet and liquid: constraints on early
1643 differentiation of the mantle. *Earth and Planetary Science Letters* 89 (1): 123-145.
- 1644 Kent, R.W., Hardarson, B.S., Saunders, A.D., and Storey, M., 1996. Plateaux ancient and
1645 modern: Geochemical and sedimentological perspectives on Archaean oceanic
1646 magmatism. *Lithos* 37 (2-3): 129-142.
- 1647 Kimura, G., Ludden, J.N., Desrochers, J.-P., and Hori, R., 1993. A model of ocean-crust
1648 accretion for the Superior province, Canada. *Lithos* 30 (3-4): 337-355.
- 1649 Kimura, K., Lewis, R.S., Anders, S., 1974. Distribution of gold and rhenium between nickel-
1650 iron and silicate melts; implications for abundance of siderophile elements on the Earth
1651 and Moon. *Geochimica et Cosmochimica Acta* 38 (5): 683-701.
- 1652 Kleine, T., Münker, C., Mezger, K., Palme, H., 2002. Rapid accretion and early core
1653 formation on asteroids and the terrestrial planets from Hf-W chronometry. *Nature* 418
1654 (6901): 952-955.
- 1655 Kleine, T., Mezger, K., Palme, H., Münker, C., 2004. The W isotope evolution of the bulk
1656 silicate Earth: constraints on the timing and mechanisms of core formation and accretion.
1657 *Earth and Planetary Science Letters* 228 (1-2): 109-123.
- 1658 Kleine, T., Touboul, M., Bourdon, B., Nimmo, F., Mezger, K., Palme, H., Jacobsen, S.B.,
1659 Yin, Q.-Z., and Halliday, A.N., 2009. Hf-W chronology of the accretion and early
1660 evolution of asteroids and terrestrial planets. *Geochimica et Cosmochimica Acta* 73 (17):
1661 5150-5188.
- 1662 Kleine, T., Walker, R. J., 2017. Tungsten Isotopes in Planets. *Annual Review of Earth and
1663 Planetary Sciences* 45 (1): 389-417.
- 1664 König, S., Münker, C., Schuth, S., and Garbe-Schönberg, D., 2008. Mobility of tungsten in
1665 subduction zones. *Earth and Planetary Science Letters* 274 (1-2): 89-92.
- 1666 König, S., Münker, C., Hohl, S., Paulick, H., Barth, A. R., Lagos, M., Pfander, J., Büchl, A.,
1667 2011. The Earth's tungsten budget during mantle melting and crust formation. *Geochimica
1668 et Cosmochimica Acta* 75 (8): 2119-2136.
- 1669 Koppers, A.A.P., Becker, T.W., Jackson, M.G., Konrad, K., Müller, R.D., Romanowicz, B.,
1670 Steinberger, B., and Whittaker, J.M., 2021. Mantle plumes and their role in Earth
1671 processes. *Nature Reviews* 2: 382-401.

1672 Korenaga, J., 2021. Hadean geodynamics and the nature of early continental crust.
1673 *Precambrian Research* 359: 106178.

1674 Kruijjer, T.S., Kleine, T., Fischer-Gödde, M., Sprung, P., 2015. Lunar tungsten isotopic
1675 evidence for the late veneer. *Nature* 520 (7548): 534-537.

1676 Kruijjer, T. S., Kleine, T., 2017. Tungsten isotopes and the origin of the Moon. *Earth and*
1677 *Planetary Science Letters* **475** (Supplement C): 15-24.

1678 Kusky, T.M. and Kidd, W.S.F., 1992. Remnants of an Archean oceanic plateau, Belingwe
1679 greenstone belt, Zimbabwe. *Geology* 20 (1): 43-46.

1680 Labrosse, S., Hernlund, J.W., and Coltice, N., 2007. A crystallizing dense magma ocean at the
1681 base of the Earth's mantle. *Nature* 450 (7171): 866-869.

1682 Lassiter, J.C. and Hauri, E.H., 1998. Osmium-isotope variations in Hawaiian lavas: evidence
1683 for recycled oceanic lithosphere in the Hawaiian plume. *Earth and Planetary Science*
1684 *Letters* 164 (3-4): 483-496.

1685 Lassiter, J.C., 2006. Constraints on the coupled thermal evolution of the Earth's core and
1686 mantle, the age of the inner core, and the origin of the $^{186}\text{Os}/^{188}\text{Os}$ "core signal" in plume-
1687 derived lavas. *Earth and Planetary Science Letters* 250 (1-2): 306-317.

1688 Liebske, C., Corgne, A., Frost, D.J., Rubie, D.C., and Wood, B.J., 2005. Compositional
1689 effects on element partitioning between Mg-silicate perovskite and silicate melts.
1690 *Contributions to Mineralogy and Petrology* 149 (1): 113-128.

1691 Liu, J., Touboul, M., Ishikawa, A., Walker, R.J., and Pearson, D.G., 2016. Widespread
1692 tungsten isotope anomalies and W mobility in crustal and mantle rocks of the Eoarchean
1693 Saglek Block, northern Labrador, Canada: Implications for early Earth processes and W
1694 recycling. *Earth and Planetary Science Letters* 448: 13-23.

1695 Loper, D.E., 1991. Mantle plumes. *Tectonophysics* 187 (4): 373-384.

1696 Maier, W.D., Barnes, S.J., Campbell, I.H., Fiorentini, M.L., Peltonen, P., Barnes, S.-J.,
1697 Smithies, R.H., 2009. Progressive mixing of meteoritic veneer into the early Earth's deep
1698 mantle. *Nature* 460 (7255): 620-623.

1699 Mallmann, G. and O'Neill, H.St.C., 2007. The effect of oxygen fugacity on the partitioning of
1700 Re between crystals and silicate melt during mantle melting. *Geochimica et*
1701 *Cosmochimica Acta* 71 (11): 2837-2857.

1702 Marchi, S., Canup, R.M., Walker, R.J., 2018. Heterogeneous delivery of silicate and metal to
1703 the Earth by large planetesimals. *Nature Geoscience* 11: 77-81.

1704 Marchi, S., Walker, R.J., and Canup, R.M., 2020. A compositionally heterogeneous martian
1705 mantle due to late accretion. *Science Advances* 6 (7): eaay2338.

1706 Maya, J.M., Bhutani, R., Balakrishnan, S., and Rajee Sandhya, S., 2017. Petrogenesis of 3.15
1707 Ga old Banasandra komatiites from the Dharwar craton, India: Implications for early
1708 mantle heterogeneity. *Geoscience Frontiers* 8 (3): 467-481.

1709 McDonough, W.F. and Sun, S.S., 1995. The composition of the Earth. *Chemical Geology* 120
1710 (3-4): 223-253.

1711 McKenzie, D. and Bickle, M.J., 1988. The volume and composition of melt generated by
1712 extension of the lithosphere. *Journal of Petrology* 29 (3): 625-679.

1713 Meisel, T., Walker, R.J., Irving, A.J., Lorand, J.-P., 2001. Osmium isotopic compositions of
1714 mantle xenoliths: A global perspective. *Geochimica et Cosmochimica Acta* 65 (8): 1311-
1715 1323.

- 1716 Michael, P., 1995. Regionally Distinctive Sources of Depleted MORB - Evidence from Trace-
1717 Elements and H₂O. *Earth and Planetary Science Letters* 131 (3-4): 301-320.
- 1718 Mole, D.R., Fiorentini, M.L., Thebaud, N., Cassidy, K.F., McCuaig, T.C., Kirkland, C.L.,
1719 Romano, S.S., Doublier, M.P., Belousova, E.A., Barnes, S.J., and Miller, J., 2014. Archean
1720 komatiite volcanism controlled by the evolution of early continents. *Proceedings of the*
1721 *National Academy of Sciences* 111 (28): 10083-10088.
- 1722 Montelli, R., Nolet, G., Dahlen, F.A., Masters, G., Engdahl, E.R., and Hung, S.-H., 2004.
1723 Finite-Frequency Tomography Reveals a Variety of Plumes in the Mantle. *Science* 303
1724 (5656): 338-343.
- 1725 Moore, J.G., 1970. Water Content of Basalt Erupted on the ocean floor. *Contributions to*
1726 *Mineralogy and Petrology* 28 (4): 272-279.
- 1727 Morino, P., Caro, G., Reisberg, L., and Schumacher, A., 2017. Chemical stratification in the
1728 post-magma ocean Earth inferred from coupled ^{146,147}Sm-^{142,143}Nd systematics in
1729 ultramafic rocks of the Saglek block (3.25-3.9 Ga; northern Labrador, Canada). *Earth and*
1730 *Planetary Science Letters* 463: 136-150.
- 1731 Mundl, A., Touboul, M., Jackson, M.G., Day, J.M.D., Kurz, M.D., Lekic, V., Helz, R.T., and
1732 Walker, R.J., 2017. Tungsten-182 heterogeneity in modern ocean island basalts. *Science*
1733 356 (6333): 66-69.
- 1734 Mundl, A., Walker, R.J., Reimink, J.R., Rudnick, R.L., and Gaschnig, R.M., 2018. Tungsten-
1735 182 in the upper continental crust: Evidence from glacial diamictites. *Chemical Geology*
1736 494: 144-152.
- 1737 Mundl-Petermeier, A., Walker, R.J., Jackson, M.G., Blichert-Toft, J., Kurz, M.D., and
1738 Haldórsson, S.A. (2019) Temporal evolution of primordial tungsten-182 and ³He/⁴He
1739 signatures in the Iceland mantle plume. *Chemical Geology* 525, 245-259.
- 1740 Mundl-Petermeier, A., Walker, R.J., Fischer, R.A., Lekic, V., Jackson, M.G., and Kurz, M.D.,
1741 2020. Anomalous μ¹⁸²W signatures in high ³He/⁴He ocean island basalts – fingerprints of
1742 Earth's core? *Geochimica et Cosmochimica Acta* 271: 194-211.
- 1743 Murphy, D.T., Brandon, A.D., Debaille, V., Burgess, R., and Ballentine, C., 2010. In search
1744 of a hidden long-term isolated sub-chondritic ¹⁴²Nd/¹⁴⁴Nd reservoir in the deep mantle:
1745 Implications for the Nd isotope systematics of the Earth. *Geochimica et Cosmochimica*
1746 *Acta* 74 (2): 738-750.
- 1747 Murphy, D., Rizo, H., O'Neil, J., Hepple, R., Wiemer, D., Kemp, A., and Vervoort, J., 2021.
1748 Combined Sm-Nd, Lu-Hf, and ¹⁴²Nd study of Paleoarchean basalts from the East Pilbara
1749 Terrane, Western Australia. *Chemical Geology* 578: 120301.
- 1750 Nakagawa, T., 2020. A coupled core-mantle evolution: review and future prospects. *Progress*
1751 *in Earth and Planetary Science* 7 (1): 57.
- 1752 Nakanishi, N., Giuliani, A., Carlson, R.W., Horan, M.F., Woodhead, J., Pearson, D. G., and
1753 Walker, R.J., 2021. Tungsten-182 evidence for an ancient kimberlite source. *Proceedings*
1754 *of the National Academy of Sciences* 118 (23): e2020680118.
- 1755 Newsom, H.E., Sims, K.W.W., Noll, P.D., Jaeger, W.L., Maehr, S.A., and Beserra, T.B.,
1756 1996. The depletion of tungsten in the bulk silicate Earth: Constraints on core formation.
1757 *Geochimica et Cosmochimica Acta* 60 (5): 1155-1169.
- 1758 Nicklas, R.W., Puchtel, I.S., and Ash, R.D., 2018. The Redox Evolution of the Archean
1759 Mantle: Evidence from Komatiites. *Geochimica et Cosmochimica Acta* 222: 447-466.

1760 Nicklas, R.W., Puchtel, I.S., Ash, R.D., Piccoli, P.M., Hanski, E., Nisbet, E.G., Waterton, P.,
1761 Pearson, D.G., and Anbar, A.D., 2019. Secular mantle oxidation across the Archean-
1762 Proterozoic boundary: Evidence from V partitioning in komatiites and picrites.
1763 *Geochimica et Cosmochimica Acta* 250: 49-75.

1764 Nesbitt, R.W., Sun, S.S., and Purvis, A.C., 1979. Komatiites: geochemistry and genesis.
1765 *Canadian Mineralogist* 17 (2): 165-186.

1766 Nisbet, E.G., Cheadle, M.J., Arndt, N.T., and Bickle, M.J., 1993. Constraining the potential
1767 temperature of the Archaean mantle: a review of the evidence from komatiites. *Lithos* 30:
1768 291-307.

1769 Ohtani, E., 1984. Generation of komatiite magma and gravitational differentiation in the deep
1770 upper mantle. *Earth and Planetary Science Letters* 67 (2): 261-272.

1771 O'Neil, J., Carlson, R.W., Francis, D., and Stevenson, R.K., 2008. Neodymium-142 evidence
1772 for Hadean mafic crust. *Science* 321 (5897): 1828-1831.

1773 O'Neil, J., Carlson, R.W., Paquette, J.-L., and Francis, D., 2012. Formation age and
1774 metamorphic history of the Nuvvuagittuq Greenstone Belt. *Precambrian Research* 220-
1775 221: 23-44.

1776 O'Neil, J., Rizo, H., Boyet, M., Carlson, R.W., Rosing, M.T., 2016. Geochemistry and Nd
1777 isotopic characteristics of Earth's Hadean mantle and primitive crust. *Earth and Planetary
1778 Science Letters* 442: 194-205.

1779 O'Neill, C. and Debaille, V., 2014. The evolution of Hadean-Eoarchean geodynamics. *Earth
1780 and Planetary Science Letters* 406: 49-58.

1781 Parman, S.W., Dann, J.C., Grove, T.L., and de Wit, M.J., 1997. Emplacement conditions of
1782 komatiite magmas from the 3.49 Ga Komati Formation, Barberton greenstone belt, South
1783 Africa. *Earth and Planetary Science Letters* 150 (3-4): 303-323.

1784 Parman, S.W., Grove, T.L., and Dann, J.C., 2001. The production of Barberton komatiites in
1785 an Archean subduction zone. *Geophysical Research Letters* 28 (13): 2513-2516.

1786 Parman, S.W., Grove, T.L., Dann, J.C., and de Wit, M.J., 2004. *South African Journal of
1787 Geology* 107 (1-2): 107-118.

1788 Patchett, P.J. and Tatsumoto, M., 1980. Hafnium isotope variations in oceanic basalts.
1789 *Geophysical Research Letters* 7 (12): 1077-1080.

1790 Patchett, P.J., Kauvo, O., Hedge, C.E., and Tatsumoto, M., 1981. Evolution of continental
1791 crust and mantle heterogeneity: evidence from Hf isotopes. *Contributions to Mineralogy
1792 and Petrology* 78 (3): 279-297.

1793 Patchett, P. J., White, W. M., Feldmann, H., Kielinczuk, S., Hofmann, A. W., 1984.
1794 Hafnium/rare earth element fractionation in the sedimentary system and crustal recycling
1795 into the Earth's mantle. *Earth and Planetary Science Letters* 69 (2): 365-378.

1796 Peters, B.J., Carlson, R.W., Day, J.M.D., and Horan, M.F., 2018. Hadean silicate
1797 differentiation preserved by anomalous ¹⁴²Nd/¹⁴⁴Nd ratios in the Réunion hotspot source.
1798 *Nature* 555: 89-106.

1799 Peters, B.J., Mundl-Petermeier, A., Carlson, R.W., Walker, R.J., and Day, J.M.D., 2021.
1800 Combined lithophile-siderophile isotopic constraints on Hadean processes preserved in
1801 ocean island basalt sources. *Geochemistry, Geophysics, Geosystems* 22 (3):
1802 e2020GC009479.

1803 Puchtel, I.S., Hofmann, A.W., Mezger, K., Jochum, K.P., Shchipansky, A.A., and Samsonov,
1804 A.V., 1998. Oceanic plateau model for continental crustal growth in the Archaean: A case
1805 study from the Kostomuksha greenstone belt, NW Baltic Shield. *Earth and Planetary*
1806 *Science Letters* 155 (1-2): 57-74.

1807 Puchtel, I.S. and Humayun, M., 2000. Platinum group elements in Kostomuksha komatiites
1808 and basalts: Implications for oceanic crust recycling and core-mantle interaction.
1809 *Geochimica et Cosmochimica Acta* 64 (24): 4227-4242.

1810 Puchtel, I.S., Brandon, A.D., and Humayun, M., 2004a. Precise Pt-Re-Os isotope systematics
1811 of the mantle from 2.7-Ga komatiites. *Earth and Planetary Science Letters* 224 (1-2): 157-
1812 174.

1813 Puchtel, I.S., Humayun, M., Campbell, A., Sproule, R., and Lesher, C.M., 2004b. Platinum
1814 group element geochemistry of komatiites from the Alexo and Pyke Hill areas, Ontario,
1815 Canada. *Geochimica et Cosmochimica Acta* 68 (6): 1361-1383.

1816 Puchtel, I.S. and Humayun, M., 2005. Highly siderophile element geochemistry of ¹⁸⁷Os-
1817 enriched 2.8-Ga Kostomuksha komatiites, Baltic Shield. *Geochimica et Cosmochimica*
1818 *Acta* 69 (6): 1607-1618.

1819 Puchtel, I.S., Brandon, A.D., Humayun, M., and Walker, R.J., 2005. Evidence for the early
1820 differentiation of the core from Pt-Re-Os isotope systematics of 2.8-Ga komatiites. *Earth*
1821 *and Planetary Science Letters* 237 (1-2): 118-134.

1822 Puchtel, I.S., Humayun, M., and Walker, R.J., 2007. Os-Pb-Nd isotope and highly siderophile
1823 and lithophile trace element systematics of komatiitic rocks from the Volotsk suite, SE
1824 Baltic Shield. *Precambrian Research* 158 (1-2): 119-137.

1825 Puchtel, I.S., Walker, R.J., Brandon, A.D., and Nisbet, E.G., 2009a. Pt-Re-Os and Sm-Nd
1826 isotope and HSE and REE systematics of the 2.7 Ga Belingwe and Abitibi komatiites.
1827 *Geochimica et Cosmochimica Acta* 73 (20): 6367-6389.

1828 Puchtel, I. S., Walker, R. J., Anhaeusser, C. R., Gruau, G., 2009b. Re-Os isotope systematics
1829 and HSE abundances of the 3.5 Ga Schapenburg komatiites, South Africa: Hydrous
1830 melting or prolonged survival of primordial heterogeneities in the mantle? *Chemical*
1831 *Geology* **262** (3-4): 355-369.

1832 Puchtel, I.S., Blichert-Toft, J., Touboul, M., Walker, R.J., Byerly, G., Nisbet, E.G., and
1833 Anhaeusser, C.R., 2013. Insights into early Earth from Barberton komatiites: Evidence
1834 from lithophile isotope and trace element systematics. *Geochimica et Cosmochimica Acta*
1835 108: 63-90.

1836 Puchtel, I.S., Walker, R.J., Touboul, M., Nisbet, E.G., and Byerly, G.R., 2014. Insights into
1837 early Earth from the Pt-Re-Os isotope and highly siderophile element abundance
1838 systematics of Barberton komatiites. *Geochimica et Cosmochimica Acta* 125: 394-413.

1839 Puchtel, I.S., Blichert-Toft, J., Touboul, M., Horan, M.F., and Walker, R.J., 2016a. The
1840 coupled ¹⁸²W-¹⁴²Nd record of early terrestrial mantle differentiation. *Geochemistry,*
1841 *Geophysics, Geosystems* 17 (6): 2168-2193.

1842 Puchtel, I.S., Touboul, M., Blichert-Toft, J., Walker, R.J., Brandon, A.D., Nicklas, R.W.,
1843 Kulikov, V.S., and Samsonov, A.V., 2016b. Lithophile and siderophile element
1844 systematics of the mantle at the Archean-Proterozoic boundary: Evidence from 2.4 Ga
1845 komatiites. *Geochimica et Cosmochimica Acta* 180: 227-255.

- 1846 Puchtel, I.S., Blichert-Toft, J., Touboul, M., and Walker, R.J., 2018. ^{182}W and HSE
1847 constraints from 2.7 Ga komatiites on the heterogeneous nature of the Archean mantle.
1848 *Geochimica et Cosmochimica Acta* 228: 1-26.
- 1849 Puchtel, I.S., Mundl-Petermeier, A., Horan, M., Hanski, E.J., Blichert-Toft, J., and Walker,
1850 R.J., 2020. Ultra-depleted 2.05 Ga komatiites of Finnish Lapland: Products of grainy late
1851 accretion or core-mantle interaction? *Chemical Geology* 554: 119801.
- 1852 Puchtel I.S., Nicklas R.W., Slagle J., Horan M., Walker R.J., Nisbet E.G., and Locmelis M.,
1853 2022. Early global mantle chemical and isotope heterogeneity revealed by the komatiite-
1854 basalt record: The Western Australia connection. *Geochimica et Cosmochimica Acta* (in
1855 press).
- 1856 Rehkämper, M., Halliday, A.N., Fitton, J.G., Lee, D.-C., Wieneke, M., and Arndt, N.T., 1999.
1857 Ir, Ru, Pt and Pd in basalts and komatiites: New constraints for the geochemical behavior
1858 of the platinum group elements in the mantle. *Geochimica et Cosmochimica Acta* 63 (22):
1859 3915-3934.
- 1860 Reimink, J.R., Chacko, T., Carlson, R.W., Shirey, S.B., Liu, J., Stern, R.A., Bauer, A.M.,
1861 Pearson, D.G., and Heaman, L.M., 2018. Petrogenesis and tectonics of the Acasta Gneiss
1862 Complex derived from integrated petrology and ^{142}Nd and ^{182}W extinct nuclide-
1863 geochemistry. *Earth and Planetary Science Letters* 494: 12-22.
- 1864 Reimink, J.R., Mundl-Petermeier, A., Carlson, R. W., Shirey, S.B., Walker, R.J., and Pearson,
1865 D.G., 2020. Tungsten isotope composition of Archean crustal reservoirs and implications
1866 for terrestrial $\mu^{182}\text{W}$ evolution. *Geochemistry, Geophysics, Geosystems* 21 (7):
1867 e2020GC009155.
- 1868 Richard, D., Marty, B., Chaussidon, M., and Arndt, N.T., 1996. Helium isotopic evidence for
1869 a lower mantle component in depleted Archean komatiite. *Science* 273 (5271): 93-95.
- 1870 Richards, M.A., Jones, D.L., Duncan, R.A., and DePaolo, D.J., 1991. A mantle plume
1871 initiation model for the Wrangellia flood basalt and other oceanic plateaus. *Science* 254
1872 (5029): 263-265.
- 1873 Richter, F.M., 1985. Models for the Archean Thermal Regime. *Earth and Planetary Science*
1874 *Letters* 73 (2-4): 350-360.
- 1875 Richter, F.M., 1988. A major change in the thermal state of the Earth at the Archean-
1876 Proterozoic boundary: Consequences for the nature and preservation of continental
1877 lithosphere. *Journal of Petrology, Special Lithosphere Issue*: 39-52.
- 1878 Righter, K. and Drake, M.J., 1997. Metal-silicate equilibrium in a homogeneously accreting
1879 earth: new results for Re. *Earth and Planetary Science Letters* 146 (3-4): 541-553.
- 1880 Righter, K., Walker, R.J., and Warren, P.H., 2000. Significance of highly siderophile
1881 elements and osmium isotopes in the lunar and terrestrial mantles. In: Righter, K. and
1882 Canup, R.M. (Eds.). *Origin of the Earth and Moon*. University of Arizona Press. Tucson,
1883 AZ, 291-322.
- 1884 Rizo, H., Boyet, M., Blichert-Toft, J., Rosing, M., 2011. Combined Nd and Hf isotope
1885 evidence for deep-seated source of Isua lavas. *Earth and Planetary Science Letters* 312 (3-
1886 4): 267-279.
- 1887 Rizo, H., Boyet, M., Blichert-Toft, J., O'Neil, J., Rosing, M.T., and Paquette, J.-L., 2012. The
1888 elusive Hadean enriched reservoir revealed by ^{142}Nd deficits in Isua Archaean rocks.
1889 *Nature* 491 (7422): 96-100.

- 1890 Rizo, H., Boyet, M., Blichert-Toft, J., and Rosing, M.T., 2013. Early mantle dynamics
1891 inferred from ^{142}Nd variations in Archean rocks from southwest Greenland. *Earth and*
1892 *Planetary Science Letters* 377-378: 324-335.
- 1893 Rizo, H., Walker, R.J., Carlson, R.W., Touboul, M., Horan, M.F., Puchtel, I.S., Boyet, M.,
1894 and Rosing, M.T., 2016. Early Earth differentiation investigated through ^{142}Nd , ^{182}W , and
1895 highly siderophile element abundances in samples from Isua, Greenland. *Geochimica et*
1896 *Cosmochimica Acta* **175**: 319-336.
- 1897 Rizo H., Andrault D., Bennett N.R., Humayun M., Brandon A.D., Vlastelic I., Moine B.,
1898 Poirier A., Bouhifd M.A., and Murphy D.T., 2019. ^{182}W evidence for core-mantle
1899 interaction in the source of mantle plumes. *Geochemical Perspectives Letters* 11: 6-11.
- 1900 Rosas, J.C. and Korenaga, J., 2018. Rapid crustal growth and efficient crustal recycling in the
1901 early Earth: Implications for Hadean and Archean geodynamics. *Earth and Planetary*
1902 *Science Letters* 494: 42-49.
- 1903 Roth, A.S.G., Bourdon, B., Mojzsis, S.J., Touboul, M., Sprung, P., Guitreau, M., and
1904 Blichert-Toft, J., 2013. Inherited ^{142}Nd anomalies in Eoarchean protoliths. *Earth and*
1905 *Planetary Science Letters* 361: 50-57.
- 1906 Roth, A.S.G., Bourdon, B., Mojzsis, S.J., Rudge, J.F., Guitreau, M., and Blichert-Toft, J.,
1907 2014. Combined $^{147,146}\text{Sm}$ - $^{143,142}\text{Nd}$ constraints on the longevity and residence time of
1908 early terrestrial crust. *Geochemistry, Geophysics, Geosystems* 15 (6): 2329-2345.
- 1909 Roy-Barman, M. and Allègre, C.-J., 1995. $^{187}\text{Os}/^{186}\text{Os}$ in oceanic island basalts: tracing
1910 oceanic crust recycling in the mantle. *Earth and Planetary Science Letters* 129 (1-4): 145-
1911 161.
- 1912 Rubie, D.C., Frost, D.J., Mann, U., Asahara, Y., Nimmo, F., Tsuno, K., Kegler, P., Holzheid,
1913 A., and Palme, H., 2011. Heterogeneous accretion, composition and core-mantle
1914 differentiation of the Earth. *Earth and Planetary Science Letters* 301 (1-2): 31-42.
- 1915 Rudnick, R.L., Barth, M., Horn, I., and McDonough, W.F., 2000. Rutile-bearing refractory
1916 eclogites: missing link between continents and depleted mantle. *Science* 287 (5451): 278-
1917 281.
- 1918 Rudnick, R.L. and Gao, S., 2014. Composition of the Continental Crust. *Treatise on*
1919 *Geochemistry*: 1-51.
- 1920 Ryder, G., 2002. Mass flux in the ancient Earth-Moon system and benign implications for the
1921 origin of life on Earth. *Journal of Geophysical Research* 107 (E4): 6.1-6.13.
- 1922 Saal, A.E., Hauri, E.H., Langmuir, C.H., and Perfit, M.R., 2002. Vapour undersaturation in
1923 primitive mid-ocean-ridge basalt and the volatile content of Earth's upper mantle. *Nature*
1924 419 (6906): 451-455.
- 1925 Saji, N.S., Larsen, K., Wielandt, D., Schiller, M., Costa, M.M., Whitehouse, M.J., Rosing,
1926 M.T., and Bizzarro, M., 2018. Hadean geodynamics inferred from time-varying
1927 $^{142}\text{Nd}/^{144}\text{Nd}$ in the early Earth rock record. *Geochemical Perspectives Letters* 7: 43-48.
- 1928 Salters, V. J. M., White, W. M., 1998. Hf isotope constraints on mantle evolution. *Chemical*
1929 *Geology* **145** (3-4): 447-460.
- 1930 Schneider, K.P., Hoffmann, J.E., Boyet, M., Münker, C., and Kröner, A., 2018. Coexistence
1931 of enriched and modern-like ^{142}Nd signatures in Archean igneous rocks of the eastern
1932 Kaapvaal Craton, southern Africa. *Earth and Planetary Science Letters* 487: 54-66.

- 1933 Schoenberg, R., Kamber, B. S., Collerson, K. D., Eugster, O., 2002. New W-isotope evidence
 1934 for rapid terrestrial accretion and very early core formation. *Geochimica et Cosmochimica*
 1935 *Acta* **66** (17): 3151-3160.
- 1936 Schubert, G. and Sandwell, D., 1989. Crustal volumes of the continents and of oceanic and
 1937 continental submarine plateaus. *Earth and Planetary Science Letters* **92** (2): 234-246.
- 1938 Shirey, S.B. and Hanson, G.N., 1986. Mantle heterogeneity and crustal recycling in Archean
 1939 granite-greenstone belts: Evidence from Nd isotopes and trace elements in the Rainy Lake
 1940 area, Superior Province, Ontario, Canada. *Geochimica et Cosmochimica Acta* **50** (12):
 1941 2631-2651.
- 1942 Shirey, S. B., Walker, R. J., 1998. The Re-Os isotope system in cosmochemistry and high-
 1943 temperature geochemistry. *Annual Reviews of Earth and Planetary Sciences* **26**: 423-500.
- 1944 Shirey, S.B., Kamber, B.S., Whitehouse, M.J., Mueller, P.A., and Basu, A.R., 2008. A review
 1945 of the isotopic and trace element evidence for mantle and crustal processes in the Hadean
 1946 and Archean: Implications for the onset of plate tectonic subduction. In: Condie, K.C. and
 1947 Pease, V. (Eds.), *When Did Plate Tectonics Begin on Planet Earth?* Geological Society of
 1948 America Special Paper 440: 1-29.
- 1949 Sivell, W.J. and McCulloch, M.T., 1991. Neodymium isotope evidence for ultra-depleted
 1950 mantle in the early Proterozoic. *Nature* **354** (6352): 384-387.
- 1951 Sizova, E., Gerya, T., Stüwe, K., and Brown, M., 2015. Generation of felsic crust in the
 1952 Archean: A geodynamic modeling perspective. *Precambrian Research* **271**: 198-224.
- 1953 Smithies, R.H., Champion, D.C., Van Kranendonk, M.J., and Hickman, A.H., 2007.
 1954 Geochemistry of volcanic rocks of the northern Pilbara Craton, Western Australia.
 1955 Geological Survey of Western Australia, Report 104. Perth, 47 pp.
- 1956 Sobolev, A.V., Asafov, E.V., Gurenko, A.A., Arndt, N.T., Batanova, V.G., Portnyagin, M.V.,
 1957 Garbe-Schönberg, D., and Krashennikov, S.P., 2016. Komatiites reveal a hydrous
 1958 Archean deep-mantle reservoir. *Nature* **531** (7596): 628-632.
- 1959 Sobolev, A.V., Asafov, E.V., Gurenko, A.A., Arndt, N.T., Batanova, V.G., Portnyagin, M.V.,
 1960 Garbe-Schönberg, D., Wilson, A.H., and Byerly, G.R., 2019. Deep hydrous mantle
 1961 reservoir provides evidence for crustal recycling before 3.3 billion years ago. *Nature* **571**
 1962 (7766): 555-559.
- 1963 Sossi, P.A., Eggins, S.M., Nesbitt, R.W., Nebel, O., Hergt, J.M., Campbell, I.H., O'Neill,
 1964 H.St.C., Van Kranendonk, M., and Davies, D.R., 2016. Petrogenesis and Geochemistry of
 1965 Archean Komatiites. *Journal of Petrology* **57** (1): 147-184.
- 1966 Storey, M., Mahoney, J.J., Kroenke, L.W., and Saunders, A.D., 1991. Are oceanic plateaus
 1967 sites of komatiite formation? *Geology* **19** (4): 376-379.
- 1968 Strom, R.G., Malhotra, R., Ito, T., Yoshida, F., and Kring, D.A., 2005. The origin of planetary
 1969 impactors in the inner Solar system. *Science* **309** (5742): 1847-1850.
- 1970 Tonks, W.B. and Melosh, H.J., 1993. Magma Ocean Formation Due to Giant Impacts. *Journal*
 1971 *of Geophysical Research* **98** (E3): 5319-5333.
- 1972 Torsvik, T.H., Steinberger, B., Ashwal, L.D., Doubrovine, P.V., and Trønnes, R.G., 2016.
 1973 Earth evolution and dynamics - a tribute to Kevin Burke. *Canadian Journal of Earth*
 1974 *Sciences* **53** (11): 1073-1087.
- 1975 Touboul, M., Puchtel, I.S., and Walker, R.J., 2012. ¹⁸²W Evidence for Long-Term
 1976 Preservation of Early Mantle Differentiation Products. *Science* **335**: 1065-1069.

- 1977 Touboul, M., Liu, J., O'Neil, J., Puchtel, I.S., and Walker, R.J., 2014. New Insights into the
1978 Hadean Mantle Revealed by ^{182}W and Highly Siderophile Element Abundances of
1979 Supracrustal Rocks from the Nuvvuagittuq Greenstone Belt, Quebec, Canada. *Chemical*
1980 *Geology* 383: 63-75.
- 1981 Touboul, M., Puchtel, I.S., and Walker, R.J., 2015. Tungsten isotopic evidence for
1982 disproportional late accretion to the Earth and Moon. *Nature* 520 (7548): 530-533.
- 1983 Trønnes, R.G. and Frost, D.J., 2002. Peridotite melting and mineral-melt partitioning of major
1984 and minor elements at 22-24.5 GPa. *Earth and Planetary Science Letters* 197 (1-2): 117-
1985 131.
- 1986 Turekian, K.K. and Clark, S.P., 1969. Inhomogeneous accumulation of the earth from the
1987 primitive solar nebula. *Earth and Planetary Science Letters* 6 (5): 346-348.
- 1988 Tusch, J., Sprung, P., van de Löcht, J., Hoffmann, J.E., Boyd, A.J., Rosing, M.T., and
1989 Münker, C., 2019. Uniform ^{182}W isotope compositions in Eoarchean rocks from the Isua
1990 region, SW Greenland: The role of early silicate differentiation and missing late veneer.
1991 *Geochimica et Cosmochimica Acta* 257: 284-310.
- 1992 Tusch, J., Münker, C., Hasenstab, E., Jansen, M., Marien, C. S., Kurzweil, F., Van
1993 Kranendonk, M. J., Smithies, H., Maier, W., and Garbe-Schönberg, D., 2021. Convective
1994 isolation of Hadean mantle reservoirs through Archean time. *Proceedings of the National*
1995 *Academy of Sciences* 118 (2): e2012626118.
- 1996 Van Kranendonk, M.J., 2008. Two types of Archean continental crust: Plume and plate
1997 tectonics on early Earth. *American Journal of Science* 310 (10): 1187-1210.
- 1998 Vervoort, J.D. and Blichert-Toft, J., 1999. Evolution of the depleted mantle: Hf isotope
1999 evidence from juvenile rocks through time. *Geochimica et Cosmochimica Acta* 63 (3-4):
2000 533-556.
- 2001 Vervoort, J.D., Patchett, P.J., Blichert-Toft, J., and Albarède, F., 1999. Relationships between
2002 Lu-Hf and Sm-Nd isotopic systems in the global sedimentary system. *Earth and Planetary*
2003 *Science Letters* 168 (1-2): 79-99.
- 2004 Vervoort, J.D., Patchett, P.J., Albarède, F., Blichert-Toft, J., Rudnick, R., and Downes, H.,
2005 2000. Hf-Nd isotopic evolution of the lower crust. *Earth and Planetary Science Letters*
2006 181 (1-2): 115-129.
- 2007 Viljoen, M.J. and Viljoen, R.P., 1969. The geology and geochemistry of the Lower
2008 Ultramafic Unit of the Onverwacht Group and a proposed new class of igneous rocks.
2009 *Geological Society of South Africa Special Publication* 2: 55-86.
- 2010 Wade, J. and Wood, B.J., 2005. Core formation and the oxidation state of the Earth. *Earth and*
2011 *Planetary Science Letters* 236 (1-2): 78-95.
- 2012 Walker, R.J., Shirey, S.B., and Stecher, O., 1988. Comparative Re-Os, Sm-Nd and Rb-Sr
2013 isotope and trace element systematics for Archean komatiite flows from Munro Township,
2014 Abitibi belt, Ontario. *Earth and Planetary Science Letters* 87 (1-2): 1-12.
- 2015 Walker, R.J., Morgan, J.W., and Horan, M.F., 1995. ^{187}Os enrichment in some plumes:
2016 evidence for core-mantle interaction? *Science* 269 (5225): 819-822.
- 2017 Walker, R.J., Morgan, J.W., Beary, E.S., Smoliar, M.I., Czamanske, G.K., and Horan, M.F.,
2018 1997. Applications of the ^{190}Pt - ^{186}Os isotope system to geochemistry and cosmochemistry.
2019 *Geochimica et Cosmochimica Acta* 61 (22): 4799-4807.

2020 Walker, R. J., Horan, M. F., Morgan, J. W., Becker, H., Grossman, J. N., Rubin, A. E., 2002.
2021 Comparative ^{187}Re - ^{187}Os systematics of chondrites: Implications regarding early solar
2022 system processes. *Geochimica et Cosmochimica Acta* **66** (23): 4187-4201.

2023 Walker, R.J., Horan, M.F., Shearer, C.K., and Papike, J.J., 2004. Low abundances of highly
2024 siderophile elements in the lunar mantle: Evidence for prolonged late accretion. *Earth and*
2025 *Planetary Science Letters* 224 (3-4): 399-413.

2026 Walker, R.J., 2009. Highly siderophile elements in the Earth, Moon and Mars: Update and
2027 implications for planetary accretion and differentiation. *Chemie der Erde - Geochemistry*
2028 69 (2): 101-125.

2029 Walker, R.J., 2014. Siderophile element constraints on the origin of the Moon. *Philosophical*
2030 *Transactions of the Royal Society of London* 372: 20130258.

2031 Walker, R.J., 2016. Siderophile Elements in Tracing Planetary Formation and Evolution.
2032 *Geochemical Perspectives* 5 (1): 1-145.

2033 Walter, M.J., Nakamura, E., Trønnes, R.G., and Frost, D.J., 2004. Experimental constraints on
2034 crystallization differentiation in a deep magma ocean. *Geochimica et Cosmochimica Acta*
2035 68 (20): 4267-4284.

2036 White, W.M. and Patchett, J., 1984. Hf-Nd-Sr isotopes and incompatible element abundances
2037 in island arcs: implications for magma origins and crust-mantle evolution. *Earth and*
2038 *Planetary Science Letters* 67 (2): 167-185.

2039 Widom, E., 1997. Sources of ocean island basalts: A review of the osmium isotope evidence.
2040 *Physica A: Statistical Mechanics and its Applications* 244 (1-4): 484-496.

2041 Willbold, M., Elliott, T., and Moorbath, S., 2011. The tungsten isotopic composition of the
2042 Earth's mantle before the terminal bombardment. *Nature* 477 (7363): 195-198.

2043 Willbold, M., Mojzsis, S.J., Chen, H.W., and Elliott, T., 2015. Tungsten isotope composition
2044 of the Acasta Gneiss Complex. *Earth and Planetary Science Letters* 419: 168-177.

2045 Willig, M. and Stracke, A., 2019. Earth's chondritic light rare earth element composition:
2046 Evidence from the Ce-Nd isotope systematics of chondrites and oceanic basalts. *Earth and*
2047 *Planetary Science Letters* 509: 55-65.

2048 Willig, M., Stracke, A., Beier, C., and Salters, V.J.M., 2020. Constraints on mantle evolution
2049 from Ce-Nd-Hf isotope systematics. *Geochimica et Cosmochimica Acta* 272: 36-53.

2050 Wilson, A.H. and Carlson, R.W., 1989. A Sm-Nd and Pb isotope study of Archaean
2051 greenstone belts in the southern Kaapvaal Craton, South Africa. *Earth and Planetary*
2052 *Science Letters* 96 (1-2): 89-105.

2053 Wyman, D.A., 2013. A critical assessment of Neoproterozoic "plume only" geodynamics:
2054 Evidence from the Superior Province. *Precambrian Research* 229: 3-19.

2055 Wyman, D., 2019. Do cratons preserve evidence of stagnant lid tectonics? *Geoscience*
2056 *Frontiers* 9 (1): 3-17.

2057 Wyman, D., 2020. Komatiites From Mantle Transition Zone Plumes. *Frontiers in Earth*
2058 *Science* **8** (383): 540744.

2059 Yin, Q., Jacobsen, S.B., Yamashita, K., Blichert-Toft, J., Telouk, P., Albarede, F., 2002. A
2060 short timescale for terrestrial planet formation from Hf-W chronometry of meteorites.
2061 *Nature* **418** (6901): 949-952.

2062 Yokoyama, T., Walker, D., and Walker, R.J., 2009. Low osmium solubility in silicate at high
2063 pressures and temperatures. *Earth and Planetary Science Letters* 279 (3-4): 165-173.

2064 Young, E.D., Kohl, I.E., Warren, P.H., Rubie, D.C., Jacobson, S.A., and Morbidelli, A., 2016.
2065 Oxygen isotopic evidence for vigorous mixing during the Moon-forming giant impact.
2066 Science 351 (6272): 493-496.
2067 Zindler, A., Jagoutz, E., Goldstein, S. L., 1982. Nd, Sr and Pb isotopic systematics in a three-
2068 component mantle: a new perspective. Nature **298** (5874): 519-523.
2069 Zindler, A., Hart, S. R., 1986. Chemical Geodynamics. Annual Reviews of Earth and
2070 Planetary Sciences **14**: 493-571.
2071
2072

2073 **Figure captions**

2074 **Fig. 1.** Variations of model-specific (see the references below for the specific models
2075 used), time-integrated Sm/Nd and Lu/Hf ratios in the mantle sources of Archean and
2076 Proterozoic komatiite-basalt systems studied to date. The individual models assume a
2077 minimum-degree fractionation of Sm/Nd and Lu/Hf in the particular mantle domains from
2078 either the chondritic values or values defined by the combined $^{142,143}\text{Nd}/^{144}\text{Nd}$ systematics
2079 (where available) to those required to bring the $\epsilon^{143}\text{Nd}$ and $\epsilon^{176}\text{Hf}$ in the mantle sources to the
2080 initial $\epsilon^{143}\text{Nd}$ and $\epsilon^{176}\text{Hf}$ by the times of the respective komatiite formation. The solid line
2081 connects Sm/Nd and Lu/Hf ratios inferred for the chondritic uniform reservoir (CHUR) and
2082 modern depleted mantle (DMM). Data are from: Ottawa – Blichert-Toft and Arndt (1999);
2083 2.05 Ga Lapland – Puchtel et al. (2020); 2.41 Ga Vetreny – Puchtel et al. (2016b); 2.72 Ga
2084 Pyke Hill and Alexo – Dupre et al. (1984), Walker et al. (1988), Blichert-Toft and Arndt
2085 (1999); 2.72 Ga Boston Creek – Puchtel et al. (2018); 2.82 Ga Kostomuksha – Puchtel et al.
2086 (1998), Blichert-Toft and Puchtel (2010); 3.48 Ga Komati and 3.26 Ga Weltevreden –
2087 Puchtel et al. (2013); 3.32 Ga Comondale – Wilson and Carlson (1989), Hoffmann and
2088 Wilson (2017); 3.55 Ga Schapenburg – Puchtel et al. (2009a, 2016a); 3.53 Ga Coonterunah,
2089 3.34 Ga Kelly, and 3.18 Ga Ruth Well and Regal – Puchtel et al. (2022). The CHUR and
2090 DMM parameters are from Jacobsen and Wasserburg (1980), Hamilton et al. (1983),
2091 Goldstein et al. (1984), Vervoort and Blichert-Toft (1999), and Bouvier et al. (2008). All
2092 uncertainties are 2SD of the mean.

2093 **Fig. 2. (a)** Initial $^{187}\text{Os}/^{188}\text{Os}$ expressed as $\gamma^{187}\text{Os}$ and **(b)** initial $^{186}\text{Os}/^{188}\text{Os}$ expressed as
2094 $\mu^{186}\text{Os}$ of Archean komatiite systems studied to date, plotted as a function of their age. The
2095 blue bars for the modern BSE estimates represent the 2SD of the mean from Meisel et al.
2096 (2001) and Brandon et al. (2006) for (a) and (b), respectively. Data are from: 2.05 Ga Lapland
2097 – Puchtel et al. (2020); 2.41 Ga Vetreny – Puchtel et al. (2016b); 2.69 Ga Belingwe and 2.72
2098 Ga Pyke Hill – Puchtel et al. (2009a); 2.72 Ga Boston Creek – Puchtel et al. (2018); 2.82 Ga
2099 Kostomuksha – Puchtel et al. (2005); 2.88 Ga Volotsk – Puchtel et al. (2007); 3.48 Ga
2100 Komati and 3.26 Ga Weltevreden – Puchtel et al. (2014); 3.55 Ga Schapenburg – Puchtel et
2101 al. (2009b, 2016a); 3.34 Ga Kelly and 3.18 Ga Ruth Well and Regal – Puchtel et al. (2022).
2102 The data for chondritic meteorites are compiled from Walker et al. (2002), Horan et al.
2103 (2003), Brandon et al. (2005; 2006), and Fischer-Gödde et al. (2010) and are plotted as an
2104 envelope enclosed between the slanting purple lines and corresponding to the entire range of
2105 calculated modern $\gamma^{187}\text{Os}$ and $\mu^{186}\text{Os}$ values projected back to the Solar System initial
2106 $^{187}\text{Os}/^{188}\text{Os}$ and $^{186}\text{Os}/^{188}\text{Os}$ ratios. All uncertainties are 2SD of the mean.

2107 **Fig. 3.** Calculated total HSE abundances in the sources of Archean and Paleoproterozoic
2108 komatiite systems plotted as *percent* of those in estimates of the modern BSE of Becker et al.
2109 (2006). The blue dashed lines correspond to the range for the BSE estimates from Becker et
2110 al. (2006). The dark-red arrow represents the regression line through the data. The dark-red
2111 vertical arrows represent the projections to the x-axis from the intersections of the regression
2112 line with the range for the BSE estimate, thus, illustrating the uncertainties on the average
2113 time of homogenization of late accreted materials within the mantle (2.5 ± 0.2 Ga). Data are

2114 from: 2.05 Ga Lapland – Puchtel et al. (2020); 2.41 Ga Vetreny Belt – Puchtel et al. (2016b);
2115 2.69 Ga Belingwe – Puchtel et al. (2009a); 2.72 Ga Pyke Hill and Alexo – Puchtel et al.
2116 (2004b, 2009a); 2.72 Ga Boston Creek – Puchtel et al. (2018); 2.82 Ga Kostomuksha –
2117 Puchtel and Humayun (2005); 2.88 Ga Volotsk – Puchtel et al. (2007); 3.26 Ga Weltevreden
2118 and 3.48 Ga Komati – Puchtel et al. (2014); 3.55 Ga Schapenburg – Puchtel et al. (2009b,
2119 2016a); 3.53 Ga Coonterunah, 3.34 Ga Kelly, and 3.18 Ga Ruth Well and Regal – Puchtel et
2120 al. (2022). Uncertainties are 2SD. The data reveal a broad trend of increasing HSE
2121 abundances in komatiite mantle sources over geological time. All uncertainties are 2SD of the
2122 mean. See text for additional details and the **Electronic Supplement** for the algorithm used to
2123 estimate the HSE abundances in the sources of the komatiite systems.

2124 **Fig. 4.** Evolution of the time-integrated $^{147}\text{Sm}/^{144}\text{Nd}$ and $^{176}\text{Lu}/^{177}\text{Hf}$ in the calculated
2125 sources of the Komati and Weltevreden komatiite systems formed during crystallization of a
2126 primordial magma ocean. The differentiation trends (shown by tick marks in percentage)
2127 depend on the relative proportions of the fractionating lower mantle mineral phases, *i.e.*,
2128 bridgmanite and Ca-Pv. The composition of the magma ocean prior to onset of crystallization
2129 is represented by that of the CHUR. The upper part of the panel represents aggregate
2130 compositions of magma ocean cumulates, while the lower part of the panel represents
2131 compositions of residual liquids after removal of the respective amounts of cumulate
2132 bridgmanite and Ca-Pv. All uncertainties are 2SD of the mean. See text for additional details
2133 of the model and the **Electronic Supplement** for the algorithm used in the calculations.

2134 **Fig. 5.** Values of $\mu^{182}\text{W}$ versus (A) $\mu^{186}\text{Os}$ and (B) $\gamma^{187}\text{Os}$ in the Kostomuksha komatiites
2135 illustrating mixing between the modern BSE and a mantle reservoir preserved from an early
2136 magma ocean crystallization event. The Re/Os, Pt/Os, and Hf/W ratios were established by
2137 high-pressure and -temperature metal-silicate equilibrium, resulting in $^{187,186}\text{Os}$ and ^{182}W
2138 enrichments at 2.82 Ga (Touboul et al., 2012). The coupled $^{186,187}\text{Os}$ and ^{182}W excesses in the
2139 source of the Kostomuksha komatiites (yellow circle) are explained by a ~50% contribution
2140 from the isotopically enriched reservoir to the modern BSE. All uncertainties are 2SD of the
2141 mean. See text for additional details.

2142 **Fig. 6.** $\mu^{182}\text{W}$ (ppm) versus calculated total HSE abundances in the sources of Archean
2143 and Paleoproterozoic komatiite-basalt systems studied to date relative to those in the estimates
2144 of the present-day BSE of Becker et al. (2006). This proportion corresponds to the fraction of
2145 the total HSE budget of the BSE added during late accretion assuming an HSE-free terrestrial
2146 mantle prior to late accretion. The average $\mu^{182}\text{W}$ value for the Moon of $+25\pm 5$ is from
2147 Kruijjer et al. (2015) and Touboul et al. (2015). The $\mu^{182}\text{W}$ of the BSE prior to late accretion is
2148 constrained *via Isoplot* regression analysis of the $\mu^{182}\text{W}$ and HSE compositions of all
2149 komatiite-basalt systems except for those of Kostomuksha and Schapenburg and the present-
2150 day BSE to be $+17\pm 7$. The W isotopic data and estimates of the HSE contents for the
2151 komatiite systems are from Puchtel and Humayun (2005), Touboul et al. (2012), and Puchtel
2152 et al. (2014; 2009b, 2016a,b; 2018; 2020; 2022). All uncertainties are 2SD of the mean. See
2153 text for additional details.

2154 **Fig. 7.** $^{182}\text{W}/^{184}\text{W}$ and $^{142}\text{Nd}/^{144}\text{Nd}$ data for the terrestrial mafic-ultramafic rock record
2155 obtained to date. The colored bands represent the 2SD uncertainty on the mean $\mu^{182}\text{W}$ and
2156 $\mu^{142}\text{Nd}$ values for each locality. The red arrows illustrate the change in direction and
2157 magnitude of the ^{182}W and ^{142}Nd anomalies. Note the relative scarcity of data for the period
2158 between ~ 2.7 Ga and present day. Data are from: 3.96 Ga Acasta – Roth et al. (2014),
2159 Willbold et al. (2015), Reimink et al. (2018); 3.85 Ga Isua – Willbold et al. (2011), Rizo et al.
2160 (2013, 2016), Dale et al. (2017), Tusch et al. (2019), Caro et al. (2006), Bennett et al. (2007),
2161 Saji et al. (2018); 3.80 Ga Nuvvuagittuq – O’Neil et al. (2012), Touboul et al. (2014); 3.78 Ga
2162 Saglek – Liu et al. (2016), Morino et al. (2017); 3.75 Ga Ukaliq – Caro et al. (2017); 3.72 Ga
2163 Isua – Rizo et al. (2011, 2016), Tusch et al. (2019), O’Neil et al. (2016); 3.50 Ga Ameralik –
2164 Saji et al. (2018); 3.37 Ga Ameralik – Rizo et al. (2012, 2016), Tusch et al. (2019); 3.55 Ga
2165 Schapenburg – Puchtel et al. (2016a); 3.53 Ga Coonterunah – Tusch et al. (2021), Puchtel et
2166 al. (2021); 3.48 Ga Komati and 3.26 Weltevreden – Touboul et al. (2012), Caro et al. (2006),
2167 Puchtel et al. (2013), Schneider et al. (2018); 3.45 Ga Warrawoona – Archer et al. (2019),
2168 Rizo et al. (2019), Murphy et al. (2021); 3.35 Ga Kelly – Puchtel et al. (2022); 3.18 Ga Ruth
2169 Well and Regal – Archer et al. (2019), Tusch et al. (2021), Puchtel et al. (2022); 3.14 Ga
2170 Banasandra – Maya et al. (2017); 2.82 Ga Kostomuksha and 2.69 Ga Belingwe – Touboul et
2171 al. (2012), Boyet and Carlson (2006); 2.72 Ga Boston Creek – Puchtel et al. (2018); 2.72 Ga
2172 Theo’s Flow – Debaille et al. (2013); 2.41 Ga Vetreny Belt – Puchtel et al. (2016b); 2.05 Ga
2173 Lapland – Puchtel et al. (2020); modern OIB – Caro et al. (2006), Andreasen et al. (2008),
2174 Murphy et al. (2010), Touboul et al. (2012), Mundl et al. (2017), Mundl-Petermeier et al.
2175 (2019, 2020), Rizo et al. (2019), Horan et al. (2018), Saji et al. (2018), Peters et al. (2018),
2176 Hyung and Jacobsen (2020); modern MORB – Caro et al. (2006), Mundl et al. (2017), Hyung
2177 and Jacobsen (2020).

2178

2179

Table 1. Summary of ages, thermodynamic parameters, and chemical features of the komatiite systems considered in this review.

Komatiite-basalt system	Age, Ga	MgO _{liq}	T _{liq} °C	T _p °C	D _{melt init.} km	D _{plume init.} km	Al ₂ O ₃ /TiO ₂	(La/Sm) _N	(Gd/Yb) _N	Nb/Nb*	W/Th
<i>Kaapvaal Craton, South Africa</i>											
Schapenburg	3.55	29.1±2.8	1582	1811	443	LM	10.0±0.8	0.93±0.04	1.57±0.10	1.2±0.1	9.7±5.5
Komati	3.48	29.9±0.5	1591	1822	494	LM	10.1±0.7	0.97±0.24	1.39±0.05	1.1±0.2	0.25±0.18
Weltevreden	3.26	31.4±0.9	1606	1841	605	LM	29.2±1.1	0.68±0.06	0.84±0.03	1.4±0.1	1.5±1.4
<i>Pilbara Craton, Western Australia</i>											
Coonterunah	3.53	23.0±0.3	1498	1705	203	MTZ	23.8±1.7	0.80±0.04	0.96±0.04	1.08±0.02	0.91±0.62
Kelly	3.34	27.4±1.0	1561	1786	351	MTZ	22.1±1.7	0.65±0.02	0.91±0.04	1.03±0.04	0.81±0.69
Ruth Well	3.18	29.3±0.7	1584	1814	455	MTZ	11.0±0.5	0.55±0.09† 0.77±0.09	1.31±0.04† 1.32±0.04	1.0±0.1† 0.51±0.05	3.4±2.3
Regal	3.18	29.3±0.7	1584	1814	455	MTZ	11.9±0.8	0.61±0.11† 0.83±0.11	1.28±0.12† 1.31±0.12	1.0±0.1† 0.55±0.09	3.5±2.8
<i>Fennoscandian Shield, northern Europe</i>											
Kostomuksha	2.82	27.6±1.0	1564	1789	361	LM	17.2±1.2	0.48±0.13	1.16±0.02	1.2±0.1	0.84±0.32
Vetreny	2.41	27.0±1.0	1556	1779	333	MTZ	19.7±0.5	0.41±0.10† 2.2±0.1	1.2±0.1† 1.3±0.1	1.0±0.1† 0.29±0.03	0.05±0.02
Lapland	2.05	25.2±0.5	1532	1748	264	LM	13.9±0.4	0.14±0.02† 0.26±0.01	1.48±0.02† 1.49±0.02	1.0±0.1† 0.58±0.01	0.16±0.06
<i>Superior Craton, Canada</i>											
Boston Creek	2.72					MTZ	5.1±0.8	1.9±0.3	2.0±0.2	1.2±0.2	0.9±1.4
Pyke Hill-Alexo	2.72	28.2±0.5	1571	1789	392	MTZ	20.4±0.6	0.53±0.16	0.98±0.03	1.0±0.1	0.15±0.06
<i>Rhodesian Craton, Zimbabwe</i>											
Belingwe	2.69	25.6±0.5	1537	1755	277	MTZ	19.8±0.6	0.68±0.02	1.02±0.04	0.97±0.05	0.20±0.06

2180

2181

2182

2183

2184

2185

†Values corrected for AFC. The italicized values are those measured in the emplaced lavas, before correction for AFC. All uncertainties are 2SD of the mean. MgO_{liq} – the MgO content of the original emplaced komatiite magma for each komatiite system compiled from Nicklas et al. (2018, 2019) and Puchtel et al. (1998, 2016a, 2020, 2022). T_{liq} °C, T_p °C – liquidus temperatures of the emplaced komatiite magmas and mantle potential temperatures for the studied komatiite systems. D_{melt init} – depths of melting initiation. D_{plume init} – inferred depths of plume initiation for the studied komatiite systems. Nb/Nb* = Nb_N/√(Th_N×La_N), where N are the BSE normalizing values from Hofmann (1988). For sources of the data see Table 2. See text and the **Electronic Supplement** for details.

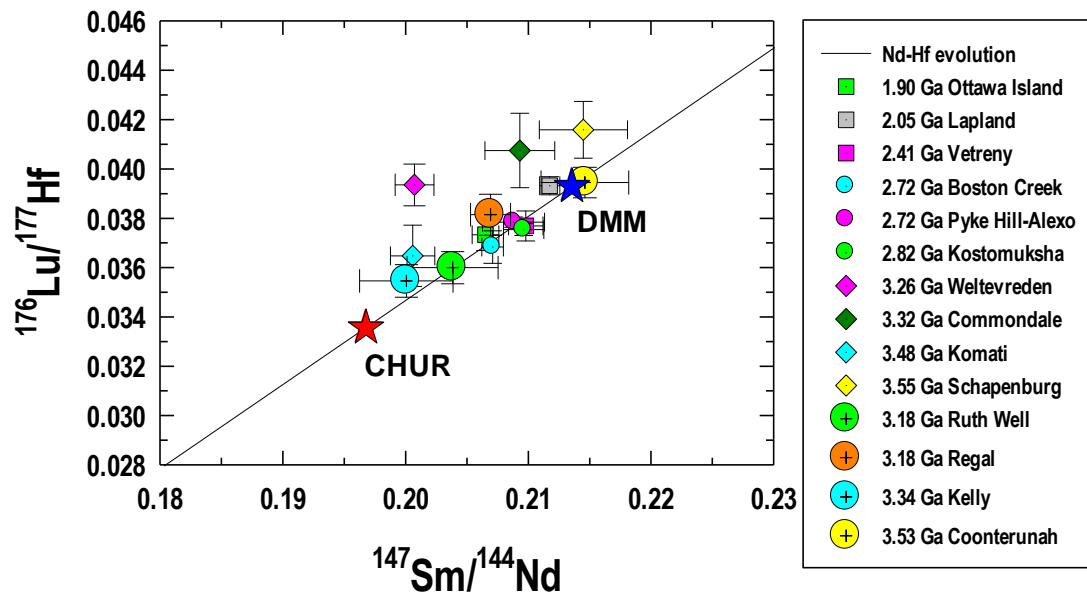
2186

Table 2. Summary of isotopic features and HSE abundances of the komatiite systems considered in this review

Komatiite-basalt system	$\epsilon^{143}\text{Nd}(\text{T})$	$\epsilon^{176}\text{Hf}(\text{T})$	$\mu^{142}\text{Nd}$	$\mu^{182}\text{W}$	$\gamma^{187}\text{Os}(\text{T})$	$\mu^{186}\text{Os}(\text{T})$	ΣHSE	Data source
<i>Kaapvaal Craton, South Africa</i>								
Schapenburg	+2.4±0.5	+5.8±0.8	-5.0±2.8	-8.4±4.1	+3.7±0.3		29±9	[1 – 2]
Komati	+0.46±0.39	+1.9±1.0	-0.9±2.7	+2.7±4.5	+0.3±0.3	-12±8	60±8	[3 – 5]
Weltevreden	+0.54±0.40	+4.7±2.1	+2.5±3.8		-0.1±0.2	+22±7	65±6	[3 – 4]
<i>Pilbara Craton, Western Australia</i>								
Coonterunah	+2.4±0.5	+4.4±0.3		+11.4±4.6			29±6	[6]
Kelly	+0.5±0.6	+1.7±0.6		+8.2±3.3	+0.8±0.4		38±7	[6]
Ruth Well	+1.3±0.7† <i>+0.6±0.7</i>	+2.4±0.4† <i>+1.7±0.4</i>	-1.8±3.8	+7.7±5.0	-0.4±0.4† <i>-0.4±0.4</i>		55±4	[6]
Regal	+1.9±0.3† <i>+1.0±0.3</i>	+4.6±0.8† <i>+4.1±0.8</i>		+7.7±5.0	+0.9±0.3† <i>+0.9±0.3</i>		70±5	[6]
<i>Fennoscandian Shield, northern Europe</i>								
Kostomuksha	+3.0±0.4	+4.9±0.3	+0.4±0.9	+15.0±4.8	+2.5±0.6	+22±6	79±6	[7 – 11]
Vetreny	+3.7±0.4† <i>-0.9±0.4</i>	+6.3±0.9† <i>+0.4±0.9</i>	+0.5±2.1	-0.5±5.2† <i>+7.5±5.2</i>	+1.3±0.2† <i>+1.7±0.2</i>	+3.2±1.7	66±10	[12]
Lapland	+4.9±0.3† <i>+3.7±0.3</i>	+10.2±0.7† <i>+8.7±0.7</i>		-10.0±5.0† <i>+1.5±3.3</i>	-0.2±0.3† <i>-0.2±0.3</i>	+29±2	120±5	[13]
<i>Superior Craton, Canada</i>								
Boston Creek	+2.5±0.2	+4.3±0.9	-3.8±2.8	+11.7±4.5	+0.1±0.3		35±10	[14]
Pyke Hill-Alexo	+3.0±0.5	+5.5±0.6	+6.8±2.5		+0.4±0.1	-0.1±4.2	85±5	[15 – 19]
<i>Rhodesian Craton, Zimbabwe</i>								
Belingwe	+2.9±0.2		+3.7±7.0		+0.1±0.2	+0.6±2.5	57±7	[20 – 21]

2187
2188
2189
2190
2191
2192

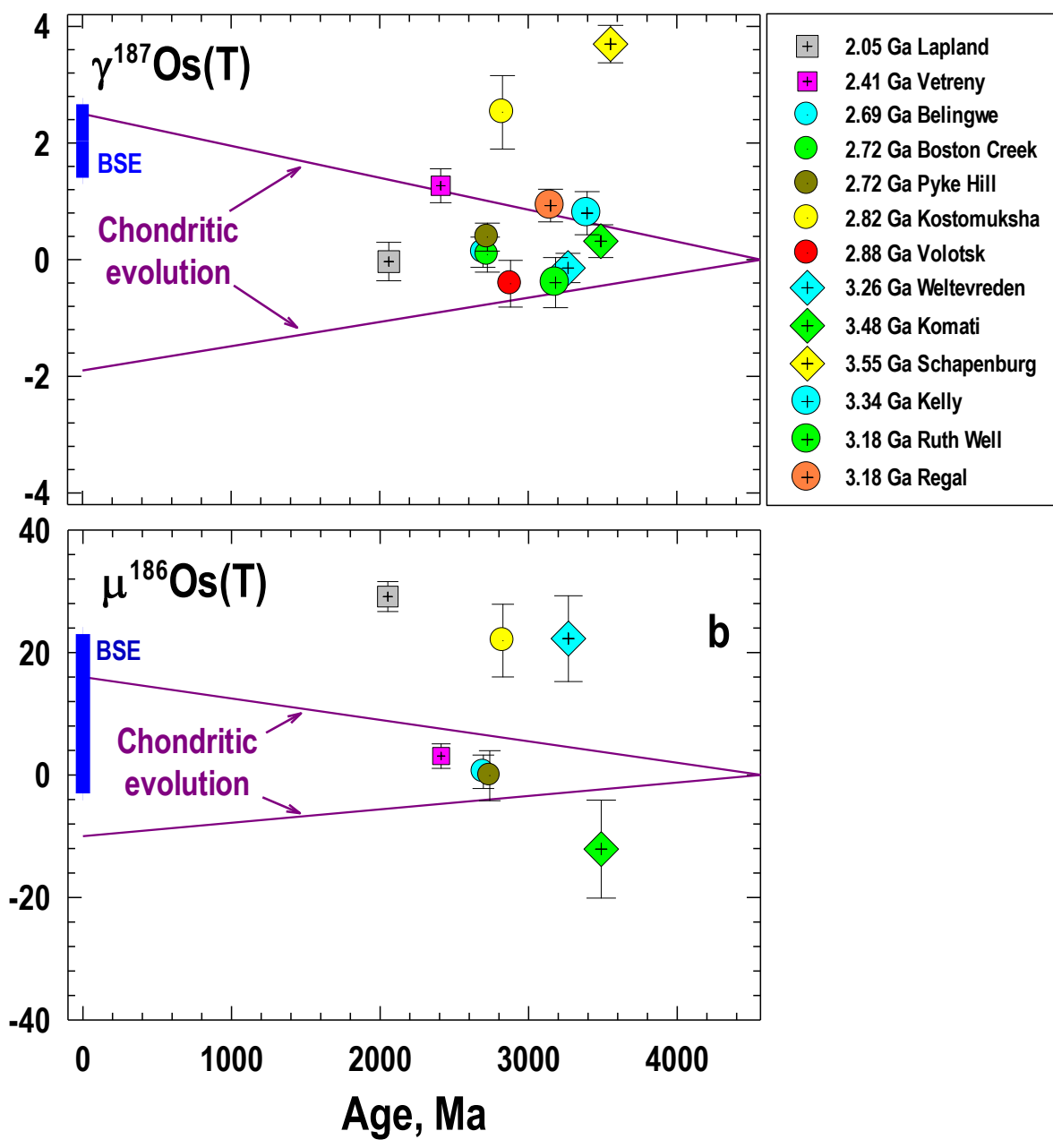
†Values corrected for AFC. The italicized values are those measured in the emplaced lavas, before correction for AFC. All uncertainties are 2SD of the mean. Data sources are as follows: [1] - Puchtel et al. (2009a); [2] - Puchtel et al. (2016a); [3] - Puchtel et al. (2013); [4] - Puchtel et al. (2014); [5] - Touboul et al. (2012); [6] - Puchtel et al. (2022); [7] - Puchtel et al. (1998); [8] - Boyet and Carlson (2006); [9] - Touboul et al. (2012); [10] - Puchtel et al. (2005); [11] - Puchtel and Humayun (2005); [12] - Puchtel et al. (2016b); [13] - Puchtel et al. (2020); [14] - Puchtel et al. (2018); [15] - Blichert-Toft and Arndt (1999); [16] - Puchtel et al. (2004a); [17] - Puchtel et al. (2004b); [18] - Puchtel et al. (2009b); [19] - Debaille et al. (2013); [20] - Puchtel et al. (2009b); [21] - Boyet and Carlson (2006).



2193

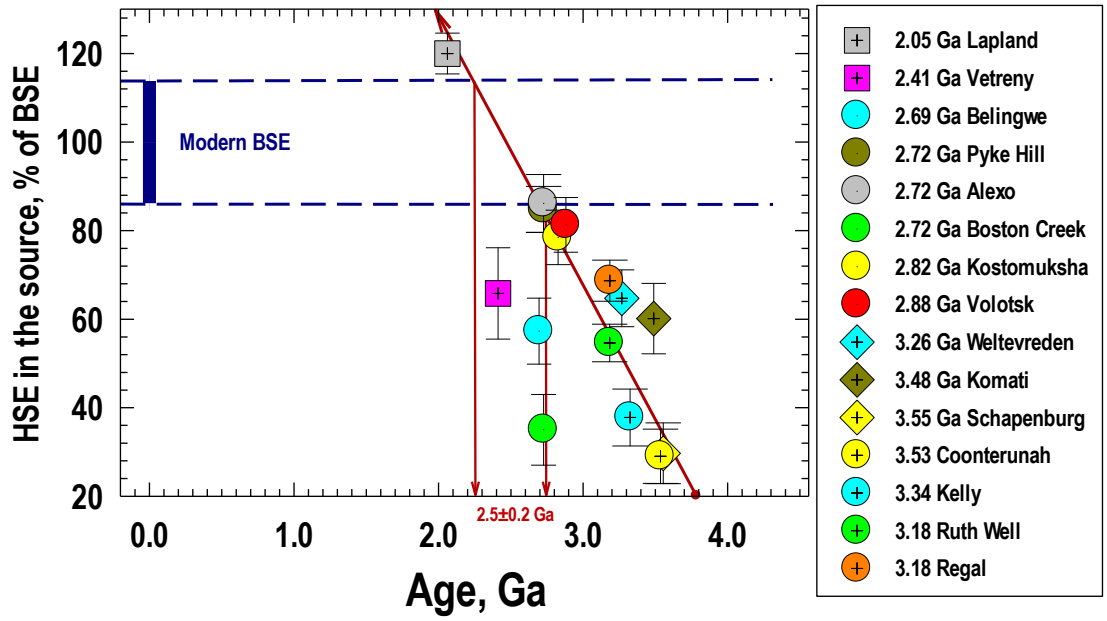
2194 **Fig. 1**

2195



2196
 2197
 2198
 2199

Fig. 2

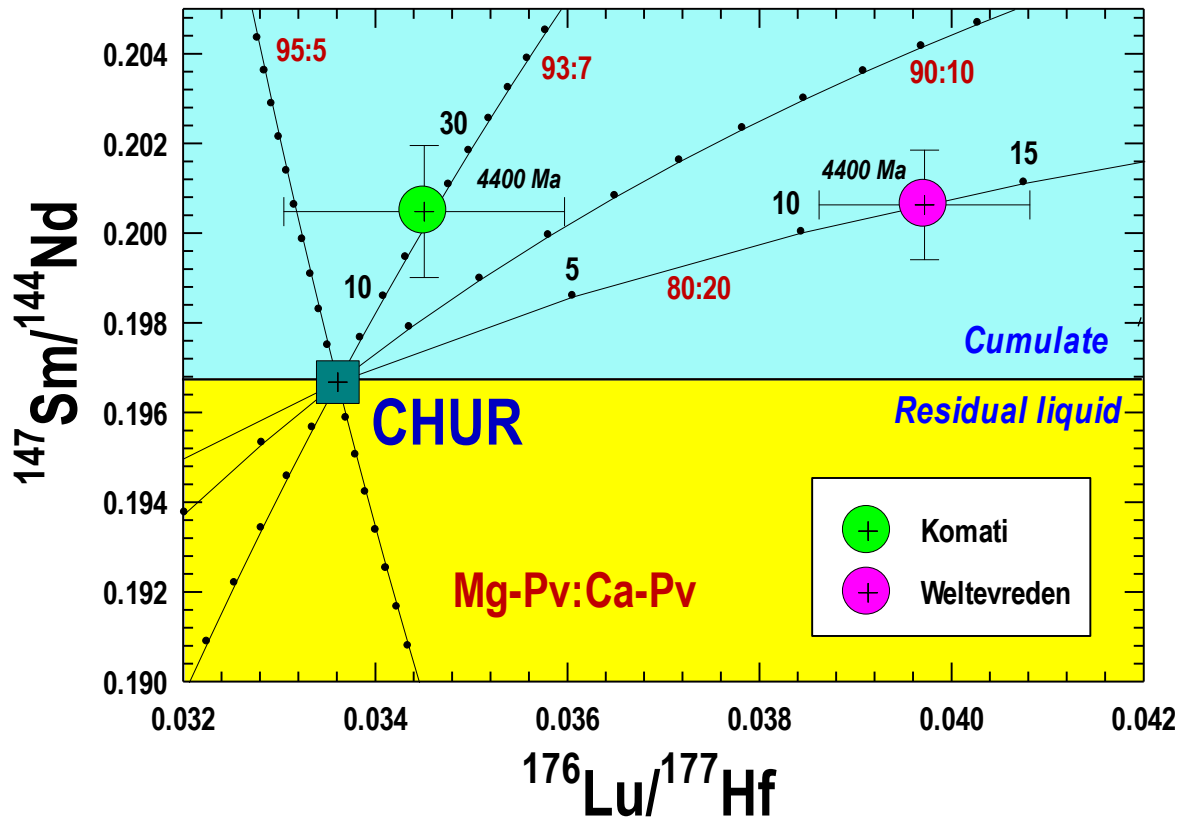


2200

2201

2202 Fig. 3

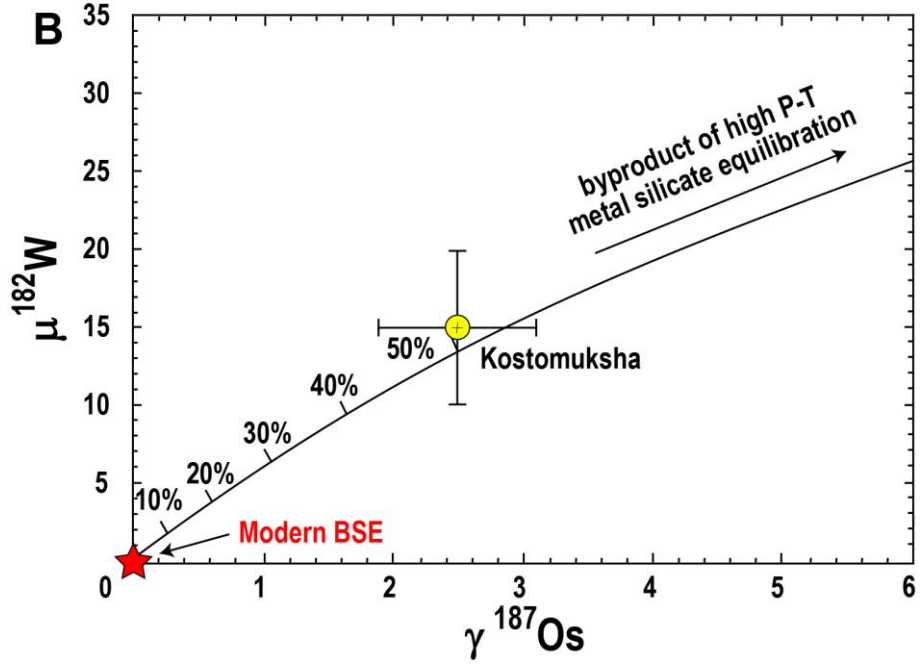
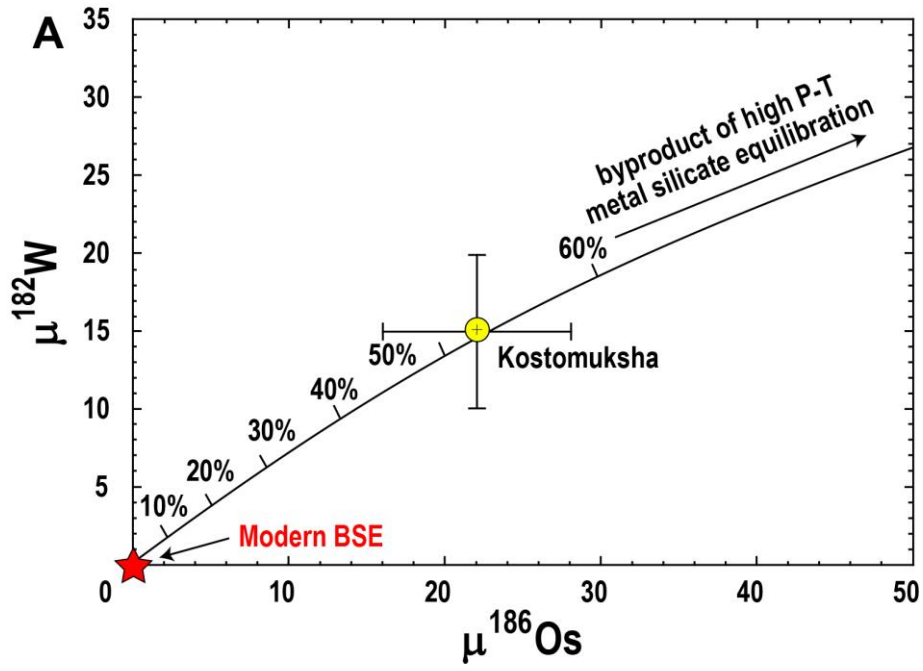
2203



2204
2205

2206 **Fig. 4**

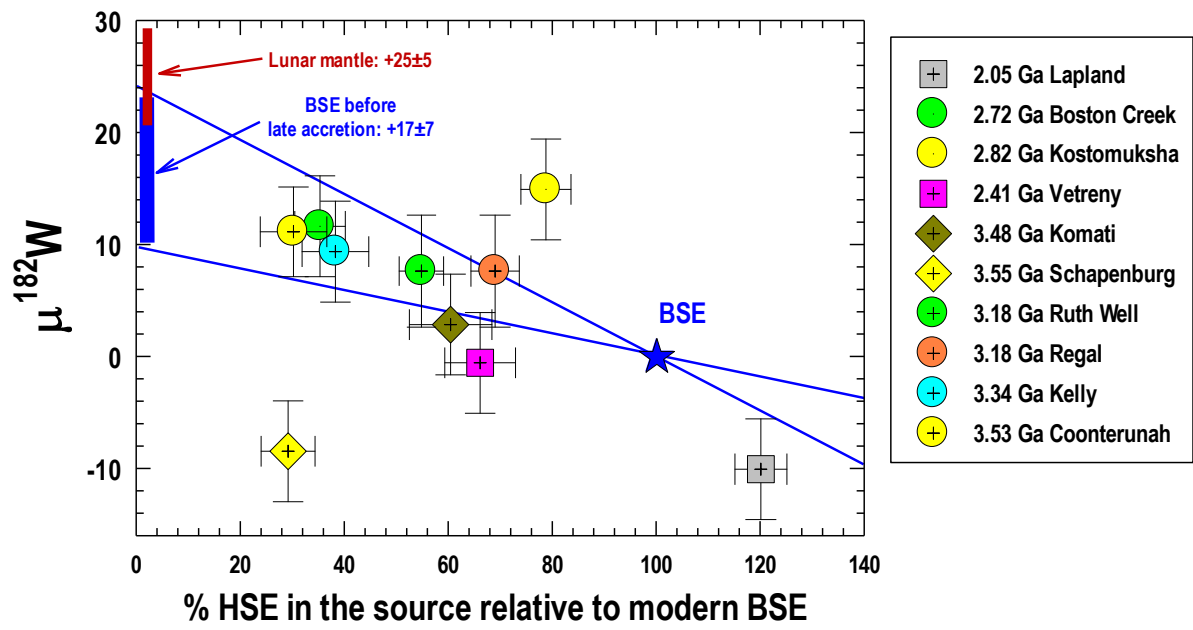
2207



2208

2209 **Fig. 5.**

2210

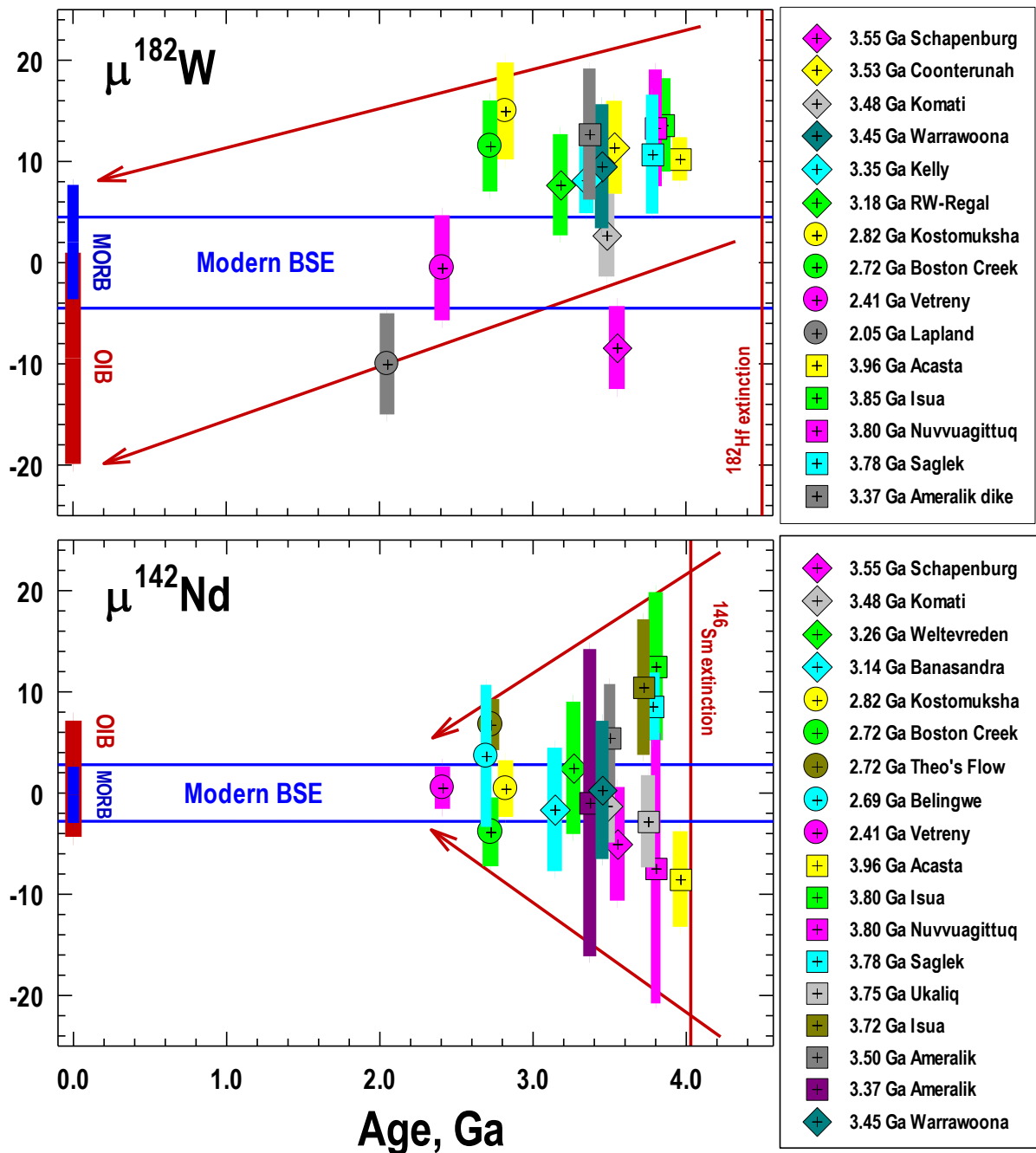


2211

2212

2213 **Fig. 6.**

2214



2215
2216

2217

2218

Fig. 7